THE DEVELOPMENT OF A DYNAMIC ENGINE - TESTING FACILITY

P.A. Conradie

Thesis presented in partial fulfilment of the requirements for the degree of Master of Mechanical Engineering at the University of Stellenbosch.

Advisor: Dr. A. B. Taylor

November 2001

Declaration

I, the undersigned, hereby declare that the work contained in this thesis is my own original work and that I have not previously in its entirety or in part submitted it at any university for a degree.

SUMMARY

The last two decades have seen many changes within the automotive industry. Many advances have been made in the design, research and development of the internal combustion engine and technological progress made in the integrated-circuit and computer industry has resulted in the availability of reliable low-cost electronic components. These components have, over time, been incorporated into the very hearts of engines, thereby allowing for the accurate control of engine functions and processes to an extent that was previously impossible. Parallel to these developments is the growing concern for the environment and the realisation that resources are being consumed at ever-increasing rates. This has placed vehicle manufacturers under continual pressure to optimise their engines, not only for fuel efficiency, but also to reduce harmful emissions while continuing to deliver better performance and drivability characteristics.

At the same time, engine testing equipment and facilities have had to keep abreast with these advances and this has required the development of more sophisticated testing facilities. One such facility is the *dynamic engine test-bed*. Among other features, this facility has the ability to subject test-bed mounted engines to loads similar to what would be experienced in a vehicle on the road. This approach allows for the optimisation of engine components and performance under more realistic conditions, yielding results far superior to those obtainable using more conventional steady-state testing and development procedures.

This document discusses the development of such a dynamic engine test-bed at the Centre for Automotive Engineering at the University of Stellenbosch. The project was initiated by conducting a literature survey to establish the current state of technology in the field. The dynamic test-bed was developed around an existing direct-current electric motor and industrial speed controller configured in a regenerative manner. This setup enabled the unit to both absorb and deliver power, essential for the simulation of vehicle dynamics. Great care was taken to ensure that signals obtained from the test-bed were accurate and useful for further computer manipulation. Anti-aliasing filters were designed and manufactured to guarantee that signals could not be misinterpreted due to sampling effects.

A computer-implemented vehicle model was developed to simulate, in real-time, vehicle response to torque developed by the engine on the test stand. The model included a manual transmission, clutch and a rigid drive-shaft. Driver input (accelerator, brake, clutch and gear selection) was by means of a set of pedals and hand-held gear selector switches. Various vehicle speed control strategies were investigated and recommendations made regarding their possible future implementation. System evaluation was accomplished by the simulated acceleration of a large truck. The simulations indicated that repeatable results could be obtained from the system. The system was also found to be adequately sensitive to reflect the effect of subtle changes made to engine parameters on vehicle acceleration. It was concluded that the dynamic engine test-bed did indeed offer the capability to conduct research and testing not previously available in South Africa. Finally, recommendations were made for the future improvement and expansion of the system's performance and capabilities.

OPSOMMING

Die laaste twee dekades het baie veranderinge in die outomobiel industrie megebring. Groot vooruitgang is gemaak in die ontwerp, navorsing en ontwikkeling van die binnebrand enjin, terwyl tegnologiese vooruitgang in die geïntegreerde-stroombaan en rekenaar industrië betroubare elektroniese komponente teen lae koste beskikbaar gemaak het. Hierdie komponente is mettertyd in enjins geïnkorporeer en het die akkurate beheer van enjin funksies en prosesse moontlik gemaak. Saam met hierdie ontwikkeling, is daar toenemende kommer oor die omgewing en `n bewuswording dat hulpbronne verbruik word teen `n groeinde tempo. Hierdie feite plaas voertuig vervaardigers onder volgehoude druk om enjins te optimeer vir brandstof doeltreffendheid, maar ook om skadelike emissies te bekamp terwyl beter werksverrigting en bestuurbaarheid vereis word.

Enjin toetstoerusting en fasiliteite moes terselfdetyd met hierdie vooruitgang byhou en het die ontwikkeling van meer gesofistikeerde toetsfasiliteite vereis. Een sodanige fasiliteit is die *dinamiese enjin toetsbank.* Een van die kenmerke van hierdie fasiliteit is dat dit toetsbank-gemonteerde enjins kan onderwerp aan `n las soortgelyk as wat ondervind sou word in `n voertuig op die pad. Hierdie benadering stel ingenieurs in staat om enjin komponente en werksverrigting te optimeer onder meer realistiese kondisies en lewer resultate van `n baie hoër gehalte as wat verkry kan word deur gebruik te maak van meer konvensionele gestadigde-toestand toets- en ontwikkelings-prosedures.

Hierdie dokument bespreek die ontwikkeling van so `n dinamiese enjin toetsbank by die Sentrum vir Automobielingenieurswese aan die Universiteit van Stellenbosch. Die projek is geïnisieer deur `n literatuurstudie te doen om die huidige stand van tegnologie in die gebied vas te stel. Die dinamiese enjintoetsbank is ontwikkel rondom `n bestaande gelykstroom-motor en industriële spoed beheerder wat in `n regeneratiewe konfigurasie opgestel is. Hierdie opstelling het die absorpsie en lewering van drywing moontlik gemaak, `n vereiste vir die simulasie van voertuig dinamika. Baie tyd is gespandeer om te verseker dat seine afkomstig van die toetsbank akkuraat en bruikbaar was vir verdere rekenaar manipulasie. Anti-aliaseringsfilters is ontwerp en vervaardig om te verseker dat seine nie verkeerd geïnterpreteer kon word as gevolg van diskritiserings effekte nie.

`n Rekenaar ge-implementeerde voertuigmodel is ontwikkel om `n voertuig se reaksie op draaimoment ontwikkel deur die enjin op die toetsbank intyds te simuleer. Die model het `n handrat transmissie, koppelaar en starre dryf-as ingesluit. Bestuurder intree (vernellingspedaal, rem, koppelaar en rat seleksie) is bewerkstellig deur middel van `n stel pedale en `n hand geoperateurde rat skakelaar. Verskeie voertuig spoed-beheerders is ondersoek en aanbevelings is gemaak aangaande die toekomstige implementering daarvan. Die sisteem is geëvalueer deur die versnellingsimulasie van `n groot vragmotor. Die simulasies het daarop gedui dat herhaalbare resultate van die sisteem verkry kon word. Daar is ook bevind dat die sisteem sensitief genoeg was om subtiele veranderinge aan enjinparameters in die resultate te weerspieël. Die gevolgtrekking is gemaak dat die dinamiese enjin toetsbank inderdaad die vermoëns gebied het om ontwikkeling en toetswerk te doen wat nie voorheen in Suid-Afrika moontlik was nie. Voorstelle is laastens gemaak aangaande die toekomstige verbetering en uitbreiding van die sisteem se vermoëns.

For my wife, Rejane

AKNOWLEDGEMENTS

I would like to express my sincere thanks to the following people for their assistance, in its various forms, towards the completion of this work:

- Dr. Andrew Taylor, my supervisor, for his support, guidance and motivation during my last five years of study;
- Prof. Garth Milne, for his advice;
- All CAE personnel who have helped and supported me in various ways, especially Willem Boshoff whose assistance I greatly valued;.
- My wife, Rejane, for all the love and understanding when I had to work until late at night and over weekends, for her motivation and inspiration and also for proof-reading this document;
- My parents, Jan and Marichen Conradie, for their encouragement, enthusiasm and love;
- And finally, my Lord and Saviour, Jesus Christ, for giving me the strength and courage (at times) to complete my studies.

CONTENTS

LIST OF SYMBOLS

A	Vehicle frontal area	[m^2]
a	Vehicle acceleration	[m/s^2]
C	Percentage clutch travel	[%]
C_D	Aerodynamic drag coefficient	
F	Force	[N]
F_b	Braking force	[N]
F_d	Aerodynamic drag force	[N]
F_r	Rolling resistance force	[N]
F_t	Tractive force	[N]
f	Frequency	[Hz]
f_0	Speed independent rolling resistance coefficient	
f_1	Speed dependent rolling resistance coefficient	
f_m	Mass factor	
f_{Nyq}	Nyquist frequency	[Hz]
f_r	Combined rolling resistance coefficient	
f_s	Sampling frequency	[Hz]
G_{ij}	Transfer function from i to j	
G_f	Final drive ratio	
G_t	Transmission ratio	
G_{tf}	Overall transmission ratio	
g	Gravitational acceleration	[m/s^2]
I_g	Thyristor gate current	[A]
J_{ave}	Average inertia	[kgm^2]
J_c	Clutch inertia	[kgm^2]

J_d	Dynamometer inertia	[kgm^2]
J_{dr}	Driveline inertia	[kgm^2]
J_{dt}	Drivetrain inertia	[kgm^2]
J_e	Engine inertia	[kgm^2]
J_f	Final drive inertia	[kgm^2]
J_t	Transmission inertia	[kgm^2]
J_v	Equivalent total vehicle inertia	[kgm^2]
J_{vl}	Equivalent vehicle inertia due to linear translation	[kgm^2]
J_w	Wheel inertial (four wheels)	[kgm^2]
K_x	Controller gain constants	
M	Mass of vehicle	[kg]
M_p	Maximum overshoot	[%]
M_r	Equivalent mass of rotating vehicle components	[kg]
N	Rotational speed	[rpm]
$\dot{N}$	Angular acceleration	[rpm/s]
n	Number of clutch plates	
P	Power	[kW]
P_L	Clutch plate load	[N]
R	Tyre radius	[mm]
R_m	Mean radius of clutch facing material	[mm]
s	Laplace variable	[ ]
T_{demand}	Torque demand	[Nm]
T_a	Dynamometer armature torque	[Nm]
T_{ax}	Axle torque	[Nm]
T_c	Clutch torque	[Nm]
T_{cap}	Clutch torque capacity	[Nm]

T_{cmax}	Maximum clutch torque	[Nm]
T_{cor}	Corrected torque	[Nm]
T_{dr}	Drive-shaft torque	[Nm]
T_e	Engine torque	[Nm]
T_f	Friction torque	[Nm]
T_{lc}	Load-cell torque	[Nm]
T_l	Load torque	[Nm]
T_s	Shaft torque	[Nm]
T_v	Total vehicle load torque as seen at the clutch	[Nm]
t	Time	[s]
t_d	Delay time	[s]
t_p	Peak time	[s]
t_r	Rise time	[s]
t_s	Settling time	[s]
U_{th}	Throttle demand signal	[%]
U_d	Dynamometer demand signal	[%]
U_g	Gear selection signal	
U_{cl}	Clutch demand signal	[%]
U_b	Brake demand signal	[%]
U_{acc}	Accelerator pedal demand	[%]
V	Vehicle speed	[km/h]
V_{actual}	Actual vehicle speed	[km/h]
V_{cycle}	Demanded cycle speed	[km/h]
$\dot{V}_{cycle}$	Differential of demanded cycle speed	[km/h/s]
V_{demand}	Demanded vehicle speed	[km/h]

V_{tacho}	Tachometer voltage	[V]
W	Vehicle weight	[N]
x_n	Raw sampled data point	
$\bar{x}_n$	Smoothed sampled data	
x_{pn}	Predicted data point at time n	
x_{pn+1}	Predicted data point at time n+1	
$\dot{\bar{x}}_n$	Derivative of smoothed data point at time n	
$\dot{\bar{x}}_{n-1}$	Derivative of smoothed data point at time n-1	
α	Track-while-scan filter parameter	
α_d	Dynamometer angular acceleration	[rad/s²]
α_e	Engine angular acceleration	[rad/s²]
α_v	Equivalent vehicle angular acceleration	[rad/s²]
Γ	Period	[s]
η_{tf}	Combined transmission and final-drive transmission efficiency	[%]
ρ	Air density	[kg/m³]
μ	Mass ratio	
μ_s	Static coefficient of friction	
ω	Rotational speed	[rad/s]
ω_a	Armature speed	[rad/s]
ω_{actual}	Actual engine speed	[rad/s]
ω_b	Bandwidth frequency	[rad/s]
ω_d	Damped natural frequency	[rad/s]
ω_{demand}	Demanded engine speed	[rad/s]

$\omega_{dynamic}$	Dynamometer speed	[rad/s]
ω_e	Engine speed	[rad/s]
ω_n	Natural frequency	[rad/s]
$\dot{\omega}_a$	Armature angular acceleration	[rad/s^2]
ω_v	Equivalent vehicle angular speed	[rad/s]

AC	Alternating Current
CAE	Centre for Automotive Engineering
CARIMA	Controlled Autoregressive Integrated Moving Average
COTS	Commercial Off The Shelf
DC	Direct Current
ECE	Economic Commission for Europe
EMS	Engine Management System
EPA	Environmental Protection Agency
FFT	Fast Fourier Transform
GPC	Generalised Predictive Control
ICE	Internal Combustion Engine
KE	Kinetic Energy
MIMO	Multiple Input Multiple Output
MISO	Multiple Input Single Output
OEM	Original Equipment Manufacturer
PDT_1	Proportional Derivative with Time lag
PID	Proportional Integral Derivative
PRBS	Pseudo Random Binary Signal
TWS	Track While Scan
VSD	Variable Speed Drive

LIST OF FIGURES

LIST OF TABLES

1. INTRODUCTION

Internal combustion engines formed the backbone of the 20th century's transport industry. The continual improvement of the ICE, specifically the optimisation for low fuel consumption, reduction of harmful emissions, and the introduction of engine management systems, has become increasingly important as the world's fossil-based energy resources dwindle, and the impact of emissions on the ecology becomes more apparent. Especially worrisome is the excessive release of oxides of nitrogen, un-burnt hydrocarbons and carbon monoxide into the atmosphere where they are key ingredients to the formation of smog, accelerate the green-house effect and cause general respiratory problems. Emphasis has been placed on the reduction of these pollutants, resulting in many countries adopting strict emissions regulations, which are enforced by the measuring of exhaust emissions over standardised driving cycles.

Vehicle manufacturers have had to go to great lengths in order to meet these emissions requirements. Both fuel efficiency and emissions are affected by the control of parameters such as air/fuel mixture and ignition timing. Engines are calibrated by a process in which these parameters are optimised for various operating conditions. Conventional engine calibration procedure involved the finding of a good, steady-state engine calibration on a test-bench, where after suitable dynamic compensation functions were obtained during extensive driving tests. These were then applied in order to meet the various drivability and transient performance requirements. Calibrated engines were installed into prototype vehicles and driven through emissions cycles by human drivers on chassis dynamometers. These tests were both cumbersome and costly, and produced data that lacked accuracy and repeatability because of the different and time-variant behaviour of human drivers. This has led to long development delays and, in many cases, to almost insurmountable difficulties. The need for more advanced testing facilities clearly existed and led many vehicle manufacturers to acquire dynamic engine test-beds.

As early as 1972, Cassidy (1972) demonstrated that a computer-controlled electric dynamometer could be used to measure vehicle exhaust emission performance. The dynamometer capabilities were also shown to be sufficient to duplicate the conditions experienced by an engine in a vehicle on a chassis-dynamometer, with regard to emissions

performance. Today these facilities are capable of simulating correct engine loading during transient operations as encountered in actual vehicles on the road, without the need for vehicle hardware other than the engine. This step has provided automotive engineers with the ability to calibrate engines to meet emissions standards while saving both time and money.

Economic competitiveness in the automotive industry, together with customer demands for better fuel efficiency and overall performance, have forced manufacturers to optimise engine control units, the dynamic behaviour, and drivability of their vehicles. This has led to experimentation into the engine-drive-train setup, such as optimising gear ratios to match a particular engine characteristic, or optimising the engine for a particular vehicle set-up. Engine-mounting characteristics and their reaction to engine and drive-line vibrations must also be considered, if the power-train system as a whole is to be fully optimised. The "time is money" cliché is particularly applicable to the automotive industry, with short lead times and costs in the design and development process often determining the success, or not, of new products.

Due to the complexity of modern engine packages including ignition, fuel injection, emissions controls and other systems, knowledge of the behaviour and interaction between these subsystems is required to meet the new design objectives for the development of power-plants and vehicles. This information is not completely available from static engine tests, since many parameters depend on the dynamic behaviour of the engine. It has for instance been shown that both fuel economy and exhaust emissions are highly dependent on transient change of engine speed and torque (Cassidy et al., 1972, Krempl et al., 1985 and Von Thun, 1987). For effective design, reliable and reproducible data obtained under dynamic conditions is thus very necessary.

On the academic side, combustion-theory, fluid-dynamics, and related fields are being better understood resulting in increasingly complex models being developed. These models are used to predict engine performance and assist in the understanding of the dynamics governing their behaviour and characteristics. They have led to a reduction in development time, minimisation of the cost of experimental work and the attainment of optimal system design. These facts, together with tremendous progress in the fields of electronics and computers, have necessitated the development of equally sophisticated

engine test-beds, capable of verifying modelled predictions, while supporting research-and-development engineers in their efforts to improve the internal combustion engine.

Complex test procedures are no longer limited to the engine as a whole unit, but are concentrated on specialised problems and their solutions, so that application oriented test procedures are required (Krebl, 1995). At present, much of the information required by these specialised procedures is not available and it is impractical to use instrumented vehicles to obtain precise, dynamic data under controlled, repeatable conditions. By placing an engine in a test cell under the control of a computer, it is possible to combine most of the advantages of vehicle testing and performing dynamometer tests. By transferring a large proportion of tests from the road to the laboratory, control can be maintained over experimental conditions in the test cell, while the use of much better equipment ensures more accurate and reproducible data.

From the above considerations it is clear that not all the information required by today's automotive engineers is available from engine tests performed under steady-state conditions. Instead, test-beds capable of both steady-state and transient capabilities are required. This need is met by the dynamic engine test-bed. Among others, applications of the facility include:

- Testing the control response and drivability of ignition and fuel supply components, the determination of their dynamic characteristics, as well as checking the efficiency of soot filters for diesel engines and the efficiency of catalysts.
- Dynamic endurance testing with load and speed points corresponding to real driving conditions. The wear and service life of the engine components and the oil consumption are of special interest.
- Comparative measurements of consumption and exhaust emissions in the early phases of development to provide the data necessary for modifications of design and engine calibration.
- Optimisation of engine management systems under specific driving conditions, for example the warm-up period, acceleration enrichment and inertia motoring.

By far the greatest advantage of the dynamic test-bed is that it can simulate engine loads as they are experienced on the road. Others include:

- Driving cycles can be simulated to much higher degrees of accuracy and repeatability since no error-prone human drivers are required for their implementation.
- Highly sophisticated equipment can be used to acquire and analyse data, since the engine being tested is now in a laboratory, not in the engine-compartment of a moving vehicle (Del Giacomo et al., 1990).
- Vehicle and road-load parameters can easily be changed using computer simulation software, allowing for optimisation over a wider range of operating conditions.
- Both development times and costs are reduced, since there is no more need for both test vehicles and drivers, but only the engines to be tested (Hong, 1995).

2. NEED IDENTIFICATION AND PROJECT OBJECTIVES

A comprehensive study of the literature available on dynamic engine testing was carried out, shedding light on what has already been achieved in the field and, to some extent, how this was achieved. This knowledge aided in identifying the need for a new engine testing facility and in formulating a set of objectives of the project. These needs and objectives were refined somewhat and are discussed in this section.

2.1. VEHICLE MODEL

The primary purpose of the dynamic test-bed was to simulate road load conditions experienced by engines. This required the modelling of vehicle and engine interactions and responses to the environment. Jacobson (1995) defines a model broadly as "everything needed to determine the solution", i.e., equations, which variables are desired to solve, etc., while Ljung (1987) defines it as an assumed relationship among observed signals of a system. An important consideration was to decide the degree of complexity the model was to assume. Too complex a model would lead to the time taken to solve the governing equations being be too long, not allowing other necessary real-time operations to be performed by the control computer. On the other hand, if the model was not complex enough, and pertinent influences and factors not included, it would lack the degree of accuracy required for acceptable simulations to be performed. The first objective of the project was thus to construct and refine a suitable vehicle model, including driveline, clutch system and tyres, that would yield as output the control parameters necessary to simulate loads on the engine as if it was located in a vehicle.

2.2. VIRTUAL VEHICLE SIMULATION ENGINE

With a suitable model at hand, the next objective of the project was to develop a virtual vehicle simulation "*engine*". The task of this engine would be the acquisition and conditioning of required input data, the manipulation of data and solving of equations, and providing output to the relevant subsystems of the facility. This engine would in essence constitute the real-time element of the computer programme overseeing the running of the test facility.

2.3. SYSTEM TEST FUNCTIONS

Having established the vehicle simulation engine to take care of the simulation aspect of the system, this subsystem should be available to do useful work. A third objective was thus to identify and develop the necessary subsystems and structures enabling the user to configure the system in such a way as to extract useful information and insight from it. Consequently, it was required to develop a user-friendly interface by means of which the user could input all relevant cycle, vehicle, engine, and driver information needed for the running of virtual-vehicle engine test cycles.

One such test consisted of performing acceleration tests such as from 0 to 100 km/h, as this can be used as a valuable tool by providing useful comparative data required for engine management system (EMS) and transmission optimisation. A second possible test was to perform standard emissions cycles, consisting of driving a virtual vehicle through a pre-determined speed profile. By collecting emissions in sampling bags using a CVS (constant volume sampling) system, integrated emissions values can be obtained, while transient emissions can be obtained by means of high-speed emissions test equipment. These emission values are then compared to the permissible values as prescribed by many countries in order for new engines to be certified. This type of work is highly specialised and well-suited to the dynamic test-bed.

Both types of test described above required real-time driver input in the form of accelerator, brake and clutch pedal position, as well as gear selection. These could be provided either by a human driver, or by the system computer using a suitable control algorithm. In the case of a human driver, the appropriate input devices had to be made available and integrated with the system. For the system under computer control, suitable control algorithms were investigated for possible implementation.

2.4. SYSTEM INTEGRATION AND STRUCTURING

With suitable vehicle models determined, and the virtual vehicle simulation engine and testing subsystems developed, these components had to be integrated into a computer programme. The structuring of the programme, especially the real-time element thereof, would require a great deal of attention to ensure the timely execution of data handling and

manipulation routines. Requirements of the programme were quite extensive, and will be discussed in more detail in Section 3.1. The objective here was to make sure that the programme was well structured and optimised for the task at hand. Aspects such as graphical feedback and system robustness required particular attention. Due to the real-time nature of the application, it was important for it to work from an accurate time-base.

3. FUNCTIONAL ANALYSIS

Blanchard et al. (1998) describes functional analysis as the process of translating system requirements into detailed design criteria, along with the identification of specific resource requirements at the subsystem level and below. One starts with an abstraction of the needs of the customer and works down to identify the requirements for hardware, software, facilities, data, or combinations thereof. The initial step in this process results in the definition of system requirements. Functional analysis actually begins with the initial identification of the "functions" that the proposed system is to accomplish. A function refers to specific or discrete action that is necessary to achieve a given objective, the objective being to specify the "whats" and not the "hows" (i.e. *what* is needed to be accomplished versus *how* it should be done). Functional analysis is the iterative process of breaking down, or decomposing, requirements from the system level to the subsystem level, and as far down the hierarchical structure as necessary to identify specific resources and components of the system.

3.1. REQUIREMENTS ANALYSIS

The following operating requirements were identified as the first step in the process of the functional analysis:

3.1.1.) Setup of cycle, vehicle, engine and driver configurations.

- Each setup should consist of either opening an existing setup from file, the editing of an existing file, or the creation of a new file.

- Cycle files allow for the setting up of one of two modes. Firstly, a vehicle speed profile (km/h vs. time), which in turn creates the need to enter profile node-points and to interpolate between them to produce demand values at every time instance (*cycle-mode*). Cycle editing aspects that need to be addressed include node-point insertion, deletion, and modification.

A mode must be allowed for that enables the driver to operate the system in *free-style* mode as will be used for the execution of acceleration runs. Further allowance must also be made for specifying:

- cycle description
- the gear in which the vehicle operates at each point during the cycle,
- tolerance settings for the current cycle,
- the number of cycles to be repeated.
- idle time before starting with the first cycle.

- Vehicle setup should allow for the setup of a "virtual vehicle" including all parameters required for the simulation of relevant vehicle dynamics. These include:
  - vehicle description
  - gear ratios
  - clutch characteristics
  - vehicle mass
  - drag coefficient
  - drive-train efficiency
  - maximum braking torque
  - frontal area
  - air density
  - tyre specifications
  - effective vehicle inertia at wheels
  - rolling resistance coefficients

- Engine setup must allow for:
  - engine description
  - engine inertia

- maximum engine speed
- idle speed

- Driver setup should allow for:
  - driver description
  - gear shifting mode – whether gear shifting occurs automatically at a specified speed (during acceleration runs) or manually as selected by the driver.
  - acceleration run shifting speeds – speeds at which gear changes are effected are entered for each gear.
  - up and down-shift times are entered for each shift combination – this determines how long it takes before the clutch starts re-engaging following a shift.

3.1.2.) Signal acquisition and condition

- Torque and speed signals need to be acquired from the test-bed during engine testing. These signals generally have a lot of noise superimposed on them due to electro-magnetic interference and need to be filtered before use. Also, since the signals are digitised, anti-aliasing filtering needs to be performed to prevent signal aliasing during the digitising process. In addition, the torque read from the load-cell is not equal to that at the flywheel during transient operation due to the inertial effects of the dynamometer. This discrepancy needs to be accounted for on-line before the corrected torque signal can be used in the vehicle model.

- Driver input in the form of accelerator, brake, clutch pedal positions and gear selection need to be read, filtered and manipulated.

3.1.3.) Running of cycles

- The system must have the ability to run cycles, whether the throttle is controlled by a human operator or computer algorithm. Cycles that are controlled by humans receive input from a set of pedals operated by a driver, whether he is trying to follow a specific cycle (*cycle-mode*), to perform an acceleration run or just arbitrarily "driving"

around (*free-style* mode). During computer controlled cycles (cycle mode) a control algorithm is used to determine what throttle position is required to drive the virtual vehicle to within specified tolerance limits. Possible control strategies will be further investigated in Section 9. Both of these cycle modes require a similar software "engine" to operate and co-ordinate the various processes needed to achieve the required results.

3.1.4.) Simulation of "virtual vehicle" dynamics in real-time

- During the running of any cycle, real-time vehicle simulation is performed by the computer. This simulation should have as input:
  - torque currently developed by the engine [Nm]
  - current engine speed [rpm]
  - brake pedal position [%]
  - clutch position and [%]
  - selected gear [ ]
  - accelerator position [%]
  - demanded vehicle speed (if running a specific cycle) [km/h]

- Using this data, the simulation program calculates the response of the virtual vehicle to the torque currently being developed by the engine, and also the way in which the engine would have accelerated if it were in the vehicle (coupled to the wheels via the transmission). Outputs of the simulation are then:
  - engine speed demand [rpm]
  - vehicle speed [km/h]
  - corrected engine torque [Nm]
  - clutch speed [rpm]
  - clutch torque [Nm]
  - aerodynamic drag force [N]
  - rolling resistance [Nm]

3.1.5.) Real-time graphical representation of pertinent information

- It is necessary that some of the more pertinent information be displayed graphically while cycles are being run. This is especially important when humanly controlled cycles are run, since feedback is necessary to control the vehicle speed to any degree of accuracy. During pull-away it is very useful to graphically witness what the clutch speed is doing since the usual feedback one has in a vehicle, i.e. acceleration, is not available under these simulated circumstances.

- Various methods of displaying other important parameters are needed to provide researchers with the necessary information needed to successfully operate the system. These displays should be user configurable and may include any combination of the following:

  - engine speed [rpm]
  - engine speed demand [rpm]
  - clutch speed [rpm]
  - clutch torque [Nm]
  - vehicle speed [km/h]
  - vehicle speed demand [km/h]
  - vehicle speed demand tolerance bands [km/h]
  - engine torque [Nm]
  - aerodynamic drag [N]
  - rolling resistance [Nm]
  - accelerator pedal position [%]
  - brake pedal position [%]
  - clutch pedal position [%]
  - selected gear [ ]

3.1.6.) Recording, analysis and presentation of data

- In order to extract meaningful data from the system it is necessary to record all test data and store it in a format that it is easily understandable and presentable. For analytical purposes, data should be in a spreadsheet compatible format (easily exportable) and time-stamped. The necessary systems must be in place to ensure that data is properly dealt with, since the system is of no use if the data is not available in the correct format.

3.2. FUNCTIONAL BLOCK DIAGRAMS

Given the identified needs of the system, it is necessary to translate this information into meaningful design criteria. This translation task constitutes an iterative process of breaking down system-level requirements into successive levels of detail, which is determined by system complexity. The objective is to progressively and systematically work down to the level where resource can be identified with *how* a task should be accomplished. A convenient mechanism for communicating this information is by using *functional flow diagrams.* APPENDIX A contains a series of functional block diagrams describing the Centre for Automotive Engineering (CAE) system, along with tables describing the contents of individual block elements. This diagrammatic approach to the functional breakdown of the system served as a useful mechanism in the structuring and integration of the computer programme.

4. OPERATING PRINCIPLES

As has been mentioned, the dynamic test-bed is a very versatile testing facility. Apart from its more specialised uses as a dynamic engine testing facility, it can also perform more traditional steady-state engine testing. Although these modes of testing share many common characteristics, they also differ substantially in some ways. This section will discuss and define the different modes of engine testing used most frequently, as well as the operating principles involved in each. Also to be discussed will be the operating principles of the system that has been developed at CAE.

4.1. STEADY-STATE ENGINE TESTING

Steady-state engine testing is probably the most often-used method for testing engines, and can provide engineers with a large amount of useful information. It is typically used to measure such engine characteristics as torque, fuel consumption, emissions and other parameters at constant engine speed and load conditions. These conditions are adequately representative of those experienced by a vehicle driven on a road at constant speed and are therefore frequently used to conduct durability tests. Water or Eddy-current absorption dynamometers have traditionally been used for this purpose, since they can provide adequately stable loads at constant speeds, while the electronics necessary for regenerative, variable speed driving of electric motors have only become available fairly recently.

During steady-state testing control is based on set values, meaning that fixed load and speeds points are approached and maintained for extended periods of time. Here it is required of the control electronics of the system to maintain these set values of speed and torque by using some sort of closed-loop feedback. Actual engine speed and torque values are compared with demanded values and the errors between these values used to initiate corrective action. The most often used type of controller is the PID controller in which the corrective action consists of a proportional, an integral and a derivative element of the error signal. This type of control works well for steady-state testing, but often lacks the stability and accuracy required for the control of time-varying, multi-input systems. The situation is worsened in the event of non-linear systems, as is the case for internal

combustion engines. Possible control strategies for such cases will be discussed in Section 9. A diagram of a typical steady-state engine test-bed setup is illustrated in Figure 4.1.

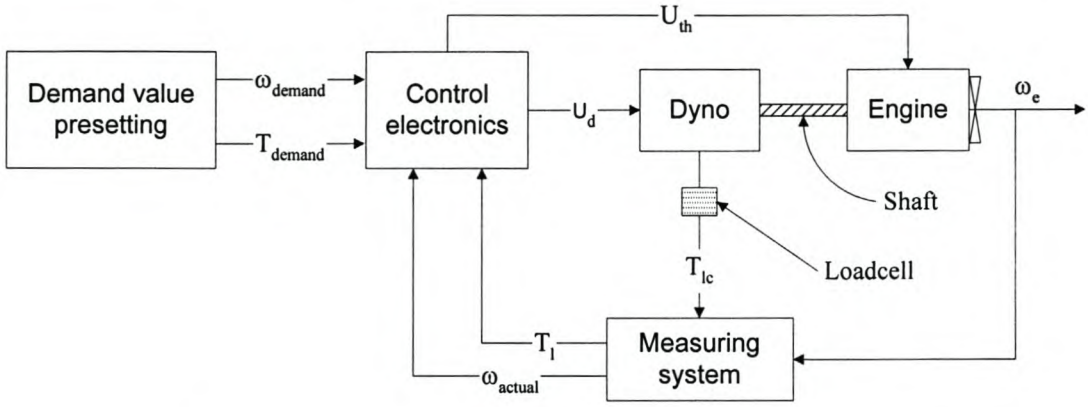

Figure 4.1. Steady-state engine test-bed setup

4.2. DYNAMIC ENGINE TESTING

Dynamic engine testing has become increasingly important in the development and testing of internal combustion engines. In contrast with steady-state test-beds, where command variables are kept constant for longer periods of time, they are changed on a continuous basis during dynamic engine testing. This involves more than a continual change of engine speed and torque as required by many durability tests, but also requires the inclusion of a vehicle model for the generation of engine speed and torque demand values. Depending on whether this model is run beforehand or in real-time, the distinction is made by Voos (1992) between a *simulation test stand* and a *transient test stand* respectively (see Figure 4.2).

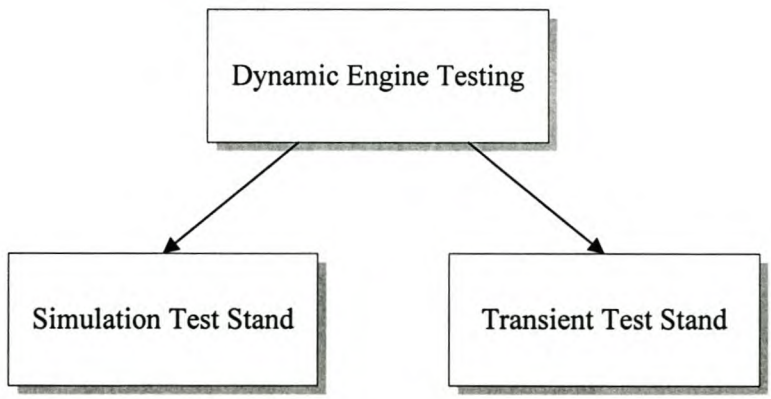

Figure 4.2. Types of dynamic engine test stands

4.2.1. Simulation Test Stand (Off-line tests)

If command values are not directly preset, but are determined prior to testing, one speaks of a simulation test stand. In this case, reference values are determined off-line in one of the following ways:

1. From measurements taken in an actual vehicle: in this case the parameters of vehicle speed, accelerator pedal position and gear selected are recorded while the vehicle is being driven on the road. This data is then used in reconstructing conditions on the engine test-bed similar to those experienced on the road.

2. As computational results from an off-line computer where both the vehicle and the engine are simulated by mathematical models. Here a model of the complete vehicle power-train system (engine and drive-line) is used to compute reference values of engine speed and throttle position required to simulate road conditions (see Figure 4.3).

3. From tables established for engine certification purposes. This method is based on steady-state engine performance predictions and/or experiments. They are normally termed *"transient-reconstruction"* or *"quasi-stationary"* methods because they reconstruct the transient performance from steady-state engine performance maps to emulate the real transient operation (Hong, 1996). One such a steady-state map of engine torque as a function of throttle position and engine speed is shown in Figure 4.4.

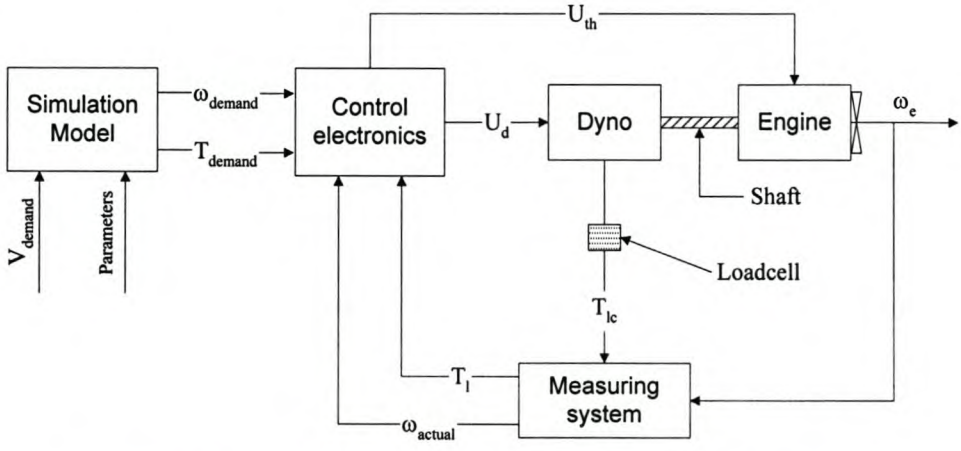

Figure 4.3. Simulation engine test-bed operational diagram.

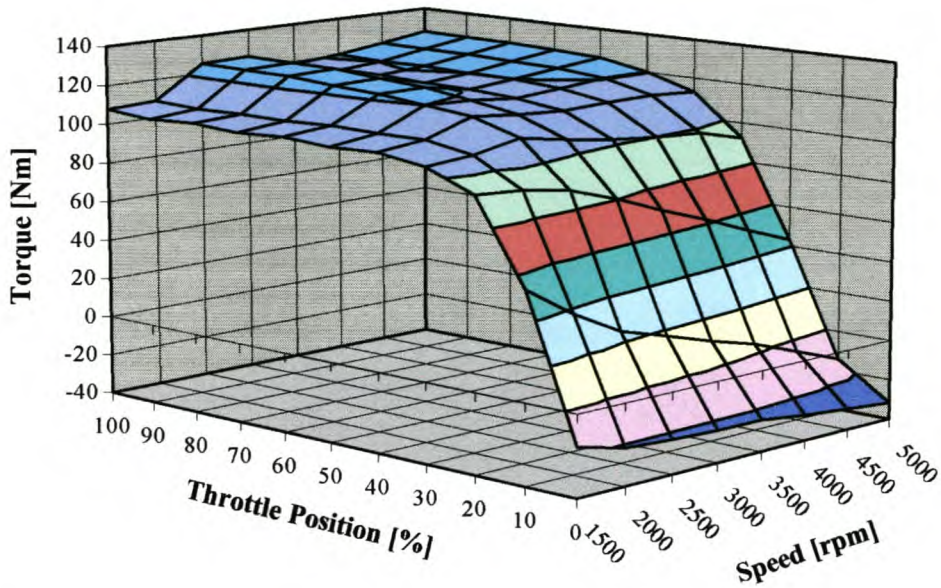

Figure 4.4. Steady-state torque map of a Toyota 4A-FE, 1600i engine (Conradie, 1995)

Von Thun (1987) points out that off-line tests tend to show significant errors with regard to the correct dynamic loading of the engine being tested. The main reason is the absence of modelling the dynamic characteristics of the thermal power engine, such as transient effects during acceleration and deceleration. These effects are due mainly to three reasons, namely, flow inertia, thermal inertia and mechanical inertia (Hong, 1996).

Flow inertia has to be considered since sudden throttle changes during transient runs do not bring enough gas flow into the cylinder due to flow lag. This is normally termed "throttle lag" and occurs in most spark ignition engines. Heat transfer plays an important role in engine power prediction, as is evident by the loss of almost one third of the power developed in the cylinder. This occurs mainly through heat transfer, which is a function of the heat convection coefficient, the heat transfer area, and the temperature difference between the combustion gas and the cylinder walls. The wall temperature increment during transient runs is influenced by the *thermal inertia* which can be derived from an energy balance at the cylinder wall boundary. The third important factor is the *mechanical inertia* of the rotating parts inside the power-train system. These can either be measured or calculated from their geometry and need to be taken into account for the correct transient simulation of engine performance.

4.2.2. Transient Test Stand (On-line tests)

In the case of command values being generated in *real-time* by a "driver", whether it be in the form of a human or computer, and a suitable vehicle simulation model, the test-bed is referred to as a *transient test-bed.* These command values will include throttle, brake and clutch-pedal position, as well as the currently selected gear ratio. Under the control of a human driver, these command values are obtained externally from a "Driver Box" (Figure 4.5), whereas they are available internally when generated by computer. Possible control strategies will be discussed in Section 9.

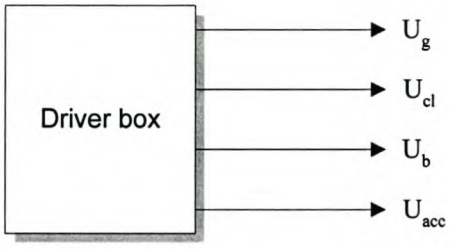

Figure 4.5. Driver box for command value generation during transient engine testing

The following discussion refers to Figure 4.6 in which the general operating principles of the transient engine test-bed are illustrated.

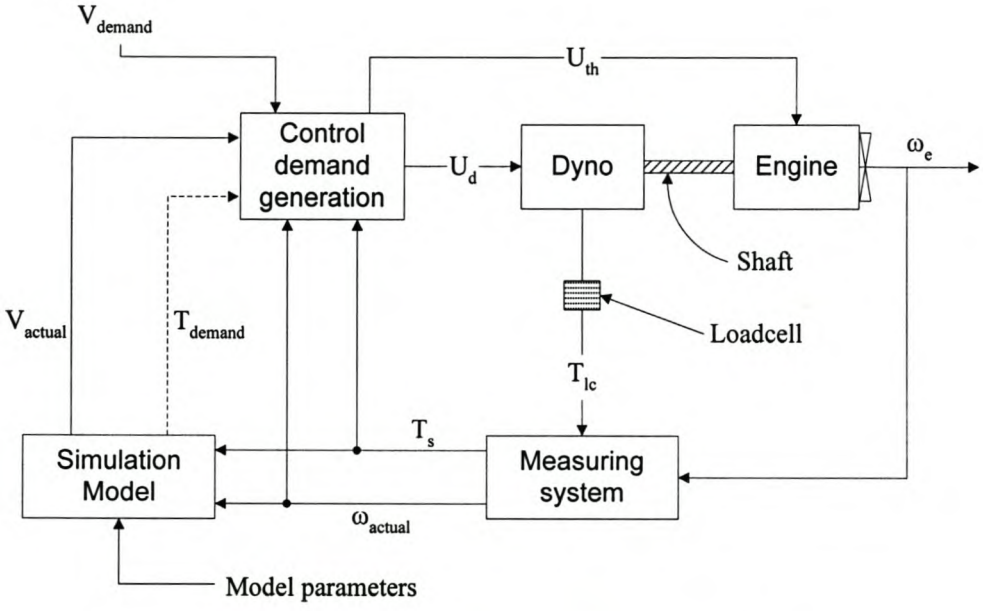

Figure 4.6. Transient test-bed operational diagram

In the above setup, load-cell torque and engine speed are acquired by the measuring system. This subsection of the system may include a torque correction component that estimates true shaft torque after dynamometer inertia has been accounted for, while filtering components may be used in order to eliminate unwanted signal noise and frequency content. The measuring system thus has as output actual shaft torque and engine speed. These test-bed variables, together with model parameters specific to the type of vehicle being simulated, then serve as input to the simulation model.

The objective of the simulation model is to make use of the current input variables and parameters to solve the equations governing vehicle dynamics. This is performed each time the cycle is executed, yielding as output simulated vehicle speed, and possibly engine torque (for multi-input multi-output (MIMO) control) required to attain the demanded vehicle speed at the next time step. These two outputs, together with the current engine speed, shaft torque and vehicle speed demand, constitute the input to the control demand generation subsystem, where throttle and dynamometer command settings originate. These demand values can either be calculated using a control algorithm, or by a human driver using the driver's box to input pedal and gear selection information in trying to follow the demanded vehicle speed.

The above discussion pertains to the essential operating principles of a transient engine test-bed as described by Voos (1992). In the following section the operating principles of the CAE engine test-bed will be discussed in terms of its major functional units, as were discussed in Section 3.

4.2.3. The CAE Test Stand

Before discussing the operating principles of the CAE engine test-bed, it is necessary to briefly consider the principles of *causal* and *non-causal* systems. Causality can simply be described as the direction of cause and effect. In mathematical terms, it is the direction of the transport of variables between subsystems in a system. Consider the test-bed configuration illustrated in Figure 4.7, representing the *conventional model* employed for vehicle simulation on an engine test-bed. In this model, vehicle speed is prescribed to exactly follow a function of time. Such a system is quasi-transient, in that the transient behaviour of the system is not fully accounted for. The direction of cause and effect is

unnatural, and in the field of mechanics such an unnatural causality is sometimes referred to as *inverse dynamics* (Jacobson, 1995).

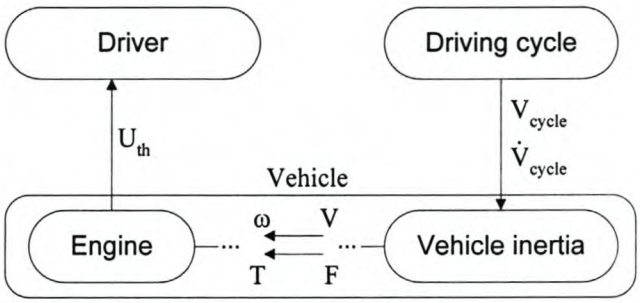

Figure 4.7. Conventional model (unnatural causality)

In contrast to this configuration, is that illustrated in Figure 4.8, which represents a *driver controlled model* having *natural causality*. In this configuration the only signal from the driver is the accelerator pedal position. However, a driver-controlled model is the most suitable platform to introduce other driver signals, such as gear selection, brake and clutch pedal, etc., all of which have natural causality from the driver to the vehicle. The "driver" here should be understood to be either a human driver or a computer control system, and acts as a regulator of the vehicle speed. It is advisable to model with natural causality since unique solutions to the equations governing the dynamics of the system will probably exist, and transient analysis will be a straightforward method required to find them. The need for more accurate simulations and studies on new driveline concepts call for transient driving cycle analysis and modelling. The CAE engine test-bed is such a system.

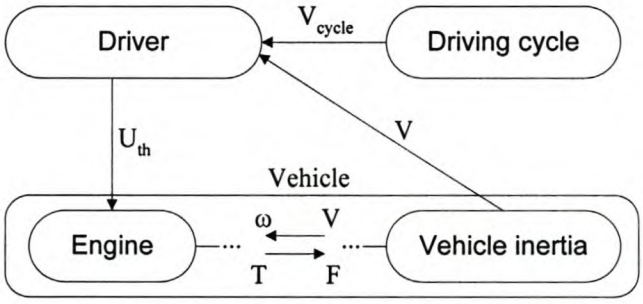

Figure 4.8. Driver controlled model (natural causality)

A diagram of the CAE engine test-bed is shown in Figure 4.9. The operating principles are very similar to those described in the previous section, and will now be discussed in more

detail. Dynamometer reaction-torque readings are acquired using a load-cell connected to the dynamometer frame, while speed readings are obtained using a tachometer connected to the free end of the dynamometer from where signals are fed to the Siemens Variable Speed Drive (VSD) for speed control purposes. For this system the shaft between dynamometer and engine was assumed to be rigid, engine and dynamometer speeds thus being equal.

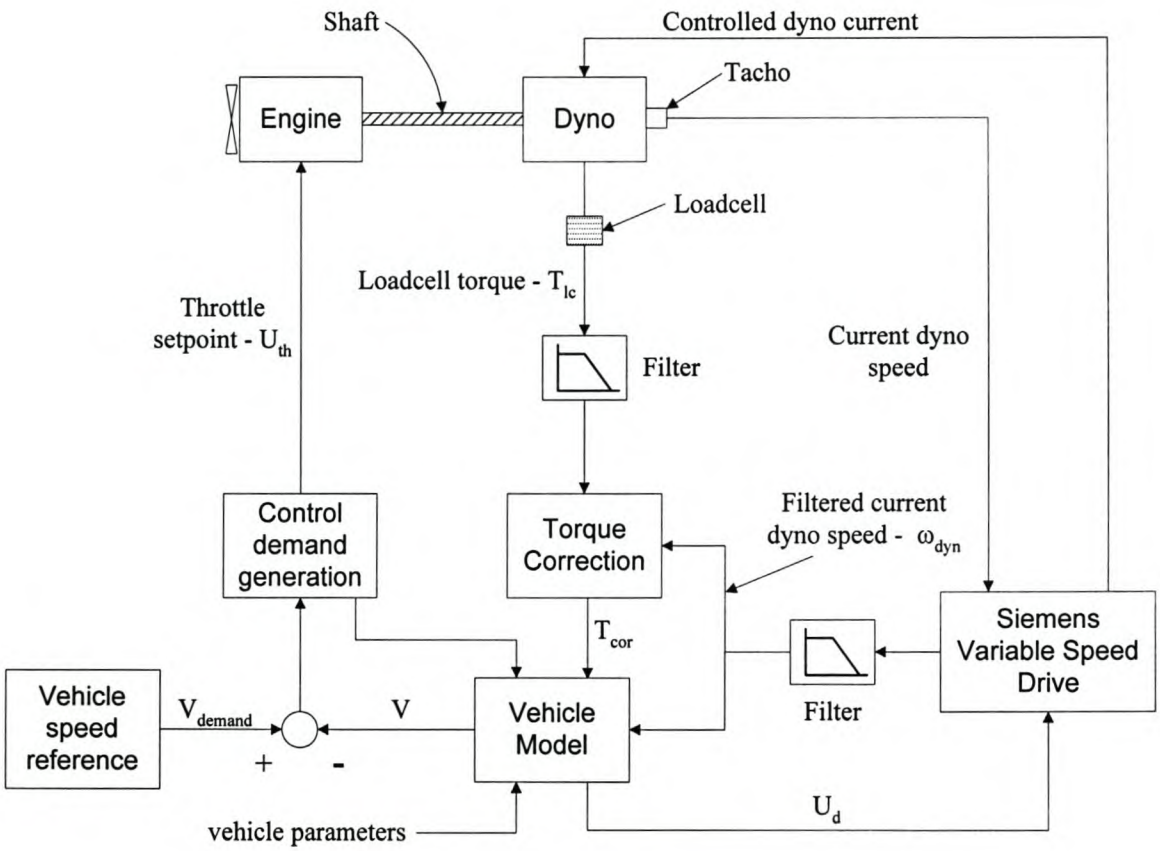

Figure 4.9. CAE engine test-bed operational diagram

From the load-cell and VSD, signals are filtered through anti-aliasing filters before being sampled by the system computer. Filtered torque and speed signals are utilised by the torque correction subsystem to correct for the inertia reaction effect the dynamometer has on the torque signal, yielding a corrected engine flywheel torque signal. This system is fully described later in Section 7. Corrected engine torque and speed signals are fed to the vehicle model, together with the vehicle parameters and selected gear ratio necessary to solve for the vehicle dynamics equations. The vehicle model has two outputs, namely that of the engine and vehicle speed. Engine speed is fed to the Siemens VSD where is serves

as a speed demand reference for the next time step. Simulated vehicle speed together with demanded vehicle speed for the current time step are fed to the control demand generation subsystem. Here the control demands of throttle, brake and clutch position, as well as gear ratio are generated. This is achieved either by a human driver or a computer control algorithm using feedback of actual vehicle speed referenced against the vehicle speed profile demanded by the currently selected simulation cycle.

5. TEST SYSTEM COMPONENTS

The dynamic engine test facility consists of several integrated components. Some of the components were available in the laboratory, some were acquired as *commercial off-the-shelf* (COTS) items, while others were designed and manufactured locally. Individual system components will now be discussed and their functional requirements and specifications identified.

5.1. REGENERATIVE DYNAMOMETER

At the heart of the dynamic engine test facility is the regenerative dynamometer. As was described in Section 2, the dynamometer, or loading unit, must be capable of both absorbing power from, and delivering power to, the engine. This allows for the loading and motoring of engines, thereby providing accurate vehicle simulation capabilities under all conditions. From this point onwards, the term *dynamometer*, refers to the electric motor as well as the variable speed drive (VSD) used for realising speed control.

5.1.1. Electric Motor Specifications and Configuration

The system under discussion consists of a direct current electric motor and a thyristor-controlled variable-speed drive. The speed of a DC motor is approximately proportional to the armature voltage and inversely proportional to the magnetic flux. The torque developed is proportional to the product of the armature current and the flux per pole (Hughes, 1987). By controlling these variables, the speed and torque of the DC motor can be manipulated, a necessity when dynamic engine testing is to be performed. Speed and torque control will be further discussed in the following section. Specifications of the DC motor used (Blocher-Motor KG Metzingen Type GNG 2800034) are summarised in Table 5.1.

Table 5.1. DC-motor specifications

Mode	Power [kW]	Speed [rpm]	Anchor Voltage [V]	Anchor Current [A]	Excitation Voltage [V]	Excitation Current [A]
Motor	154	5500	400	380	90	1.3
Generator	160	5500	400	380	95	1.4

The engine/dynamometer setup is illustrated in Figure 5.1.

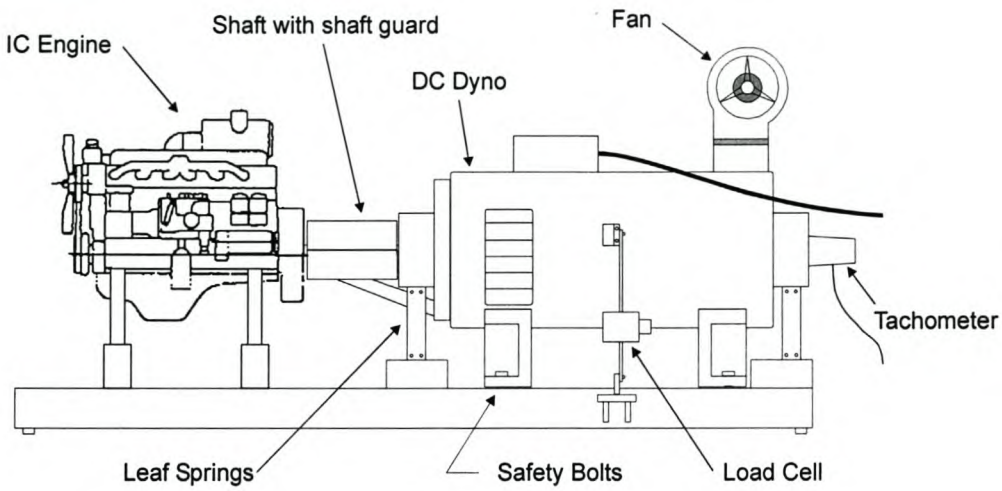

Figure 5.1. DC Dynamometer/Engine setup

The DC motor is mounted on four leaf springs which, if extended, would intersect at the motor axis and therefore do not apply any moment to the motor frame. This configuration ensures that any reaction torque on the motor frame will be sensed by the load cell which is connected between the frame and the test-bed. Safety bolts guard against the motor separating from the test-bed should one or more of the leaf springs fail. An electric motor drives a fan that provides cooling air for the motor brushes. Dynamometer speed is determined using a tachometer that provides a voltage proportional to the rotation speed according to the formula:

$$V_{tacho} = \frac{240.N}{5500} \quad [V] \tag{5.1}$$

This voltage is fed back to the variable-speed drive where it is used in the speed control loop.

5.1.2. DC Dynamometer Inertia

It was seen in Section 3 that a correction has to be made to the torque measurement received from the load-cell during dynamic conditions. This is necessary since the substantial inertia of the dynamometer has to be overcome when accelerated by the engine, requiring a certain amount of torque. When the system decelerates, the dynamometer

tends to keep rotating *(Newton's first law)* and torque is again required to overcome this inertia. What is read at the load-cell is thus not at all representative of the load on the engine during dynamic conditions. The following simple equation was developed to correct for this effect.

$$T_l = T_{lc} + J_d \alpha_d \tag{5.2}$$

From equation (5.2) it is seen that the inertia and acceleration of the dynamometer has to be known in order to correctly determine the true load torque. Tests performed on the dynamometer to determine its inertia were based on *Newton's second law* as it applies to rotating bodies.

$$T_{lc} = J_d \alpha_d \tag{5.3}$$

In order to measure dynamometer inertia the load cell was calibrated, then by controlling the speed of the dynamometer (with the engine now disconnected), known accelerations were realised, while reaction torques were measured at the load-cell. Triangular speed functions were demanded, starting from standstill. This would require constant torque values which could be averaged and, using equation (5.3), the inertia of the dynamometer can be calculated. The periods and amplitudes of the input functions were varied to determine whether the results obtained would remain the same.

A set of results of one of these tests is shown in Figure 5.2. It is immediately apparent how noisy the unfiltered torque signal was. This was due to noise on the signal line and resonances in various parts of the system. Two prominent occurrences of resonance were seen at approximately 120 and 170 rad/s, corresponding to 1145 rpm and 1625 rpm respectively.

Looking at Figure 5.2, one can see that the dynamometer speed was indeed very accurately controlled by the Siemens VSD. A closer look at the transition points shows how the controller over-compensates when changing between acceleration and deceleration. A slight curve can be seen in the speed line, coinciding with an overshooting of the reaction torque.

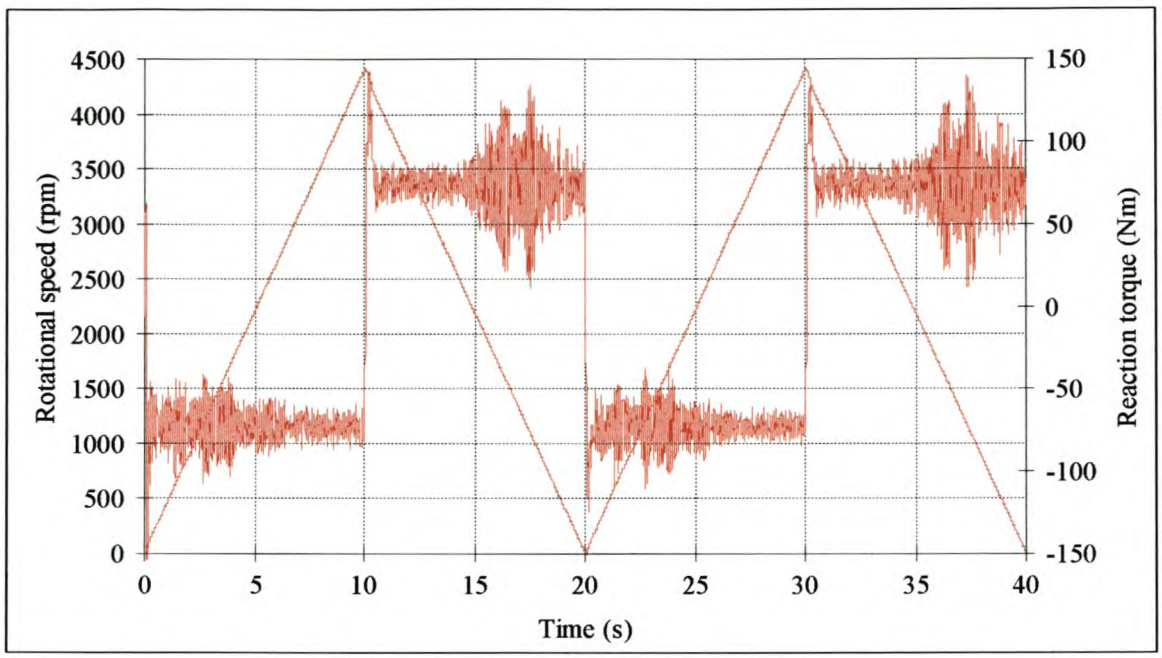

Figure 5.2. Dynamometer inertia test

Figure 5.3 shows a close-up of the first 10 seconds of the test.

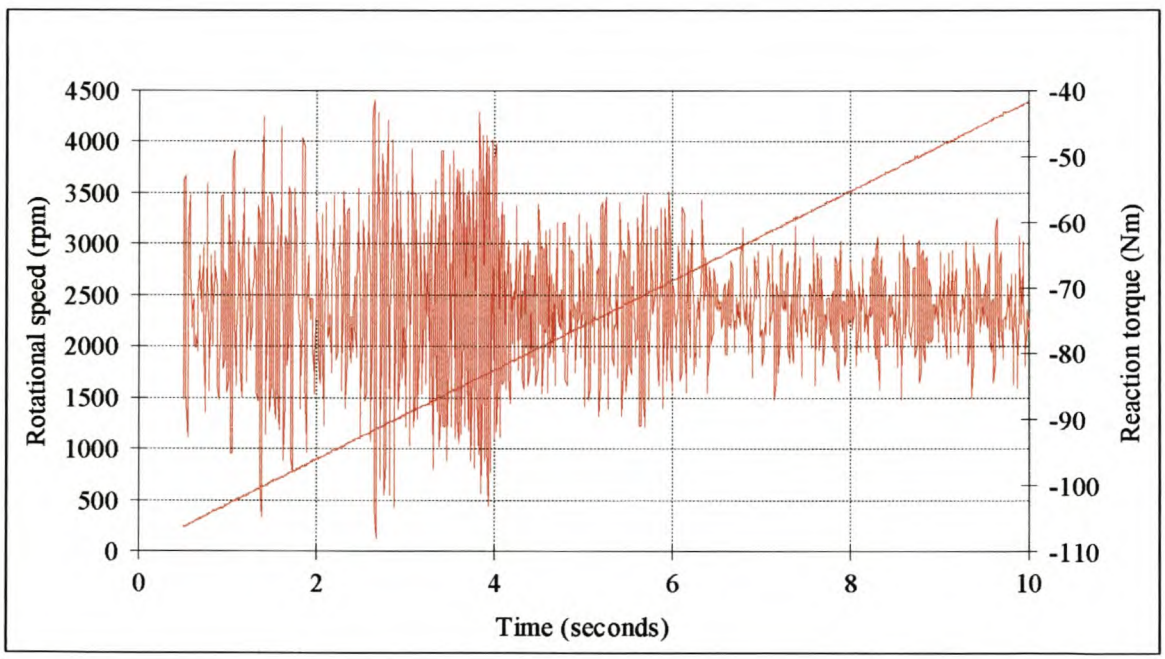

Figure 5.3. Dynamometer inertia test (enlarged)

A regression was performed on the speed curve of the dynamometer, the slope of the line yielding the acceleration. A block average was taken of torque values. The first 0.5

seconds of speed and torque data for each acceleration was disregarded because of excess "noise" caused by over-correction applied by the control software. Table 5.2 shows the results obtained during four tests, the speed functions having periods of 20, 50, 20 and 40 seconds respectively.

Table 5.2. Dynamometer inertia test results

α_d (rad/s^2)	T_{lc} (Nm)	J_d (kgm^2)	J_{ave} (kgm^2)
45.891	-72.991	-1.591	
-45.878	73.767	-1.608	
45.920	-73.204	-1.594	
-45.898	73.746	-1.607	**-1.600**
18.368	-28.911	-1.574	
-18.362	29.828	-1.624	**-1.599**
45.918	-72.858	-1.587	
-45.908	74.164	-1.615	
45.892	-73.065	-1.592	
-45.918	73.882	-1.609	**-1.601**
22.958	-36.410	-1.586	
-22.954	37.052	-1.614	**-1.600**

It is seen that the reaction torque was higher during deceleration. This was probably due to an inaccurate zero-point of the torque calibration. An average was taken over the four tests, yielding an inertia of **1.600 kgm^2** and a standard deviation of 0.014 kgm^2. This value was used in further development of the system.

5.2. VARIABLE-SPEED DRIVE SPECIFICATIONS AND OPERATING PRINCIPLES

As was discussed in Section 4.2, accurate speed control of the electric motor under transient operating conditions is a crucial aspect of the system. It is this quality that gives it the ability to perform dynamic engine testing, setting the facility apart from other types of engine testing.

5.2.1. Specifications

Speed control of the dynamometer was achieved by a Siemens (type Simoreg K) DC variable-speed drive (Siemens AG, 1993). This drive is fully regenerative, meaning that any absorbed power is conditioned and returned to the electricity supply network, thus

acting as a generating facility. This has major electricity saving advantages and obviates the need to dispose of waste heat. Table 5.3 lists some of the more important technical specifications of the drive.

Table 5.3. Technical specifications for Siemens variable-speed DC drive

Order no.		6RA2481-6DV62
Rated voltage/output	[V]	3-ph. AC 400 (+15% / -20%)
Rated supply voltage, field	[V]	2-ph. AC400 (+15% / -20%)
Rated DC voltage	[V]	420
Rated DC current	[A]	400
Overload capability	[%]	max. 150% rated DC current
Rated output	[kW]	168
Power loss at rated current	[W]	1250
Rated DC voltage, field	[V]	max. 325
Rated DC current, field	[A]	25
Control stability	[%]	$\Delta n = 0.1\%$ of the rated speed

The drive is extensively configurable with various parameters that can be set. Some of the parameters used in the development of the system included:

(1) System current limits

This parameter limits the current that can be delivered to the motor, and can be adjusted from 0.0 to 300.0 % of the rated motor armature current (380 A) in steps of 0.1%. Both positive and negative limits can be individually set. This feature is intended to protect the motor from overheating or burning out.

The drive is capable of exceeding the rated converter current (equal to the maximum permissible continuous DC current) during operation. The absolute value and duration of the overload are limited and will be briefly discussed. An absolute upper limit for the absolute overload current is 150 % of the rated converter current. The duration of overload is determined by the overload current characteristic as well as the overload condition prior to this. A reduced loading phase must always precede the overload condition (phase with load current less than rated converter current). When the maximum permissible overload duration has expired, the load current must be reduced to a value less than or equal to the rated converter current.

Dynamic overload is made possible by thermal monitoring (I^2t monitoring) of the power section. The I^2t monitoring system calculates the theoretical temperature rise of the thyristor junction layer above ambient from the load current value characteristics (over time). The I^2t monitoring responds if the calculated equivalent junction layer temperature rise exceeds the permissible value by (a) raising an alarm with reduction of the armature current set-point to the rated converter current, and (b) giving a fault with converter trip.

For maximum dynamometer response during transients such as gear change simulation, the current limit was set to 150 % of the rated converter current. Dynamometer response characteristics will be discussed in Section 5.3.1.

(2) Maximum motor torque

This parameter limits the current delivered to the motor in such a way as to restrict the maximum torque that can be exerted by the motor. It can be adjusted from 0.0 to 300.0 % of the rated motor torque in steps of 0.1%. It can also be set for both positive and negative torque directions and is again intended as a protection feature. It must be remembered that this type of drive is used mainly in industrial environments where current and torque limiting for protection purposes is often used.

A setting of 150 % of the rated motor torque was used to ensure good transient response of the dynamometer.

(3) Ramp-up (down) times

This parameter sets the time it takes the motor to accelerate from standstill to its maximum rated speed. The armature current will thus be limited in such a way as to prevent the motor from accelerating faster than the set value. If the current/torque limits are set such that the ramp-up (down) rate can not be attained, the motor will accelerate at a rate as permitted by the lowest limit.

There are three ramp-rate settings available on the drive of which two were set for the system. Ramp-rate #1 was set to 10 seconds, i.e. about 550 rpm/s, and used during start-up and shut-down when higher rates were not required. Ramp-rate #2

was set to 0 seconds, i.e. the maximum acceleration allowed as limited by parameter settings (1) and (2). Either setting could be selected via a binary switch activated by the control computer.

(4) Analogue input/output selection and conditioning

The drive allows for three analogue inputs besides the main speed set-point and speed actual value. These are all configurable in terms of gain, range and offset, while filtering of incoming variables is also possible. The main speed set-point was obtained from the simulation computer at intervals of 50 ms, while actual speed was obtained from the tachometer.

There are also four similarly configurable analogue outputs that can make available any parameter available within the control unit with a resolution of 11 bits. The actual dynamometer speed was output on one of these channels for use in the simulation computer.

In Section 5.1.1 it was mentioned that it is necessary to be able to control the armature voltage, current and flux in order to control the speed and torque of the dynamometer. Although transistors can be used as switches, their current capacity is generally quite small. There are many applications in which it would be advantageous to have a high-speed switch that could handle up to 1000A. The thyristor is such a device, which also has the advantage of no moving parts and no arcing.

5.2.2. The Thyristor

A thyristor is essentially an on/off switch used to switch high capacity (up to 1000A) alternating-current supplies. A 2000 V, 300 A device would typically be a silicon wafer with a diameter of 30 mm and thickness 0.7 mm (Lander, 1987). In essence, the thyristor consists of four layers of alternating P-type and N-type silicon semiconductors, forming three P-N junctions, with a third terminal, the *gate*, as shown in Figure 5.4.

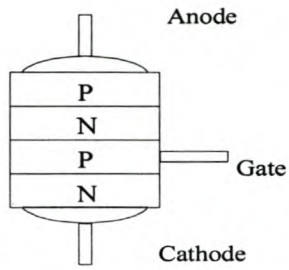

Figure 5.4. Thyristor structure

In the off state, conduction is prevented in either direction with the thyristor effectively acting as three diodes in a back-to-back configuration. Characteristics of the thyristor in this state, without any external connection to the gate, are shown in Figure 5.5.

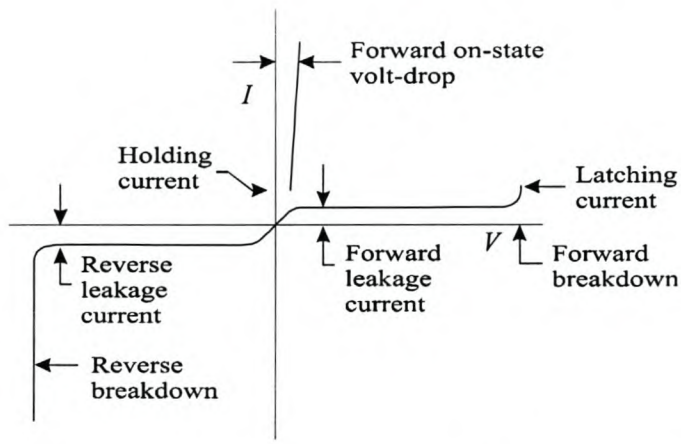

Figure 5.5. Thyristor characteristics with no gate current

The reverse characteristics of the thyristor, that is, with the cathode positive, exhibit similar features to the diode. The forward characteristic, with the anode positive, exhibits no current flow except leakage until the *break-over voltage* of the centre control junction is exceeded. Forward and reverse break-over voltages are similar in magnitude. Once break-over in the forward direction has occurred, the centre P slice is neutralised by electrons from the cathode, and the device acts as a conducting diode having two junctions giving a forward voltage drop approximately double that of the diode. For the thyristor to retain the on-state, the anode current must reach its *latching level*, and not fall below its *holding level*, as shown in Figure 5.6.

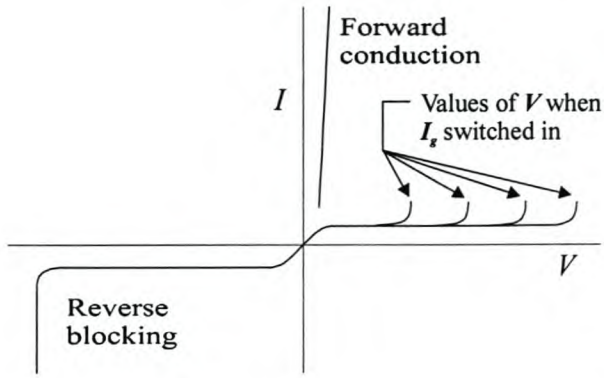

Figure 5.6. Thyristor characteristics with gate current

The latching current is typically double that of the holding current, both being much less that 1% of the full-load rated value. For instance, the holding current may be about 10 mA for a thyristor having a forward-current rating of 40 A (Hughes, 1987). A forward biased thyristor (anode positive), can be switched to the on-state by injecting current into the gate terminal by means of a firing circuit. This has the effect of injecting holes into the inner P slice, which, together with the electrons form the cathode N layer, break over the centre control junction, switching the thyristor into the on-state. Once the anode current has exceeded the latching level, the gate current can cease and the thyristor remains in the on-state, irrespective of conditions in the gate circuit.

To turn on the thyristor in the shortest possible time, it is desirable to have a gate current with a fast rise time. This is best achieved using pulse techniques in which the firing circuit generates a fast pulse of sufficient length to allow the anode current enough time to reach its latching value. The advantage of using this pulsing technique is that much less power is dissipated in the gate compared with continuous currents, and the instant of firing can be accurately timed. In A.C. applications it is essential that the thyristor be turned on at time a related to the A.C. supply voltage phase. The phase of the firing pulse in relation to the A.C. supply voltage zero must also be capable of variation. Practical commercial firing circuits will typically deliver pulses with a rise time of 1 μs from a voltage source of 10 V, capable of delivering 1 A. Pulse lengths of 10 μs with a rise of 2 V in 1 μs may suffice for many applications, whereas others may require lengths of up to 100 μs. By varying the instant at which the thyristor is triggered, it is possible to vary the thyristors duty cycle, thereby effective controlling the current over a wide range (Lander, 1987).

To turn off conduction in the forward direction (also known as commutation), the forward-current must be reduced to below the holding level. A relatively long time must be allowed to elapse for the thyristor control junction to recover its blocking state, before a forward voltage can again be applied without conduction. The thyristor described above is that which was first developed, and can be referred to as the conventional thyristor. More recent developments have introduced the *gate turn-off thyristor* which can be turned off by removal of current from the gate, unlike the conventional thyristor which can only be turned off by reduction of its anode current to near zero (Lander, 1987). In practise the device is turned off by injecting a negative signal into the gate. It will remain off until the conditions of a positive anode and gate with respect to the cathode are met.

5.3. DYNAMOMETER SPECIFICATIONS

Dynamometers have to comply with certain requirements if they are to be used for the purposes of dynamic engine testing. Two characteristics that are of special interest are:

- the dynamometer *control response*
- the parameters of *mass ratio* and *speed gradient*

5.3.1. Control Response

Control response is one of the more important parameters of a dynamic engine dynamometer. It is this parameter that determines how fast and with what degree of accuracy the dynamometer can follow demanded speed or torque values. The faster the dynamometer response, the better the degree with which vehicle behaviour can be simulated.

Control response can be determined by measuring the dynamometer response to a sinusoidal pre-setting of the command value. This response will also be sinusoidal, with amplitude and phase deviations being functions of the input frequency. This deviation is determined by a number of factors, namely (1) power-to-mass ratio of the electric motor, (2) power capacity of the variable-speed drive, and (3) control characteristics of the drive. These control responses are termed *amplitude frequency response* and *phase response*. The parameter describing the amplitude frequency response is the *cut-off frequency*, at

which point the actual response value is 70.7% (-3 dB) of the excitation amplitude (see Section 7.2). In general, the parameter used when looking at the phase response is the frequency at which the phase displacement is –90° (Voos, 1992). Cut-off frequency is often considered an important factor when judging the capabilities of a dynamic loading unit. This is especially the case with the assumption being made that the unit should be capable of simulating vehicle drive-line dynamics.

Cut-off frequency is, however, not the only factor to be considered. Since the engine and dynamometer are connected via a shaft, vibrations emanating from either side have to be transmitted via the dynamometer shaft. This shaft is inevitably flexible in nature and therefore acts as a mechanical filter, only transmitting frequencies below its natural frequency. Shaft dimensions on test stands are generally restricted by space considerations, while engines initiate vibrations particular to their type and construction. Speeds at which these shaft/engine combinations become resonant are referred to as "torsion-critical speed". At these speeds damage to the test stand and/or engine may occur, and operating the test stand within these speed ranges should be avoided at all cost. This requires that the dynamometer shaft must be designed such that its torsion-critical speed is well below the idling speed for the particular engine. For a 4-cylinder four-stroke engine (2 excitations by ignition per revolution) idling at 600 rpm, this cut-off frequency is 20 Hz and for a 6-cylinder four-stroke engine (3 excitations by ignition per revolution), 30 Hz.

In this way the shaft connecting the engine and dynamometer further limits the frequency range within which the dynamometer is allowed to be operated safely, without encountering resonance problems. Investigations carried out by Voos (1992). have shown that the natural mode shapes of the simplified models used for representing different vehicles are always very similar. The first of these modal shapes lies in the frequency range from 3–9 Hz depending on the gear selected. In this case the engine oscillates against the vehicle and the entire vehicle shows the characteristics of a 2-mass oscillator. This is called "Jerk-vibration". With the second mode shape, the vibration occurs on the wheel drive-shafts or the wheel respectively. These modes appear in the frequency range from 30-40 Hz. Two further mode shapes are defined and occur in the frequency range from 50-80 Hz and 120-180 Hz respectively. These frequencies can no longer be seen, but only heard. The implication of this is that only the first natural shape can be simulated during the driveline simulation before running into possible resonance problems. This

observation compares well with that of Shafai and Geering (1989) in which they suggest good load torque matching in the frequency range from 0 – 60 rad/s (0 to ±10 Hz). The frequencies involved can be attained by most modern dynamic loading units. Already the second natural shape with frequencies in the range from 30-40 Hz cannot be simulated.

A comparison between three common dynamometer systems was made by Voos (1992). The systems tested were:

- DC machine with belt drive (Schenck type GSR)
- Hydrostatic unit with 1-step gearbox (Schenck type HSE)
- Directly coupled asynchronous machine (Schenck type DYNAS) also referred to herein as an AC dynamometer.

The control responses of the DC and asynchronous machines, (i.e. the parameters of rise time and settling time) were found to be about identical. The hydrostatic unit was a little inferior. The DC machine offered significant advantages regarding reference frequency, i.e. the parameters of cut-off frequency and frequency at a phase displacement of –90°. Hydrostatic units and asynchronous machines were about identical. Control responses of DC-, AC-machine and a Hydrostatic unit can be seen in Figure 5.7. The asynchronous machine does well on all characteristics and features a simpler mechanical design compared to DC machines and hydrostatic units. Its price-performance ratio is also more favourable than those of the other two units.

The dynamometer available to the CAE was tested to judge its control response. This would give an idea of the extent to which vehicle simulations could be performed. Since the dynamometer was used in speed-control mode, sinusoidal speed signals of increasing frequency were generated and fed to the dynamometer as speed demands. Data gathered during one such a test is shown in Figure 5.8, in which the nominal speed was 5000 rpm with oscillation amplitude of 400 rpm.

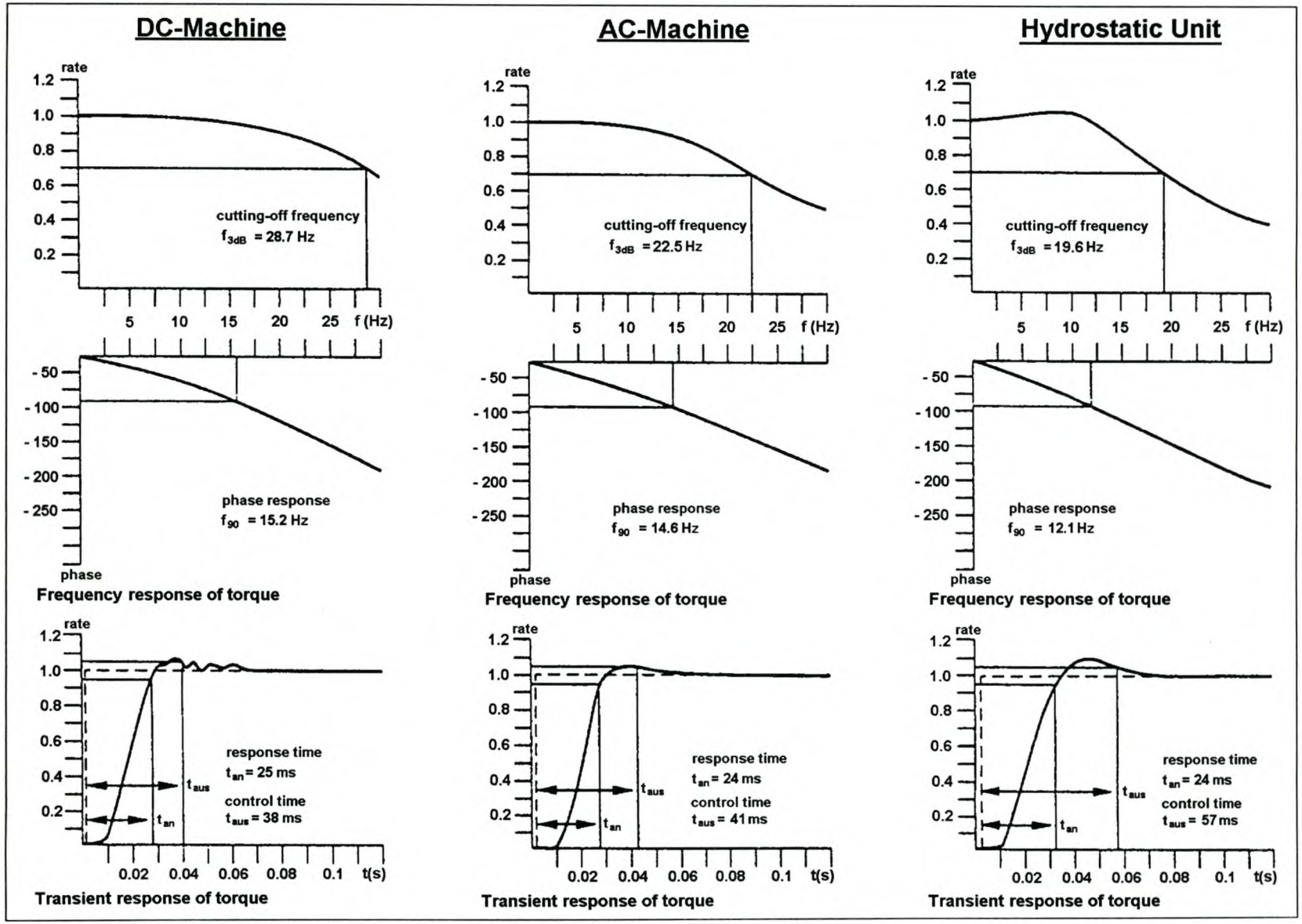

Figure 5.7. Control response of DC-, AC-machine and Hydrostatic unit (Voos, 1992)

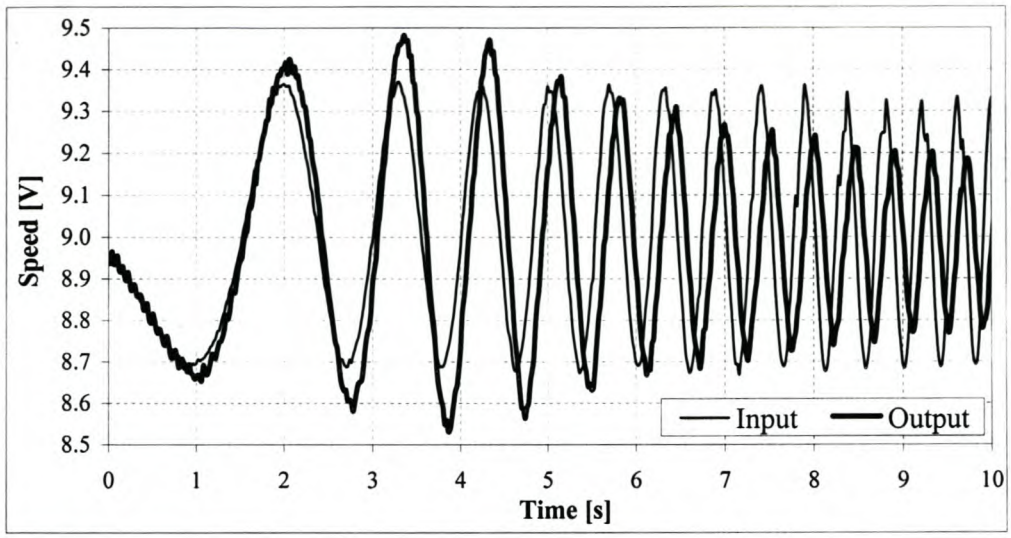

Figure 5.8. Data gathered during dynamometer bandwidth determination

Actual speed output was recorded and Fast Fourier Transforms performed on both signals. The frequency at which the magnitude of the output signal was 3 dB less than that of the input signal was taken to be the cut-off frequency for that specific test. Figure 5.9 shows such a Fourier Transform performed on the data presented in Figure 5.8. The cut-off frequency for this particular case can be seen to be about 2.15 Hz.

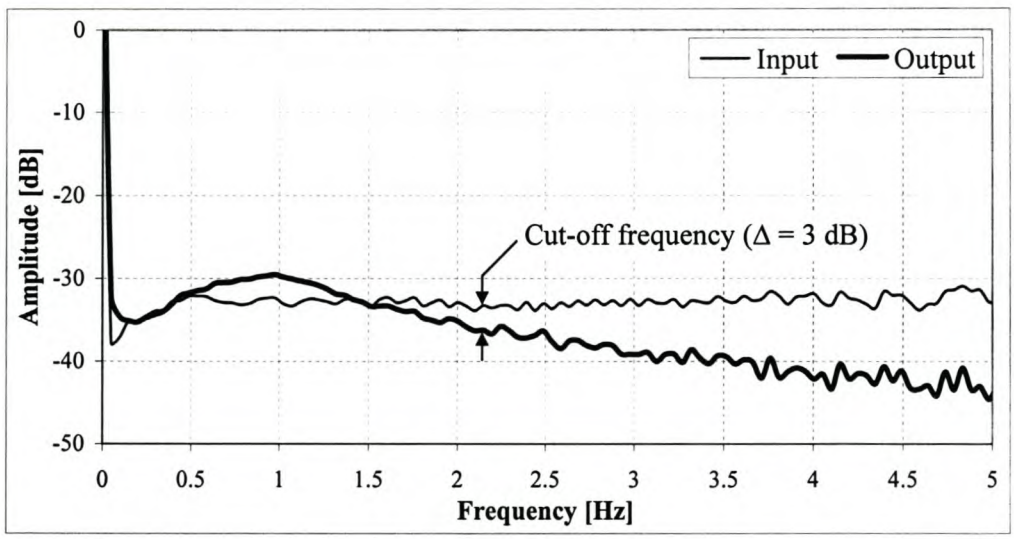

Figure 5.9. Fourier transform of gathered bandwidth data

Various tests were performed during which both the nominal dynamometer speed and amplitude of the input sinusoids were varied, since both these parameters influence the

bandwidth. At lower speeds, torque is the limiting factor, whereas maximum power limits the bandwidth at higher speeds. A matrix of dynamometer operating conditions were tested, as shown in Table 5.4, with shaded areas indicating the combinations that were tested.

Table 5.4. Dynamometer operating conditions tested for bandwidth

Nominal Speed [rpm]	Amplitude [rpm]											
	50	**100**	**150**	**200**	**250**	**300**	**350**	**400**	**450**	**500**	**750**	**1000**
500	5.08	4.89	5.06	5.11	5.03	4.79	4.32	-	-	-	-	-
1000	5.07	5.10	5.15	5.13	4.79	4.70	4.45	4.14	4.11	3.45	2.30	-
1500	5.30	4.79	5.11	4.93	5.08	4.75	4.24	4.38	3.57	3.49	-	1.74
2000	4.99	4.97	5.27	5.33	4.91	4.74	4.30	4.20	3.33	3.50		-
2500	5.06	4.83	5.01	5.06	5.23	4.60	4.36	3.96	3.30	3.59	-	-
3000	4.13	4.14	4.60	4.27	4.17	3.87	3.83	3.49	3.16	2.93	1.88	1.45
3500	3.65	3.95	3.52	3.74	3.81	3.35	3.06	2.71	2.40	2.36	-	-
4000	3.07	3.29	3.44	3.32	3.26	2.89	2.80	2.37	2.30	2.13	-	-
4500	2.99	2.94	3.13	2.90	2.97	2.69	2.36	2.42	1.88	2.02	1.21	0.92
5000	2.71	2.96	2.69	2.76	2.93	2.59	2.17	2.11	1.86	1.77	-	-

Results of these tests are shown in Figure 5.10. Here it is clearly seen that a maximum bandwidth of about 5.30 Hz is obtained for small oscillations at low speeds. At these lower speeds the dynamometer momentum is overcome more easily, resulting in the ability to follow higher speed demand frequencies.

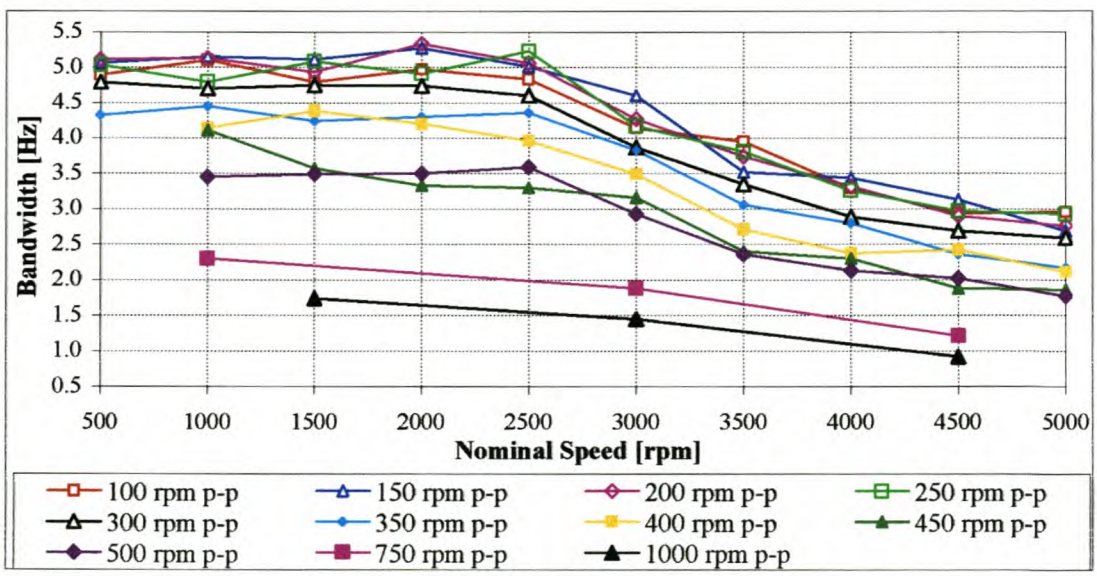

Figure 5.10. Dynamometer bandwidth test results

As the dynamometer speed increases its kinetic energy increases at a rate that is proportional to the square of its rotational speed and more power is required to bring about speed changes than for equivalent changes at lower speeds. This fact is illustrated in the following example in which the power required to effect two equal dynamometer speed changes is calculated. In both cases an increase of 500 rpm is achieved starting at 4000 rpm and 4500 rpm respectively. The following energy equations apply:

$$\Delta KE = \frac{1}{2} J\left(\omega_2{}^2 - \omega_1{}^2\right) \tag{5.4}$$

$$\text{Power (P)} = \frac{\Delta KE}{\Delta t} \tag{5.5}$$

For the first acceleration from 4000 rpm to 4500 rpm (using J = 1.600 kgm^2)

$$\Delta KE = \frac{1}{2} \cdot 1.600 \left(\left(\frac{4500 \cdot 2\pi}{60} \right)^2 - \left(\frac{4000 \cdot 2\pi}{60} \right)^2 \right)$$
$$= 37\,285 \text{ J}$$

$$\therefore P = \frac{37\,285 \text{ J}}{1 \text{ s}}$$
$$= 37.285 \text{ kW}$$

For the second acceleration from 4500 rpm to 5000 rpm (using J = 1.600 kgm^2)

$$\Delta KE = \frac{1}{2} \cdot 1.600 \left(\left(\frac{5000 \cdot 2\pi}{60} \right)^2 - \left(\frac{4500 \cdot 2\pi}{60} \right)^2 \right)$$
$$= 41\,672 \text{ J}$$

$$\therefore P = \frac{41\,672 \text{ J}}{1 \text{ s}}$$
$$= 41.672 \text{ kW}$$

Since the drive can only deliver a limited amount of power (Power [W] = Torque [Nm] x Speed [rad/s]), the torque drops off at higher speeds, resulting in slower response. Also, as the input amplitude was increased, the dynamometer had to follow a broader speed range, resulting in a smaller bandwidth. Thus, trying to follow an amplitude of 1000 rpm superimposed over a nominal speed of 4500 rpm resulted in a bandwidth of a mere 0.92 Hz.

The above tests indicated that maximum frequencies, at low dynamometer speeds and oscillation amplitudes of below approximately 5 Hz, could faithfully be followed. This is considerably less than figures quoted by Shafai and Geering (1989), meaning that, based solely on an analysis of the control response of the dynamometer, not all vehicle dynamics could be expected to be reproduced accurately by the system. Other factors to be considered were those of mass ratio and speed gradient.

5.3.2. Mass ratio and Speed gradient

The *mass-ratio* is defined as the ratio of moments of inertia:

$$\mu = \frac{J_d}{J_e} \tag{5.6}$$

This parameter is an indication of the need for *over-dimensioning* of the unit. Over-dimensioning is associated with the power-to-inertia ratio of the unit. The bigger the mass-ratio the more the unit has to be over-dimensioned. This becomes important when gear changes with a "hard" clutch must be simulated. During these transients the dynamometer shaft torque required to simulate such a situation could typically be double the maximum engine output torque. This means that a loading unit with a mass-ratio of μ=1 must produce three times the torque of the engine to enable the simulation of such gear transitions. The conditions become even more unfavourable with a higher mass ratio.

For the system under discussion the mass-ratio is worked out using a standard 2ℓ spark-ignition engine (rotational inertia of 0.23 kgm^2 used for illustrative purposes) as reference, and a load unit inertia of 1.60 kgm^2 (see Section 5.1.2):

$$\mu = \frac{1.60}{0.23} = 6.96$$

Speed-gradient is the third important characteristic of the dynamometer and is defined as

$$\dot{N} = \frac{dN}{dt} \tag{5.7}$$

This property indicates the maximum possible speed gradient that the dynamometer can achieve, which is important for the simulation of an "open clutch" situation as is the case

during gear changes. During this period, zero torque must be simulated by the system and the dynamometer must overcome its own inertia by following the engine speed as it would drop during gear shifts in a vehicle. This is clearly a desirable dynamometer characteristic if gear changes and other fast transients are to be realistically simulated. Gallacher et al. (1995) refer to typical ramp-rate requirements of up to 4000 rpm/s for dynamic engine test beds for transient testing, and a controlled speed ramp capability of 10 000 rpm/s for use with dynamic test-beds for vehicle simulation.

Of the three systems tested by Voos (1992), the superiority of the hydrostatic loading unit regarding mass ratio and speed gradient can clearly be seen in Table 5.5.

Table 5.5. Mass Ratio and Speed Gradient of Hydrostatic-, DC-, and AC unit

	Hydrostatic Unit	DC Machine	AC Machine
μ	0.16*	1.39*	1.96*
$\dot{N}$	12000	10800	8000

(* figures related to a common 2ℓ spark-ignition engine with $J_e = 0.23$ kgm^2)

Tests were performed on the CAE system to determine the ramp-rate capabilities of the dynamometer (disconnected from the engine). With the maximum current and torque limits set at 150% (as used during operation), step responses were recorded and maximum ramp-rates calculated. One such test result is shown in Figure 5.11. Here it is seen that an average maximum ramp-rate of between 4700 rpm/s and 4825 rpm/s was measured. These rates are seen at lower dynamometer speed due to torque and power limitations as explained previously. A definite change in ramp-rate can be seen at a speed of approximately 3500 rpm due to the power limitation of the VSD.

Comparing the CAE system with those tested by Voos (1992), it is evident that it is not that well-suited for the dynamic engine testing of smaller sized engines. The system's excessive inertia is its major draw-back, as this negatively influences its mass-ratio and maximum ramp-rate capability, preventing it from simulating higher frequency vehicle dynamics.

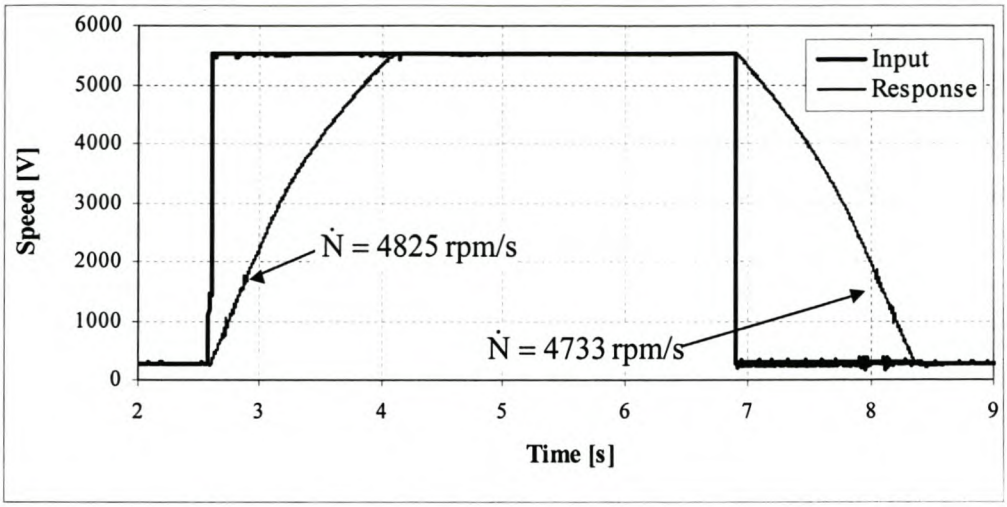

Figure 5.11. Dynamometer ramp-rate test result

5.4. TRANSDUCERS AND ACTUATORS

The transient engine test-bed used a number of transducers and actuators for obtaining signals from, and conveying signals to the system. Figure 5.12 summarises the input and output signals to and from the test-bed.

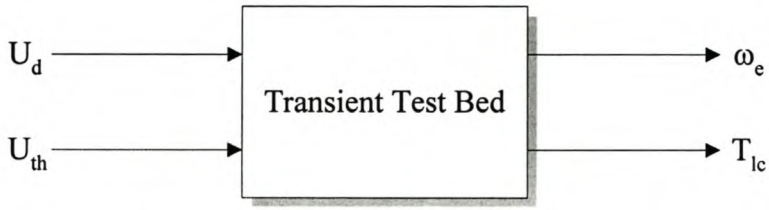

Figure 5.12. Input and output signal from the test-bed

5.4.1. Throttle Actuator

Engine torque was controlled by manipulating the engine's throttle valve (petrol engines) or the governor demand lever (diesel engines). This was realised by converting the driver throttle input (see Section 5.4.3), after the necessary scaling, to a pressure set-point by means of a current-to-pressure (I-P) converter. A pneumatically-controlled actuator then used this set-point to move the throttle/rack to the required position.

5.4.2. Load-Cell and Bridge Amplifier

Engine torque could not be measured directly on the load shaft, but had to be calculated from torque measurements obtained from a load-cell connected to the frame of the electric motor (see Section 5.1.2). The load-cell was used to measure the force with which the motor frame reacted to torque developed by the armature. By calibrating the load-cell reading using the known length of the calibration arm and calibrated masses, measured torque was amplified using a bridge amplifier unit before being filtered through an anti-aliasing filter and sampled by the simulation computer.

5.4.3. Driver Input System

As was discussed in Section 3.1, input could be obtained from a human driver in order to drive the "virtual" vehicle. These inputs consisted of the normal variables as manipulated by a driver in a true vehicle, namely, throttle pedal, brake pedal, clutch pedal and gear selection input. The driver input system consisted of three pedals connected to potentiometers, each providing a 0 to 10 Volt output. These signals were read by the data acquisition card and subsequently used by the simulation computer. Gear selection controls were based on the *"Tip-tronic"* style gearbox. Three buttons provided the driver with the ability to change up one gear, change down one gear, or select neutral. These systems are described further in Section 8, *Software Development.*

5.5. DATA PROCESSING SYSTEMS

Throughout the system, data was constantly being acquired and manipulated. The quality of these signals and the means by which they were processed were important considerations and will now be discussed.

5.5.1. Data Acquisition and Digital Cards

A number of signals were transferred to and from the simulation computer. These are illustrated in Figure 5.13. These signal were transferred using an Eagle Electronics PC30GA data acquisition board, while additional timing functions were performed using a PC14B digital board , both of which were acquired as COTS items.

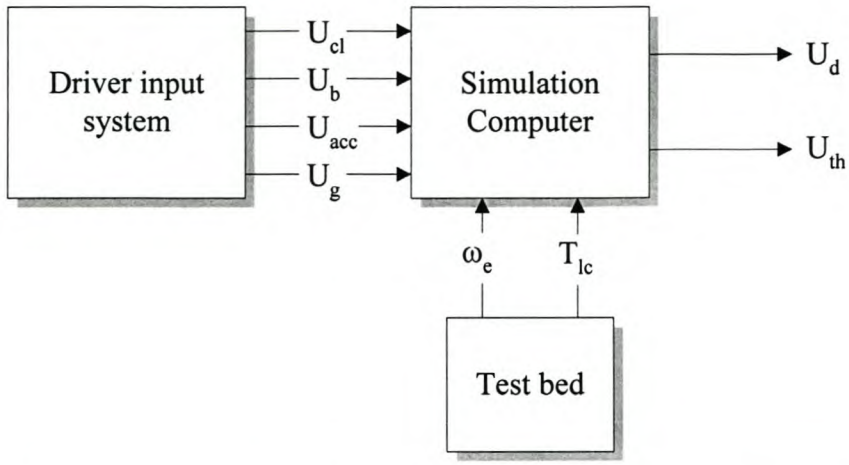

Figure 5.13. Input and output signal from the simulation computer

5.5.1.1 Description of the PC30GA data acquisition card

The PC30GA board is an enhanced data acquisition board utilising advanced design techniques such as surface-mount technology and high-density logic (FPGA). Such advanced techniques allow higher performance to be accomplished with fewer components, reducing the cost and increasing the reliability of the board. Because all features are under software control, the number of control jumpers has been dramatically reduced relative to earlier models (American Eagle Technology, 1995).

This card was used to read all voltage inputs, while the D/A subsystem was used to output throttle and dynamometer speed demands. The remaining timer/counter was used for timing of the simulation, as is discussed fully in Section 8.2. Some features of the PC30GA card used are given below, while technical specifications can be found in APPENDIX B.

5.5.1.2 Features of the PC30GA

- 12-bit A/D with 16 single-ended or 8 differential input channels.
- 100 kHz A/D sample rate.
- Extensive use of surface mount devices to reduce RF noise and maintain EMC compatibility.
- FPGA design reduces component count, increases reliability.

- Complex noise-control circuitry gives accuracies to ± 1 count
- 16-bit AT-bus interface
- Hardware channel scanning
- 16-Sample FIFO buffers
- Block-mode triggering
- 4 D/A channels: 2 @ 8 bits and 2 @ 12 bits with programmable gain.
- 24 programmable digital I/O lines.
- User-available counter/timer to measure frequency/period.
- Complete software support package.

5.5.1.3 Description of the PC14B digital board

The PC14B digital board is equipped with 48 digital lines and on-board counter/timers. The board has a higher speed version of the 8255 PPI, an advanced 8254 timer/counter, wait states, and external interrupts. It can be used as an event counter, to generate a one-shot pulse, as a rate generator, event timer, strobe, frequency generator, clock divisor, periodic interrupt, etc. A full list of technical specifications can be found in APPENDIX B.

5.5.1.4 Features of the PC14B

- Two 8255 PPI's providing the card with 48 digital lines.
- Advanced 8254 C/T providing three 2MHz clock/counters.
- Clock source for each timer is programmable to 1 of 4 sources.
- On-board 2MHz reference oscillator.
- The PC I/O clock divided by either 4 or 64
- Any external clock source with a max frequency of 8MHz.
- Complete software support package.

5.5.2. Anti-Aliasing Filter

The Anti-Aliasing Filter is a filter employed for the specific purpose of eliminating aliased data in a sampled system. This piece of equipment was designed and built at the Electrical & Electronics Engineering faculty by "Sentrale Elektroniese Dienste" (SED) using Burr-

Brown Universal Active Filters (Burr Brown Corporation, 1993). The design of and theory behind the filter will be discussed in full in Section 7.

5.5.3. System Control Computer

A large part of the dynamic engine test-bed consists of the control computer where the vehicle simulation is performed. It is here where all signals come together to be manipulated, and where signals are generated for controlling the test-bed. The computer has to be fast enough so that real-time data manipulation, graphics, and input/output can be performed, without falling behind on computations. Having a fast enough computer also means that one can perform all tasks using one machine. It is also desirable to run the simulation programme within a Windows environment as there are numerous advantages, including:

- multi-tasking of programmes
- inherent data transfer compatibility between programmes
- networking capabilities
- user-friendly interface

With this in mind, the following configuration was chosen for the control computer:

- Processor: Intel Pentium II – 350 MHz
- RAM: 128 MBytes
- Hard drive: 4 Gbytes
- Operating System: Windows NT 4.0

6. VEHICLE MODELLING AND SIMULATION

The aim of the dynamic engine testing facility is to simulate engine conditions as they are experienced on the road. In order to do this, it was necessary to develop a vehicle-dynamics model to calculate relevant road loads and how they are experienced by the engine. Forces impinging on the vehicle together with moments of inertia to be taken into consideration are illustrated in Figure 6.1. Components of this model will now be discussed individually and then synthesised into a complete vehicle dynamics model.

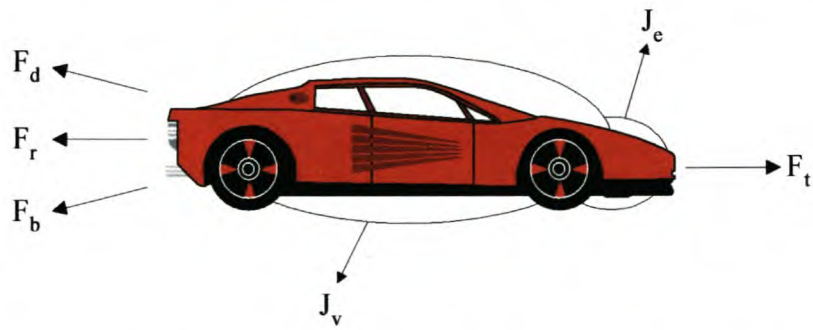

Figure 6.1. Forces and inertias pertaining to vehicle model

6.1. ENGINE INERTIA

In order to correctly simulate the dynamic aspects of the vehicle to which tested engines have to "think" they are connected, it was important to pay attention to such detail as gear changes and engine behaviour during these transient phases in the driving cycle. It will be shown later that it was necessary to know the engine inertia before the equations governing these dynamic events could be solved.

Similar tests to those performed during dynamometer inertia determination were performed in order to determine engine inertia. Again, triangular speed demands were output to the dynamometer while measuring the reaction torque on the load-cell. In this case, however, the inertia calculated would be the combined inertia of both the dynamometer and the engine connected to it. Engine inertia could then be determined by subtracting the dynamometer inertia, calculated previously. Engine friction also had to be considered and accounted for during these tests. As a result of internal engine friction, torque required by

the dynamometer to follow the demanded acceleration would be higher than when spinning a hypothetical frictionless engine, whereas it would be less during deceleration. Since only the torque needed to overcome engine inertia was required, the frictional torque had to be subtracted from the torque read at the load-cell. It was thus necessary to perform a friction test before an engine inertia test could be conducted.

A friction test was performed on a Toyota 4A-FE engine. The test consisted of running the engine warm (until all temperatures had reached operating levels) and then measuring reaction torque at the load-cell at different engine speeds with the ignition off. Results obtained during this test can be seen in Table 6.1.

Table 6.1. Engine speed versus frictional torque

Speed (rpm)	T_f (Nm)
1500	-19.298
2500	-22.136
3500	-24.850
4500	-28.508

A graph of the results, on which a second order regression was performed, is shown in Figure 6.2.

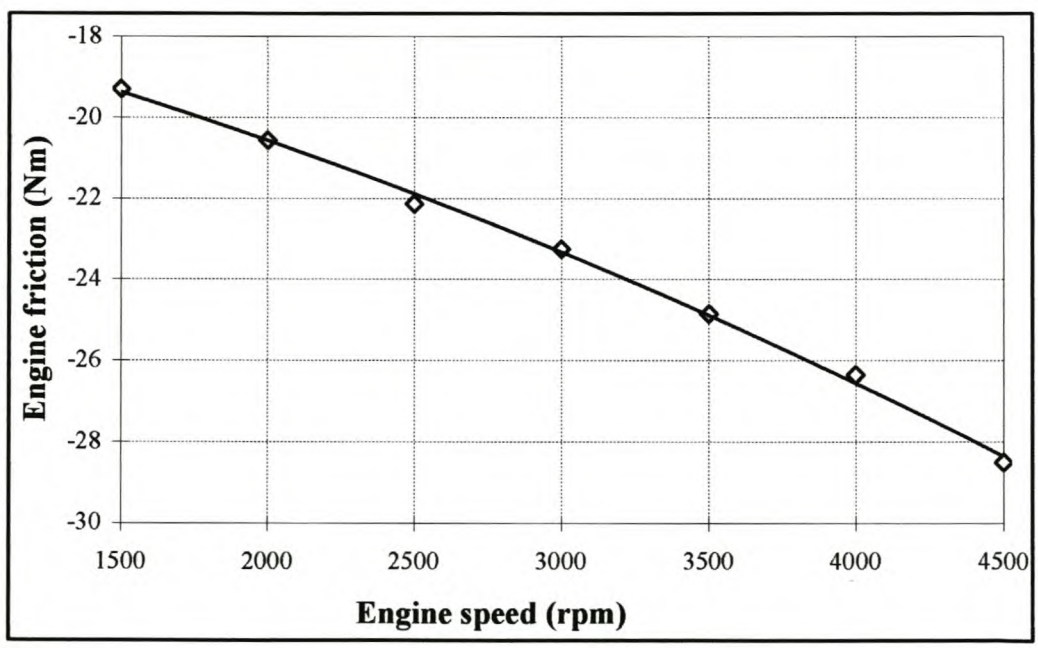

Figure 6.2. Engine speed versus friction

Figure 6.3 shows the results of one of the engine inertia tests performed. The period of the speed function was 20 seconds and the speed was varied between 2100 and 3200 rpm.

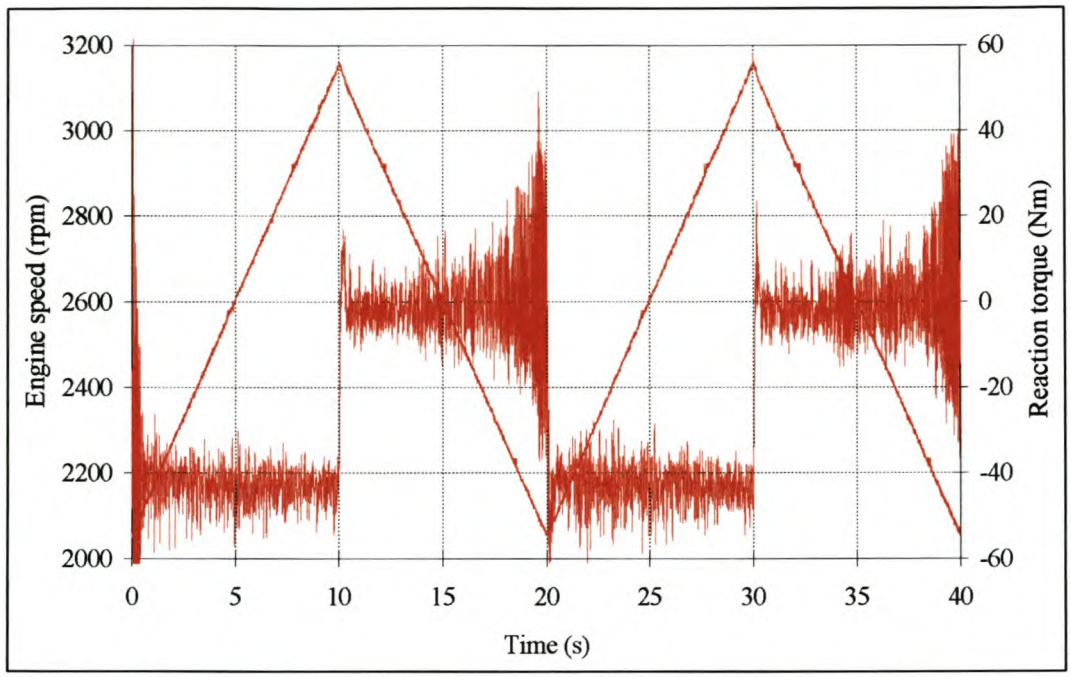

Figure 6.3. Engine inertia test result

An expansion of the first 10 seconds of the test is shown in Figure 6.4 for explanation purposes.

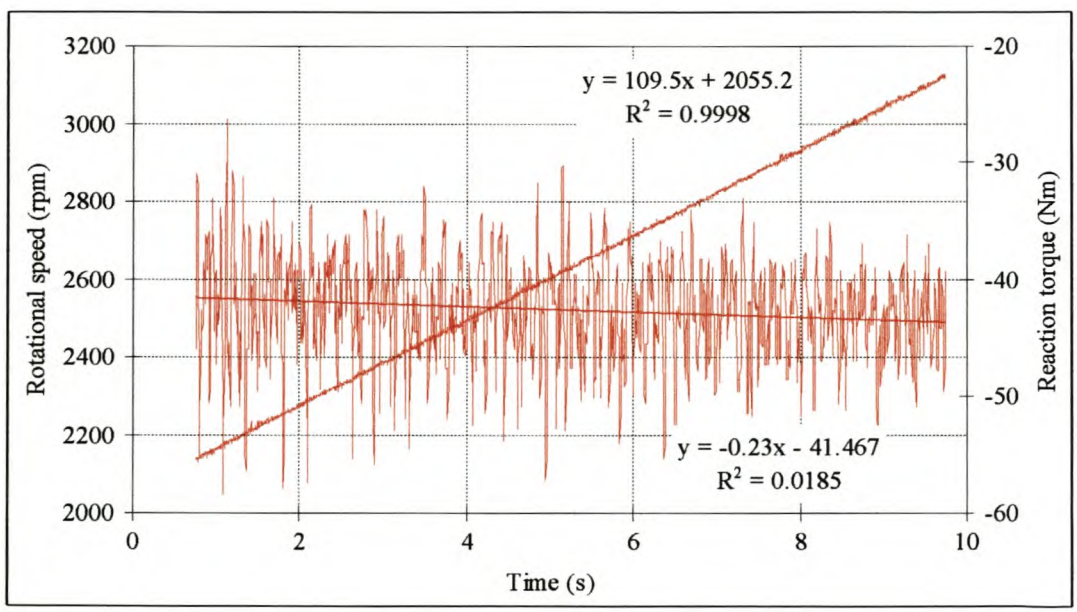

Figure 6.4. Engine inertia test (enlarged)

From the previous figure it is seen that the regression function of the reaction torque had a negative slope. This was due to the increase of engine friction as the speed increased. The engine friction at each speed was calculated using the regression curve in Figure 6.2, and this was subtracted from the reaction torque measured during the inertia tests. This yielded the torque necessary to overcome only engine and dynamometer inertia. By taking a block average of the torque, knowing the acceleration, the combined inertia was calculated using the following equation.

$$T_{lc} - T_f = (J_e + J_d)\alpha_e \tag{6.1}$$

The results of two tests are shown in Table 6.2. Both functions had periods of 20 seconds.

Table 6.2. Test results of engine inertia tests

α_e (rad/s^2)	T_{lc} -T_f (Nm)	$J_e + J_d$ (kgm^2)	J_{ave} (kgm^2)
11.467	-20.111	-1.754	
-11.465	21.220	-1.851	
11.455	-20.138	-1.758	
-11.471	21.195	-1.848	1.803
11.465	-19.408	-1.693	
-11.473	21.927	-1.911	
11.479	-19.706	-1.717	
-11.463	21.731	-1.896	1.804

It is again seen that torques during deceleration were higher than during acceleration. Averages of the two tests, however, yield similar results. The average moment of inertia for both tests was **1.804 kgm^2** with a standard deviation of 0.078 kgm^2. From this combined inertia and the dynamometer inertia as determined in Section 5.1.2, the engine inertia was calculated by subtraction as follows:

$$\begin{aligned} J_e &= (J_e + J_d) - J_d \\ &= 1.804 - 1.600 \\ &= 0.204\ \text{kgm}^2 \end{aligned}$$

Using this method, the inertia of any engine could be accurately determined for use during the solving of vehicle dynamics equations. Provision was made to input engine inertia as variable parameter in the control software, thus allowing the accurate simulation of any engine-vehicle combination.

6.2. TYRE ROLLING RESISTANCE

Tyre rolling resistance F_r is a major force acting on the vehicle, and is as a result of the deformation of the contact patch between tyre and road. At low road speeds this force constitutes the major part of the total retarding force acting to slow down the vehicle. Only at speeds of about 70 km/h and above does the aerodynamic drag force become the major contributing factor. Rolling resistance is present from the instance that the wheels of a vehicle start turning, whereas other forces are present only under certain conditions. There are at least seven factors responsible for the rolling resistance force:

- Energy loss due to deflection of the tyre side-walls near the contact area
- Energy loss due to deflection of the tread elements of the tyre
- Scrubbing in the contact patch
- Tyre slip in the longitudinal and lateral directions
- Deflection of the road surface
- Air drag on the inside and outside of the tyre
- Energy loss on bumps

Rolling resistance force is expressed by the *rolling resistance coefficient* as follows.

$$F_r = f_r W \tag{6.2}$$

This coefficient depends on many factors, most importantly:

- Tyre temperature
- Tyre inflation pressure
- Vehicle load
- Vehicle velocity
- Tyre material and design
- Tyre slip

Rolling resistance is directly proportional to the level of deformation, and inversely proportional to the radius of the tyre. The coefficient will thus increase in response to greater loads, higher speeds and lower tyre pressures. This coefficient rises approximately

linearly with speed, which gave rise to the development of equations that include a linear speed dependency (Gillespie, 1992).

$$f_r = 0.01(1 + V/44.704) \tag{6.3}$$

The Institute of Technology in Stuttgart developed the following equation for the rolling resistance coefficient. It is applicable over broader speed ranges where the coefficient was found to rise in a manner closer to the square of the vehicle speed (Gillespie, 1992).

$$f_r = f_0 + 3.24\, f_1 (V/44.704)^{2.5} \tag{6.4}$$

The two coefficients f_0 and f_1 depend on tyre inflation pressure as illustrated in Figure 6.5.

The Bosch Automotive Handbook (Bosch GmbH, 1993) presents two ways for the estimation of rolling resistance coefficients. Table 6.3 shows coefficients of different tyres under various operation conditions. Figure 6.6 can be used to estimate the rolling resistances of radial and cross-ply car tyres on smooth, level road surfaces under the prescribed tyre pressure and load conditions.

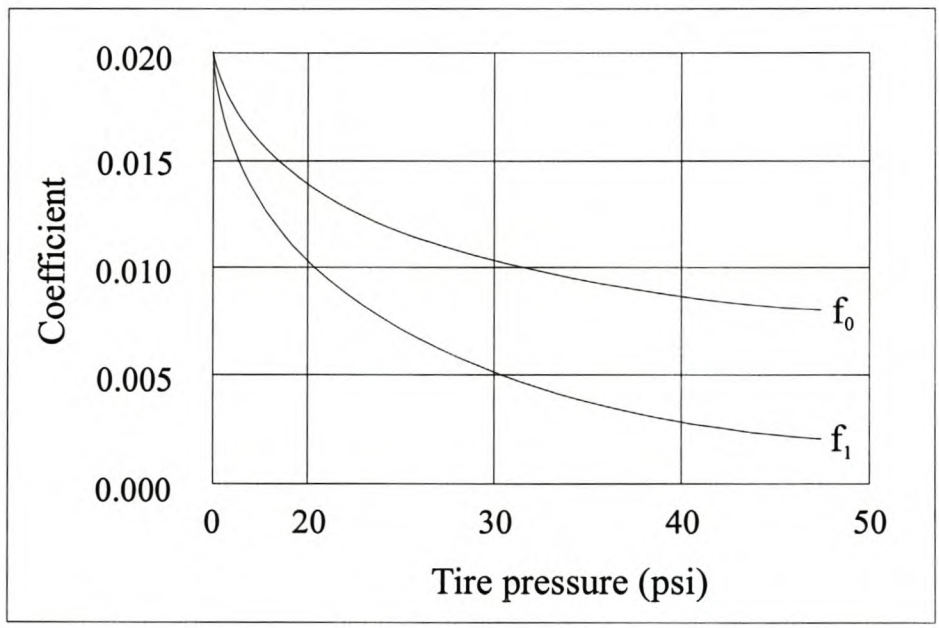

Figure 6.5. Rolling resistance as a function of tyre pressure (Bosch GmbH, 1993)

Table 6.3. Rolling resistance coefficients of various tyre-road surface combinations

Road surface	Coefficient of rolling resistance
Pneumatic car tyres on	
Large sett pavement	0.015
Small sett pavement	0.015
Concrete pavement	0.013
Rolled gravel	0.02
Tarmacadam	0.025
Unpaved road	0.05
Field	0.1 ... 0.35
Pneumatic truck tyres on concrete, asphalt	0.006 ... 0.01
Strake wheels in field	0.14 ... 0.24
Track-type tractor in field	0.07 ... 0.12
Wheel on rail	0.001 ... 0.002

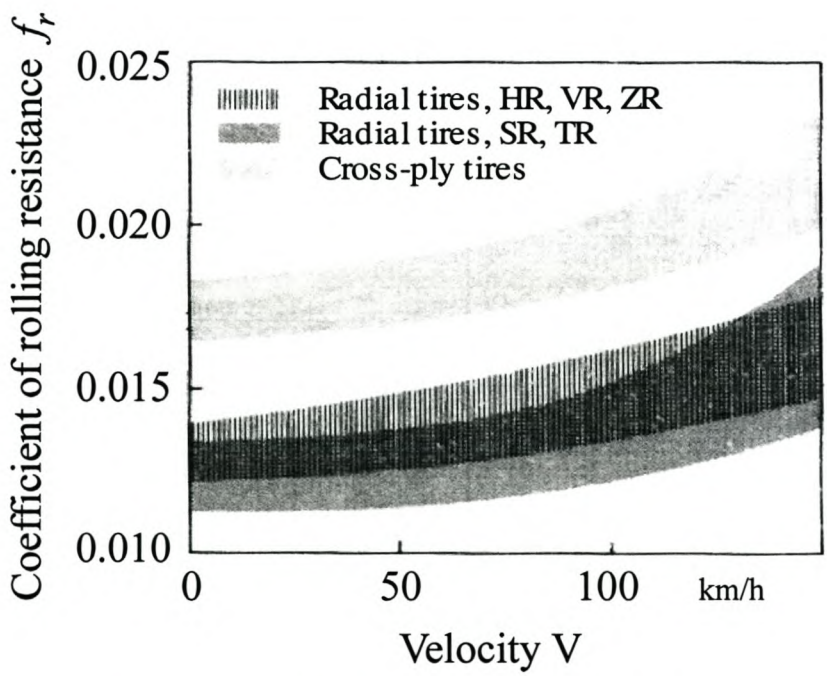

Figure 6.6. Rolling resistance coefficients (Bosch GmbH, 1993)

6.3. AERODYNAMIC DRAG FORCE

As was mentioned above, rolling resistance is the major force acting on a vehicle when travelling at low speeds. Only at higher speeds does aerodynamic drag start to play a significant part in the retardation of the vehicle. The physical origin of air resistance on vehicles is derived primarily from three sources (Germane et al., 1980):

1. Drag resistance which is a function of the aerodynamic shape of the body with respect to frontal area and the outside body surfaces and attachments.
2. Air flow through the car for purposes of cooling or ventilation.
3. Skin friction on the outside surfaces of the vehicle.

Since air flow over a body is complex and the theory of aerodynamic drag weak and inadequate, semi-empirical models have been developed to represent this effect. These three factors are thus expressed in the drag coefficient C_D in the theoretical aerodynamic drag equation (Bosch GmbH, 1993):

$$F_d = \tfrac{1}{2}\rho V^2 C_D A \qquad (6.5)$$

Typical values and associated power requirements for various body configurations can be found in the Bosch Automotive Handbook, p. 326. The drag coefficient of a vehicle is determined empirically and one method that yields both drag coefficient and rolling resistance will now be discussed.

6.3.1. Empirical determination of coefficients for aerodynamic drag and rolling resistance

This empirical technique (Bosch Automotive Handbook, p. 325) can be used to determine the drag coefficient and rolling resistance of a vehicle if the complete vehicle is available for testing. The procedure is described in the following paragraph:

The vehicle is allowed to coast down in neutral, under windless conditions on a level road surface. The time that elapses while the vehicle coasts down by a specific increment of speed is measured from two initial velocities, V_1 (high speed) and V_2 (low speed). This information is used to calculate the mean deceleration rates a_1 and a_2. The formulae required to calculate the rolling resistance and aerodynamic drag, together with an

example, are given in the following table. The example is for a vehicle weighing m = 1450kg with a cross sectional area of A = 2.2 m^2.

	1st Trial (high speed)	2nd Trial (low speed)
Initial velocity Terminal velocity Interval between v_a and v_b	V_{a1} = 60 km/h V_{b1} = 55 km/h t_1 = 6.5 s	V_{a2} = 15 km/h V_{b2} = 10 km/h t_2 = 10.5 s
Mean velocity	$V_1 = \frac{V_{a1} + V_{b1}}{2} = 57.5$ km/h	$V_2 = \frac{V_{a2} + V_{b2}}{2} = 12.5$ km/h
Mean deceleration	$a_1 = \frac{V_{a1} - V_{b1}}{t_1} = 0.77 \frac{km/h}{s}$	$a_2 = \frac{V_{a2} - V_{b2}}{t_2} = 0.48 \frac{km/h}{s}$
Drag coefficient	$C_D = \frac{6m \cdot (a_1 - a_2)}{A \cdot (V_1^2 - V_2^2)} = 0.36$	
Coefficient of rolling resistance	$f_r = \frac{28.2 \cdot (a_2 \cdot V_1^2 - a_1 \cdot V_2^2)}{10^3 \cdot (V_1^2 - V_2^2)} = 0.013$	

6.4. BRAKING FORCE

Braking plays an important part in the modelling of a vehicle. When the brakes are applied, torque acts on the wheels of the vehicle to slow it down. The braking torques on all four wheels can be assumed to be equal and only one torque value used to represent all four brakes. This is not strictly the case, but the assumption was made since we were interested only in the response of the vehicle as a whole and not in the dynamics of individual vehicle components. This assumption also simplified matters significantly during the solving of dynamic equations.

For the vehicle under the control of a human driver, brake torque was determined by the brake pedal position as is the case in any vehicle. This position was scaled by a predetermined maximum braking torque to be applied to the wheels. Tyre slip was not taken into account in this model, but can be considered for inclusion in future models. For the vehicle under computer control, braking torque has to be arrived at based on the error between demanded and actual vehicle speed and has to be applied in a realistic manner

representative of the way in which a human driver operates the brake pedal. These restrictions add extra complexity to the design of a control algorithm designed for this purpose. Once the required braking torque had been arrived at, it was accounted for by adding it to the vehicle load torque in the vehicle dynamics model.

6.5. POWER-TRAIN

The power-train system converts torque developed by the engine into traction force available at the wheels for accelerating the vehicle. Key elements of this mechanical system are shown in Figure 6.7. This represents a manual transmission which amplifies the engine torque, while reducing its speed to match the appropriate vehicle speed.

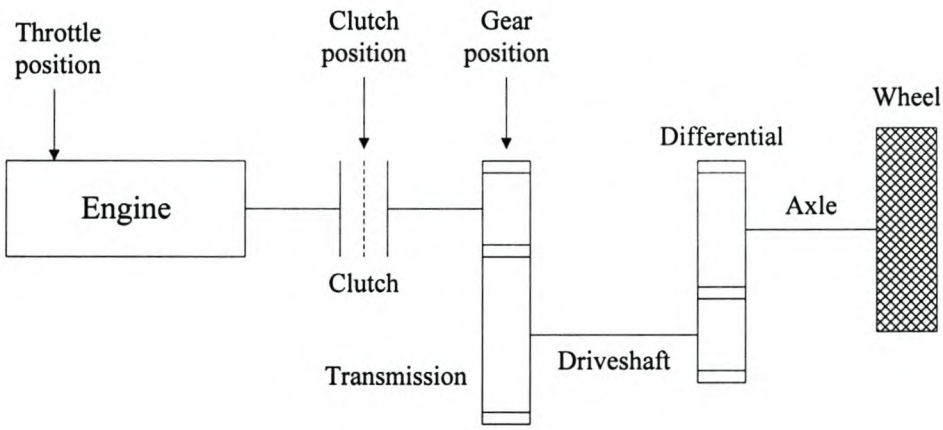

Figure 6.7. The power-train system

An analogous system, represented by a geared torsional model, is seen in Figure 6.8.

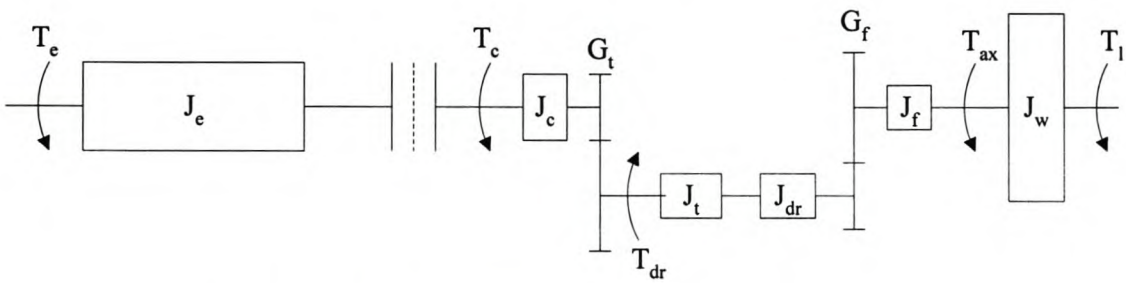

Figure 6.8. The power-train system represented by a geared torsional system

The above illustrations show that the rotational parts engaged with the engine, with the clutch pedal fully released, include the clutch, the transmission, the drive-shaft, the final drive and the wheels. The above system can be represented by an equivalent gearless system as shown in Figure 6.9 in which all torques and speeds are related back to engine/clutch interface. In this model rigid shafts are assumed and used in the following calculations of engine and vehicle behaviour. More complex drive-train equations have been developed by numerous authors (Leonhardt et al., 1992, Roberts & Dallard, 1974 and Voigt, 1991), and included elements such as driveline flexibility and damping. For reasons mentioned in Section 5.3, rigid driveline equations were used during the development of the CAE engine test-bed.

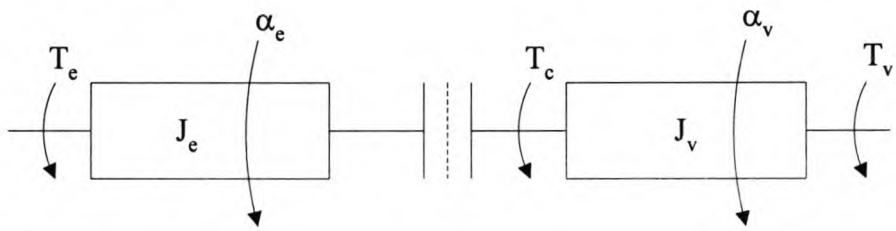

Figure 6.9. The power-train system represented by an equivalent gear-less system

Starting with the engine, it must be remembered that internal engine torque T_e and the torque available at the input of the transmission T_c differ due to the torque required to accelerate the inertia of the rotating components of the engine (as well as accessory loads not considered here). The torque thus available at the clutch (input to the transmission) is given by Newton's 2nd Law as:

$$T_c = T_e - J_e \alpha_e \tag{6.6}$$

This equation can be rewritten to express the instantaneous angular acceleration of the engine α_e in rad/s² which is the difference between the torque developed by the engine and the road-load torque applied on the flywheel, then divided by the total mechanical inertia engaged. Thus, for the case of the clutch fully depressed (engine decoupled from the vehicle), engine and vehicle accelerations can be calculated from:

$$\alpha_e = \frac{T_e - T_c}{J_e} \tag{6.7}$$

$$\alpha_v = \frac{T_c - T_v}{J_v} \tag{6.8}$$

With the clutch pedal fully released the same equations become:

$$\alpha_v = \alpha_e = \frac{T_e - T_v}{J_e + J_v} = \frac{T_c - T_v}{J_v} \tag{6.9}$$

In the above equations, T_v, the total vehicle load torque at the clutch, is comprised of the individual load torques discussed in the previous sections, together with the total driveline efficiency and gear ratios. This torque is expressed as:

$$T_v = \frac{(F_r + F_d + F_b)R}{G_t G_f \eta_{tf}} \tag{6.10}$$

With engine and vehicle accelerations known, it was possible to estimate the next engine and vehicle speeds by extrapolation, using the *Euler* integration algorithm:

$$\omega_{en} = \omega_{en-1} + \Delta t \alpha_{en-1} \tag{6.11}$$

$$\omega_{vn} = \omega_{vn-1} + \Delta t \alpha_{vn-1} \tag{6.12}$$

J_v in the above equations represents the equivalent rotational inertia of the vehicle as seen from the clutch side, and is derived from Figure 6.9 as

$$J_v = J_{vl} + J_{dt} \tag{6.13}$$

where:

J_{vl} is the effective rotational inertia due to linear acceleration of the vehicle and, J_{dt} is the rotational inertia of the drive-train from the clutch up to, and including, all four wheels and is given by:

$$J_{dt} = J_c + \frac{1}{G_t^2}\left\{J_t + J_{dr} + \frac{1}{G_f^2}(J_f + J_w)\right\} \tag{6.14}$$

J_{vl} can be found by transforming the effective vehicle mass into a rotational inertia for use in the dynamic equations. The development of this transformation can be seen in APPENDIX C. As seen from the clutch-side of the drive-train this quantity is given by:

$$J_{vl} = \frac{f_m M.R^2}{G_{tf}^2} \tag{6.15}$$

As a vehicle accelerates, all rotational parts experience an angular as well as a translational acceleration. This effectively adds to the inertial mass of the vehicle, which can be separated into the gravitational mass, the drive-train effective mass including the engine, and effective mass of the non-driving wheels. In order to model the drive-train accurately it would be required to have detailed knowledge of all its parts. Moments of inertia would have to determined either by means of physical measurements of from detailed drawings often only obtainable from OEMs.

A method has been developed by Cole (1972) that combines all these rotating and reciprocating masses into an "effective mass" so that the total contribution can be expressed in terms of the gravitational mass of the vehicle. The ratio $(M + M_r)/M$ is known as the "mass factor" and depends on the operating gear, with typical values as shown in Table 6.4 below:

Table 6.4. Typical mass factor values

		Mass Factor – f_m			
Vehicle	***Gear:***	***High***	***Second***	***First***	***Low***
Small Car		1.11	1.20	1.50	2.4
Large Car		1.09	1.14	1.30	-
Truck		1.09	1.20	1.60	2.5

A representative number is often taken as:

$$\text{Mass factor } (f_m) = 1 + 0.04 + 0.0025 G_{tf}^{\ 2} \tag{6.16}$$

With the mass factor known, the effective vehicle rotational inertia as seen at the clutch is calculated from the effective mass and wheel radius by:

$$J_v = \frac{f_m M.R^2}{G_{tf}^{\ 2}} \tag{6.17}$$

Equation (6.15) transforms the effective vehicle mass into a rotational inertia for use in the dynamic equations. With the above model established, a clutch model had to be developed for connecting the engine with the rest of the vehicle. This model will now be described.

6.6. CLUTCH MODEL

The clutch is a mechanism for the smooth engagement or disengagement of torque between the engine and transmission. A model was developed for a dry friction clutch since these are extensively used in cars and trucks. A thorough mathematical investigation into clutch dynamics and engagement has been made by Szadkowski & Morford (1992) and Szadkowski & McNerney (1992). This work was studied, leading to a more complete understanding of the principles behind the operation and simulation of clutch engagement theory. A number of assumptions were made regarding the clutch model that was developed for the system. These were made in order to simplify the model, since relatively little time would be spent in clutch engagement phases and a more accurate model would not have influenced the entire body of experimental data by much. Main assumptions included the following:

- Torque transmitted by the clutch (T_c) is a linear function of the clutch pedal position (Shigley, 1986).
- There is no torque loss during clutch slipping.
- The clutch is rigid and mass-less, its inertia being included with the rest of the transmission system.

In developing the model, the following clutch functions had to be considered and included:

- Pull-away
- Disengagement of clutch
- Changing of gears
- Clutch re-engagement
- Throttle control during the above clutch phases

Depending on the driver's gear selection and control of the clutch pedal, one of the following modes of clutch operation was selected:

6.6.1. Pull-away mode

During pull-away of a vehicle, two things happen. Firstly, torque is transferred from the engine to the wheels where it provides the tractive force necessary to accelerate the vehicle. Secondly, the clutch acts as a speed buffer between the engine and vehicle, since their rotational speeds do not initially match one another. Thus, clutch slip occurs during the first stage of engagement. During this time, torque transmitted by the clutch is regulated by the driver by means of the clutch pedal, while clutch speed is related to wheel speed by the chosen gear ratio. Maximum clutch torque capacity is determined by the clutch geometry, including such factors as frictional area and material used, spring constant, number of disks, etc., and is defined by Szadkowski & Morford (1992) as

$$T_{Cap} = 2n\mu_s P_L R_m \tag{6.18}$$

Clutch lock-up occurs when engine -and clutch-speeds coincide. During the period in which the clutch slips, engine speed is governed by equation (6.7), echoed below,

$$\alpha_e = \frac{T_e - T_c}{J_e} \tag{6.19}$$

while vehicle speed is determined by equation (6.8).

$$\alpha_v = \frac{T_c - T_v}{J_v} \tag{6.20}$$

The clutch speed is always related to the vehicle speed by the gear ratio and is determined by the gear selected. Figure 6.10 illustrates pulling-away manually with a simulated 20 ton truck on the test-bed. Both engine and clutch speeds are shown, together with throttle and clutch pedal positions. Clutch lock-up is seen to occur at approximately 500 rpm, as indicated.

For cycles under the complete control of a computer, the pull-away procedure also needs to be fully automated. In the case of a friction clutch as described above, this would involve controlling both throttle and clutch pedal positions in such a way as to ensure a smooth pull-away without stalling the engine. Clearly it would be advantageous to rather simulate an automatic gearbox and torque converter in such a case. Then the procedure would involve the control of only one variable (i.e. the throttle), making the process of control

that much simpler. These possibilities were investigated and will be considered for future enhancements made to the system.

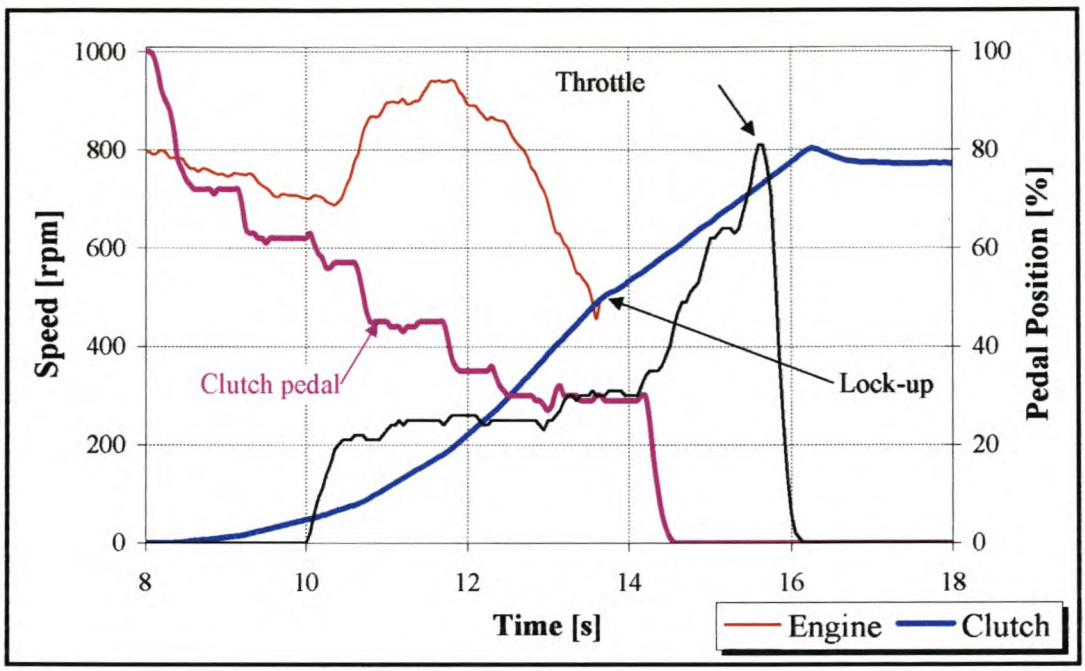

Figure 6.10. Pull-away simulation of 20 ton truck

6.6.2. Locked mode

The locked mode of clutch operation commences as soon as the engine and clutch speed match. At this time all the torque developed by the engine is transmitted by the clutch to the transmission system, and T_c in equation (6.19) is equal to the net torque as measured by the load cell T_{lc}.

$$\alpha_v = \alpha_e = \frac{T_c - T_v}{J_v} \tag{6.21}$$

6.6.3. Gear changing mode

For the modelling of gear shifting, certain assumptions had to be made regarding the procedure to ensure consistent model performance. This would in turn ensure that data obtained during experiments could be compared, knowing that the same shifting procedure was followed every time. The gear shifting process was started by setting the clutch torque and throttle position to zero, an accurate account of what happens when the clutch is fully

depressed. The assumption was made that re-engagement would only commence once the engine speed had dropped to match that of the clutch speed, now governed by the newly selected gear ratio. Although this is an idealised situation, it is in fact the way in which gear changes should be made when shifting up, since it minimises jerk due to sudden acceleration and also limits wear on clutch surfaces. An example of a gear change using the described model is shown in Figure 6.11.

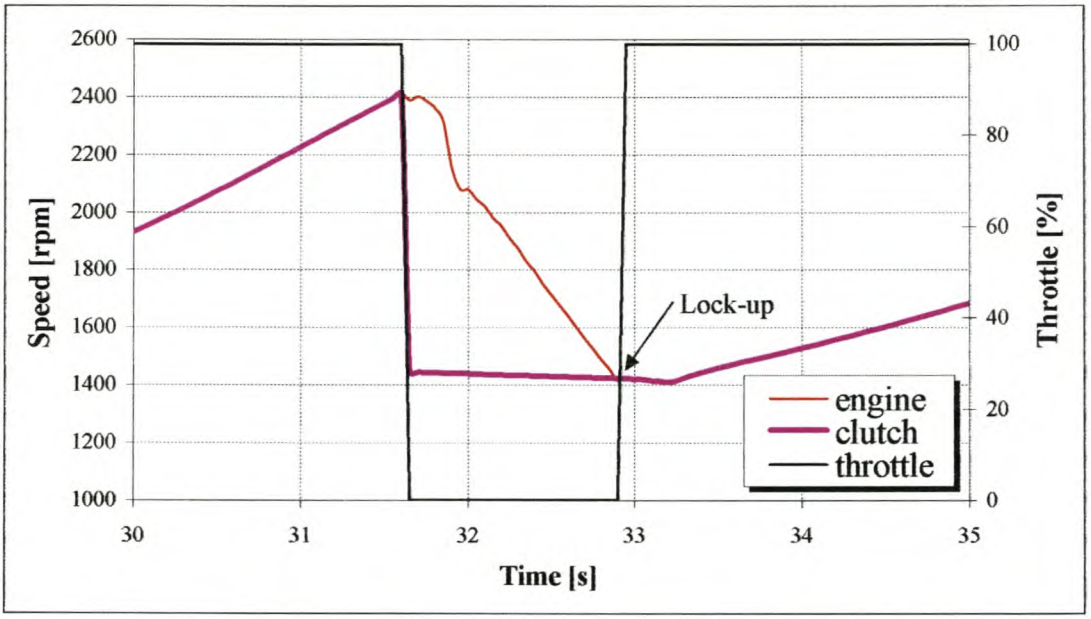

Figure 6.11. Gear-change simulation of 20 ton truck

A simplified flowchart of the clutch logic implemented by the controlling software is shown in Figure 6.12. This model will now be discussed.

- During cycles, clutch and gear input is obtained from the driver box (see Figure 4.5). This data handling process constitutes the first part of the clutch model (block *1*).
- The next step is to compare the new driver data (if any) with the previous data to determine whether the driver has requested a change in clutch status (block *2*). If not, the same clutch-torque mode is again used (block *3*) and the next cycle loop executed.
- If a clutch mode change is requested by the driver, it is determined what mode he wishes to enter (block *4*), whether it be pulling-away from standstill, changing to neutral, or changing to another gear.

- If a change to neutral is selected (block ***5***), the neutral condition is modelled by having the clutch torque fall to zero (block ***6***), while engine and vehicle accelerations are governed by equations (6.19) and (6.20).

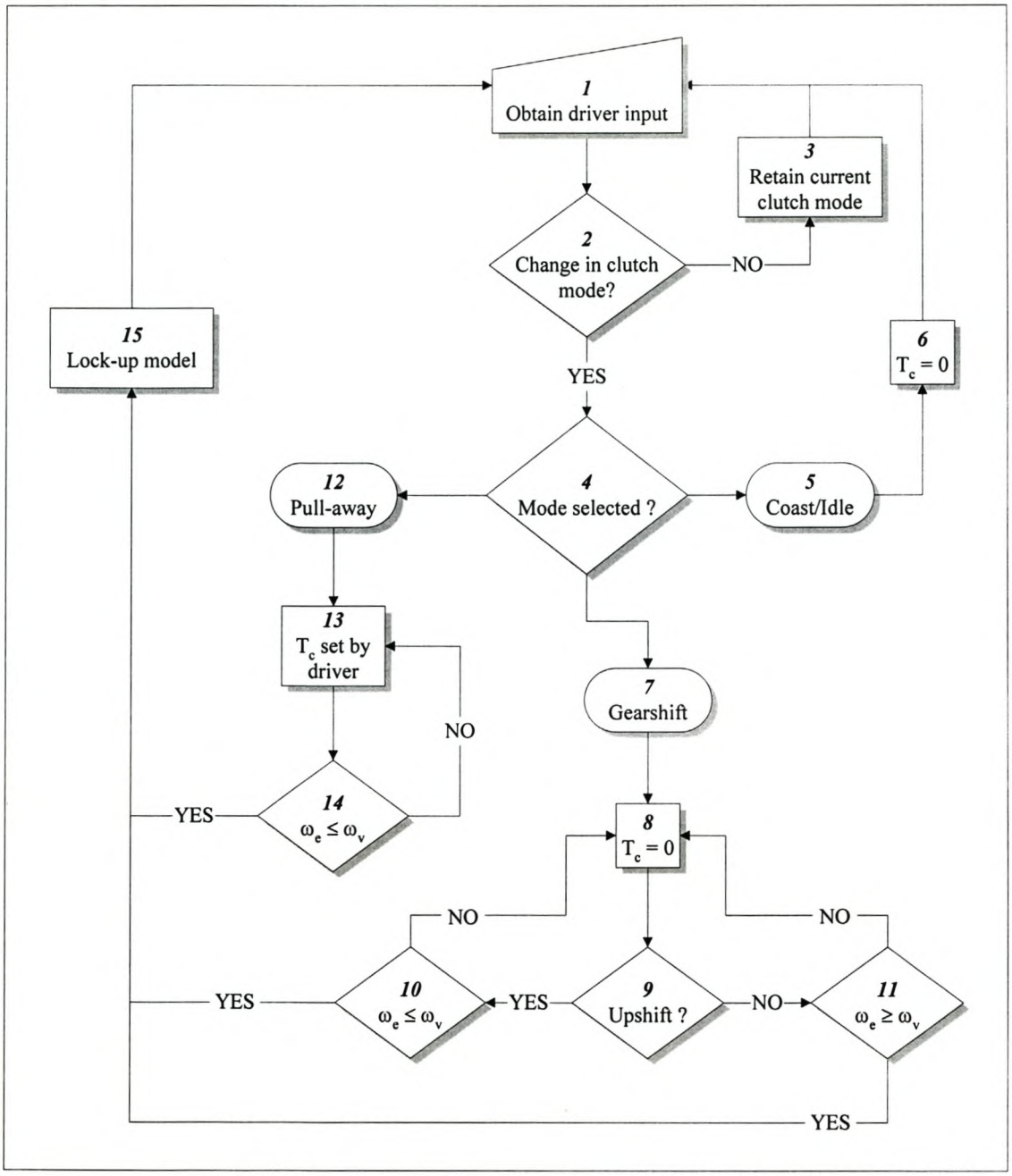

Figure 6.12. Clutch model flow chart

- If a pull-away away is about to be performed (detected by a change to first gear while the vehicle is stationary, block ***12***), the clutch torque is determined by the driver (as

explained previously, block ***13***) until such a time that the engine speed matches the clutch speed (block ***14***). At this time clutch lockup is initiated (block ***15***).

- When a gearshift is requested (initiated by changing gear while the vehicle is moving, block *7*), the clutch torque is set to zero (block ***8***) while the engine speed is updated until clutch lock-up occurs. For an up shift this is when the engine speed has dropped to match the new clutch speed (block ***10***), while for a down shift this occurs when the engine speed has risen to match the new clutch speed (block ***11***). When either condition is satisfied, the clutch lock-up mode comes into effect (block ***15)***.

With the clutch model described above most clutch functions could be simulated to a satisfactory degree of accuracy and reliability. This model was incorporated into the software programme that would control and oversee the system. More detail will be given in Section 8.

7. DATA ACQUISITION AND SIGNAL CONDITIONING

Signal acquisition and conditioning are very important aspects of any control or simulation problem. The accuracy and stability of feedback systems are very strong functions of signal quality as excessive noise-to-signal ratios often lead to unforeseen difficulties and controllability problems. As a result, certain steps had to be undertaken to ensure good signal quality. Feedback signals were analysed in order to determine the amplitude and identify the origins of possible noise sources. Fourier analyses were performed on captured data to aid in the process of pinpointing dominant noise frequencies and their possible origins. This information was used during the design phase of the inline analogue filters used to further condition the signals. Anti-Aliasing filters also had to be designed and built as part of the conditioning process, details of which will now be discussed.

7.1. THE ALIASING PHENOMENON

Aliasing is a phenomenon that occurs whenever an analogue signal, be it of a visual, audio, or any other information-carrying nature, is digitised. A classic case of aliasing is seen in cinema pictures, where analogue data (the visual images) is digitised and captured on film. This process usually happens at a rate of 26 frames per second, which is faster than the human eye can resolve. The observer reconstructs the sampled image by "filling in the gaps", leading to a smooth, continuous picture rather than a series of jerky images. This process can sometimes lead to erroneous data in which the reconstructed signal is not a faithful portrayal of the original. This is often seen in cinema pictures as rotating objects (such as wagon wheels and aircraft propellers) alternately appear to spin forwards and backwards. It is the avoidance of this phenomenon that needs special attention whenever data is sampled and reconstructed during a digital process.

In the sampling process there are two parameters that can be adjusted, namely the sampling rate, which is the frequency at which samples are recorded, $f_s = 1/\Delta t$ and the number of points recorded N. Figure 7.1 shows two examples of sampling the same waveform. In Figure 7.1(a) the sampling rate is low (Δt too large) resulting in high frequencies in the original waveform not being well resolved by the discrete samples. The reconstructed signal (the dashed curve) does not show the sharp peaks seen in the original waveform.

Furthermore the total period of sampling is also short (N is small) which results in the low frequencies of the signal being missed. It is therefore not possible to see how often the signal repeats itself.

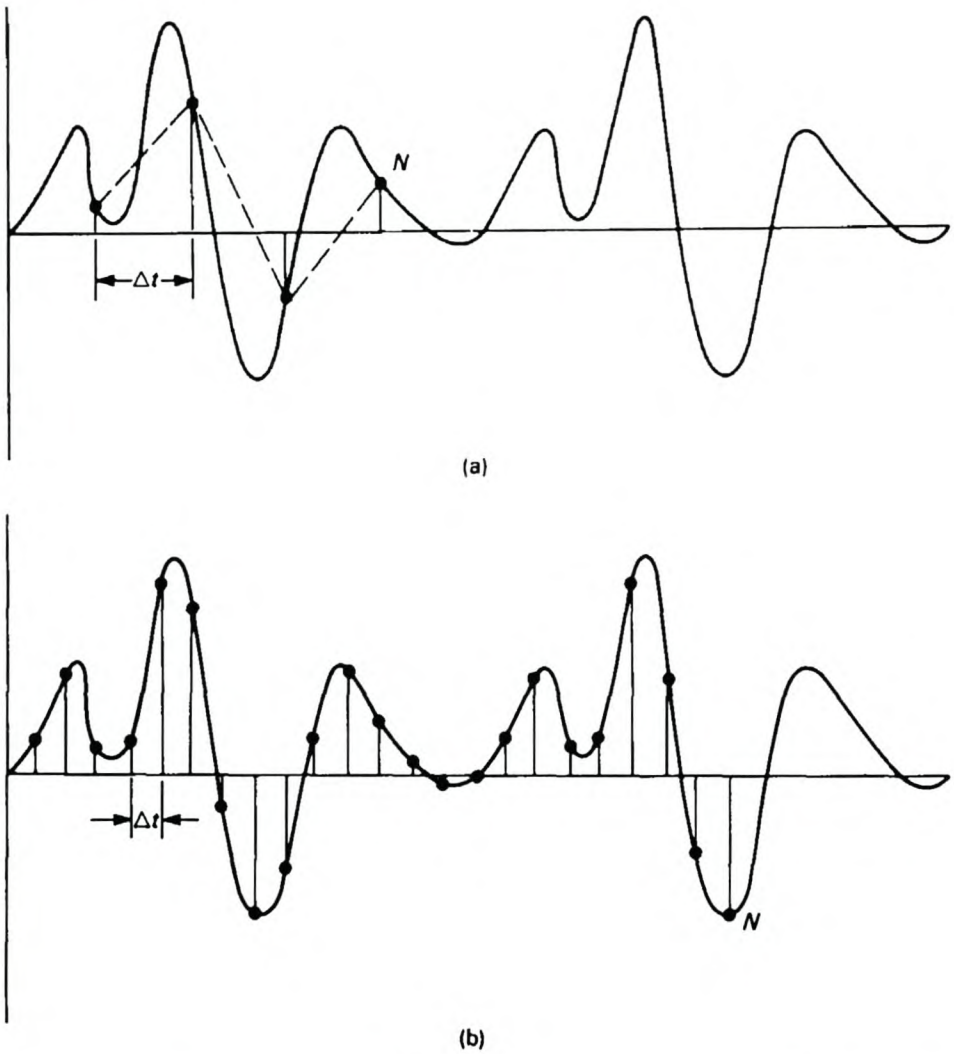

Figure 7.1. The effect of sampling rate and the number of samples taken on signal reconstruction (Beckwith et al., 1993)

Figure 7.1(b) shows the same signal sampled at a higher frequency resulting in more samples being recorded and the resolution of both high and low frequencies being improved. In the above figures the importance of the sampling frequency and number of samples taken for the accurate reconstruction of a sampled waveform is clearly illustrated. This brings us to the next question. The question of the minimum sampling frequency needed to faithfully resolve a particular frequency is illustrated in Figure 7.2 which uses a signal, with frequency f, which is sampled at increasing rates.

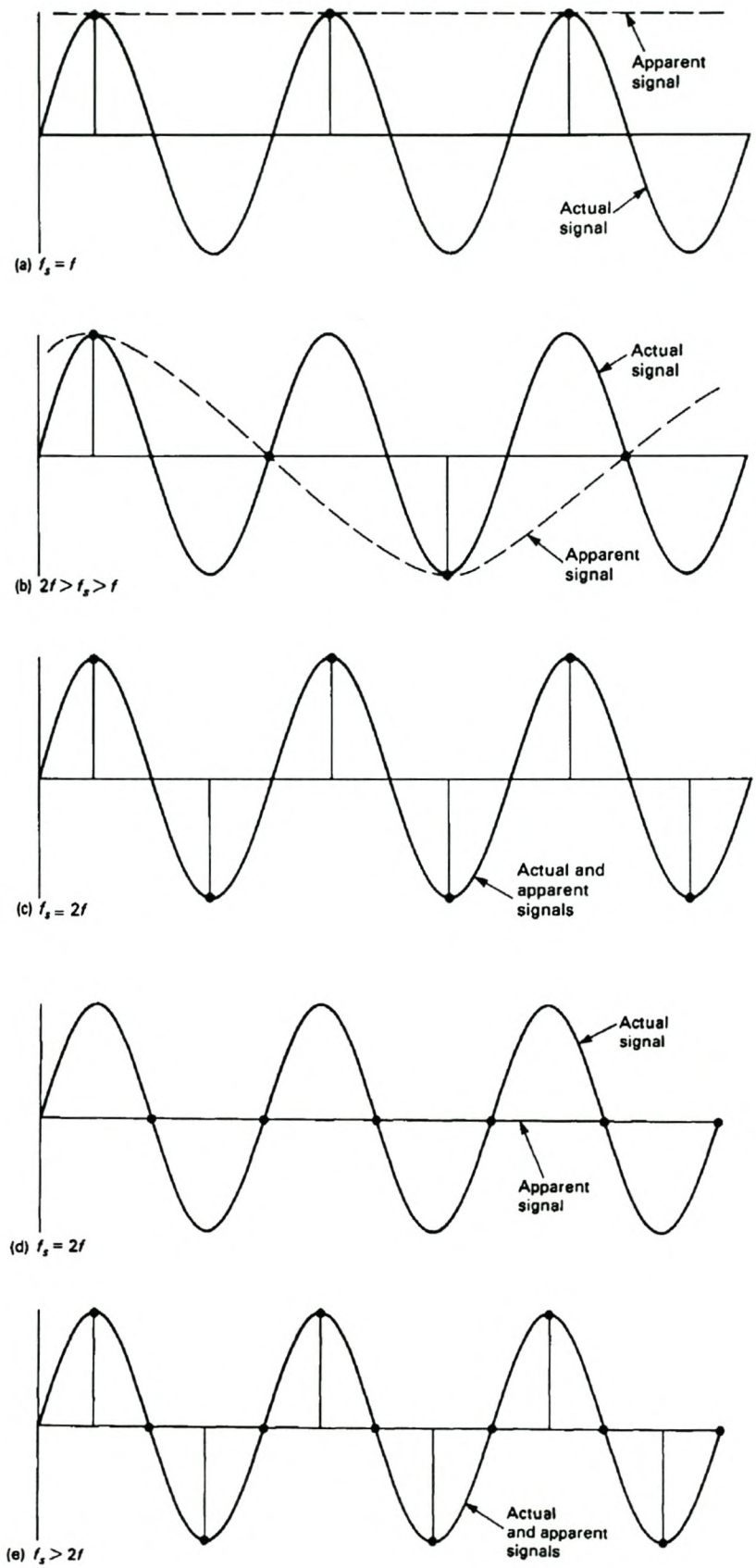

Figure 7.2. The effect of varying the sampling rate, f_s, on the apparent signal obtained by discrete sampling (Beckwith et al., 1993)

In (a) the waveform is sampled at frequency $f_s = f$ and the discretely sampled signal appears to be constant. A sinusoidal signal appears, after being digitised, as a constant. In case (b) the signal is sampled at a slightly higher frequency, between f and $2f$. Now the digitised signal does appear to be a wave, but it has a frequency lower that f. In (c) the signal is sampled at a frequency $f_s = 2f$ and the apparent signal appears with the correct frequency of f. Here again, if the sampling is started a quarter-cycle later using the same frequency, a constant sample is obtained as seen in (d). It is only when the sampling frequency is increased above $2f$, as shown in (e), that the correct signal frequency is obtained.

There is a limit to the highest signal frequency that can be resolved. This limit is determined by the *Nyquist frequency*,

$$f_{Nyq} = \frac{f_s}{2} \tag{7.1}$$

Any signal with frequency content lower than $f_{Nyq} = f_s/2$ is accurately sampled and reconstructed. If a signal has frequency content above the *Nyquist frequency,* f_{Nyq}, then those frequencies incorrectly appear as lower frequencies in the digitised signal and will lead to the subsequent misinterpretation of the signal. This phenomenon in which frequencies of a sampled signal take on lower frequencies, as in Figure 7.2(b), is referred to as *frequency folding* -or *aliasing* and occurs whenever the Nyquist frequency falls below the signal frequency. As shown in Figure 7.2(c) and (d), phase ambiguity when sampling at the Nyquist frequency means that the sampling frequency chosen should always be greater than twice that of the highest frequency (of significant amplitude) of interest in the signal.

This concept is summarised by **Shannon's Sampling Theorem (Phillips et al., 1995)**: *A function of time e(t) which contains no frequency components greater than f_o hertz is uniquely determined by the values of e(t) at any set of sampling points spaced $1/2f_o$ seconds apart.*

Frequency aliasing over the frequency range of interest can be prevented in two ways. Firstly by raising the sampling frequency f_s so that the whole frequency range where the sampled signal is of significant amplitude falls below the *Nyquist* frequency, or secondly

by low-pass filtering the signal at f_{Nyq} or lower through an analogue *anti-aliasing* filter before it is sampled, thereby ensuring that the data sampled only contain frequencies lower than the *Nyquist* frequency. The design and implementation of such a filter will be discussed in Section 7.3. The choice of sampling frequency is an important consideration in that it determines the maximum signal frequency that can be resolved. This will now be discussed.

7.2. CHOICE OF SAMPLING FREQUENCY

The digitisation of data is intrinsic to any computer-based acquisition system. In the previous section it was mentioned that the sampling frequency is an important consideration when dealing with digital systems, as it determines the maximum signal frequencies that may be resolved. This in turn determines to what frequencies the system can respond and accurately model the virtual vehicle. During the sampling process it is unavoidable that some information loss will occur and it is important to select the sampling frequency in such a way that these losses are kept to an acceptable level.

Ljung (1987) points out that a sampling frequency of about five to ten times the *bandwidth* of a system should be a good choice in most cases. Referring to Figure 7.3, the frequency at which the system response is 3 dB below its zero-frequency response is called the *cut-off-frequency.* What this means is that when the system is excited at the cut-off frequency, the system gain is 0.707 of what it is at zero hertz or steady-state conditions. The system filters out input signal components higher than the cut-off frequency and transmits those components with frequencies lower than the cut-off frequency.

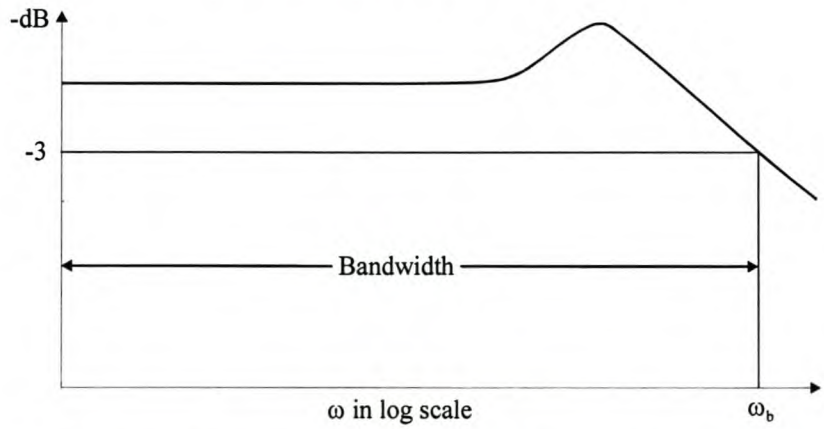

Figure 7.3. Logarithmic plot showing cut-off frequency ω_b and bandwidth

The range of frequencies $0 \leq \omega \leq \omega_b$ in which the system response does not drop with more than 3db is called the *bandwidth* of the system. System bandwidth gives an indication of how well a system will track or respond to a sinusoidal excitation, a large bandwidth corresponding to small rise times or a fast response.

In the case of the system under consideration there were two separate sub-systems to consider. Both sub-systems were of a multiple-input single-output configuration, each consisting of two transfer functions. For the first sub-system, the output was considered to be a change in engine torque (the first system variable), while inputs consisted of a change in engine throttle position and speed. For the second sub-system, the output was a change in dynamometer speed (the second system variable), the inputs being a change in dynamometer speed demand and engine torque. These systems are shown in Figure 7.4.

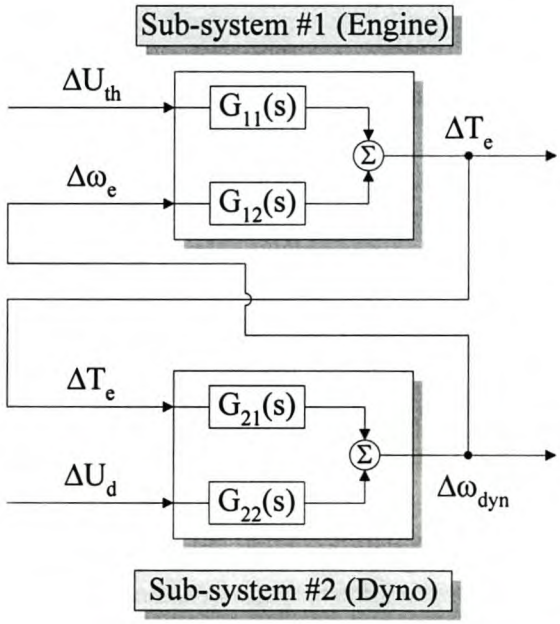

Figure 7.4. Inputs and outputs influencing sub-system bandwidths

Here we thus had to do with four transfer functions, $G_{ii}(s)$, each with bandwidth ω_{bii}. Clearly there was coupling between these two systems in that the output of one was an input to the other. Due to the dominant nature of two of these couplings, the bandwidths of only two transfer functions, namely those of $G_{11}(s)$ and $G_{22}(s)$, were taken into consideration in determining the required sampling frequency. This was the case since the bandwidth of $G_{12}(s)$ was necessarily going to be less than that of $G_{22}(s)$ due to the inertia of

the internal combustion engine, with the bandwidth of transfer function $G_{21}(s)$ being less than that of transfer function $G_{11}(s)$ due the inertia effect of the dynamometer. As the bandwidths involved in these two sub-systems were known, the sampling frequency could be chosen accordingly. It was decided that a sampling frequency based on the larger of the two bandwidths would be used, thus ensuring that all pertinent information stemming from both sub-systems would be accurately portrayed in the sampled data. The choice of a single sampling frequency would also result in the reduction of system complexity. As was discussed in Section 5.3.1, the bandwidth of a system can be calculated by exciting the system while measuring its response to that excitation. This method was used to estimate the dynamometer bandwidth. A second method can also be used to obtain the bandwidth of a system. This method involves a step command pre-setting of the input to the system, while observing the output. Based on the system output behaviour, together with prior knowledge and assumptions made regarding the system, specifications concerning its transfer function can be determined.

Starting with sub-system #1, the engine, assumptions had to be made regarding the system's order and complexity. Various attempts have been made at identifying engine models resulting from detailed mathematical descriptions (Morris et al., 1981). These were, however, found to be relatively complex and lacking in extensive verification with engine data. It has been found that a second-order MISO model can adequately represent the open-loop throttle-speed-torque system (Fullmer et al., 1992 and Tuken et al., 1990). In the frequency domain, the general form of the second-order system is:

$$\frac{C(s)}{R(s)} = \frac{K\omega_n^{\,2}}{s^2 + 2\zeta\omega_n s + \omega_n^{\,2}} \tag{7.2}$$

where ω_n is the *un-damped natural frequency*, K the gain, and ζ the damping ratio. The damping ratio, ζ, is the ratio of the actual damping to the critical damping. The dynamics of the system can then be described in terms of these two parameters. If $0 < \zeta < 1$, the system is called under-damped, and the transient response is oscillatory. If $\zeta = 1$, the system is called critically damped. Over-damped systems correspond to $\zeta > 1$. The transient response of critically damped and over-damped systems do not oscillate, while for $\zeta = 0$, the transient response does not die out.

In many practical cases, the desired performance characteristics of systems are given in terms of time-domain quantities. As was mentioned above, the performance characteristics of a system are frequently specified in terms of the transient response to a unit-step input since it is easy to generate and is sufficiently drastic (or extreme). If the response to a unit-step input is known, it is mathematically possible to compute the response to any input (Ogata, 1990). Practical systems often exhibit damped oscillations before reaching steady-state. In specifying the transient response characteristics of a system to a unit step-input, it is common to specify the following parameters:

1. Delay time, t_d
2. Rise time, t_r
3. Peak time, t_p
4. Maximum overshoot, M_p
5. Settling time, t_s

These parameters are defined in what follows and are shown in Figure 7.5.

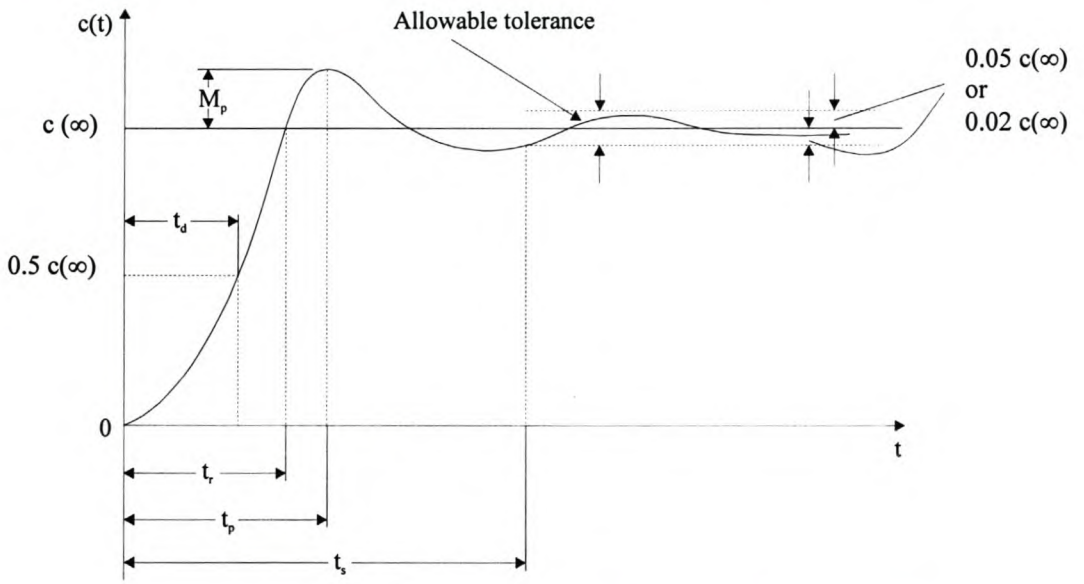

Figure 7.5. Unit-step response curve showing t_d, t_r, t_p, M_p, and t_s

1. Delay time, t_d: The delay time is the time required for the response to reach half the final value for the very first time.
2. Rise time, t_r: The rise time is the time required for the response to rise from 10% to 90%, 5% to 95%, or 0% to 100% of its final value. For under-damped second-

order systems, the 0% to 100% rise time is normally used. For over-damped systems, the 10% to 90% rise time is commonly used.

3. Peak time, t_p: The peak time is the time required for the response to reach the first peak of the overshoot.

4. Maximum (percent) overshoot, M_p: The maximum overshoot is the maximum peak value of the response curve measured from unity. If the final steady-state value of the response differs from unity, then it is common to use the maximum percent overshoot. If is defined by

$$\text{Maximum percent overshoot} = \frac{c(t_p) - c(\infty)}{c(\infty)} \times 100\%$$

The amount of the maximum overshoot directly indicates the relative stability of the system.

5. Settling time, t_s: The settling time is the time required for the response curve to reach and stay within a range about the final value of size specified by the absolute percentage of the final value (usually 2% or 5%). The settling time is related to the largest time constant of the system. The relevant percentage error criterion to use may be determined from the objectives of the system design in question.

The above terms can be related to ζ and ω_n by the following equations (see Ogata pages 266 – 268):

$$t_r = \frac{\pi - \beta}{\omega_d} \tag{7.3}$$

where $\beta = \tan^{-1}\left(\frac{\omega_d}{\zeta\omega_n}\right)$ and

$$\omega_d = \omega_n\sqrt{1-\zeta^2} \tag{7.4}$$

$$t_p = \frac{\pi}{\omega_d} \tag{7.5}$$

$$M_p = e^{-(\zeta/\sqrt{1-\zeta^2})\pi}$$

from which

$$\zeta = \frac{\sqrt{\frac{\ln^2(M_p)}{\pi^2}}}{\sqrt{1+\frac{\ln^2(M_p)}{\pi^2}}} \qquad (7.6)$$

The above equations make it possible to determine system characteristics from its response to a step-input. Such a response to a step-input of the throttle demand is shown in Figure 7.6, in which a Toyota 4A-FE engine (1600cc, fuel injection) was given a throttle step demand from 0% to 20% at a constant speed. It is seen that the torque climbed slightly with time as it reached its steady-state operation condition.

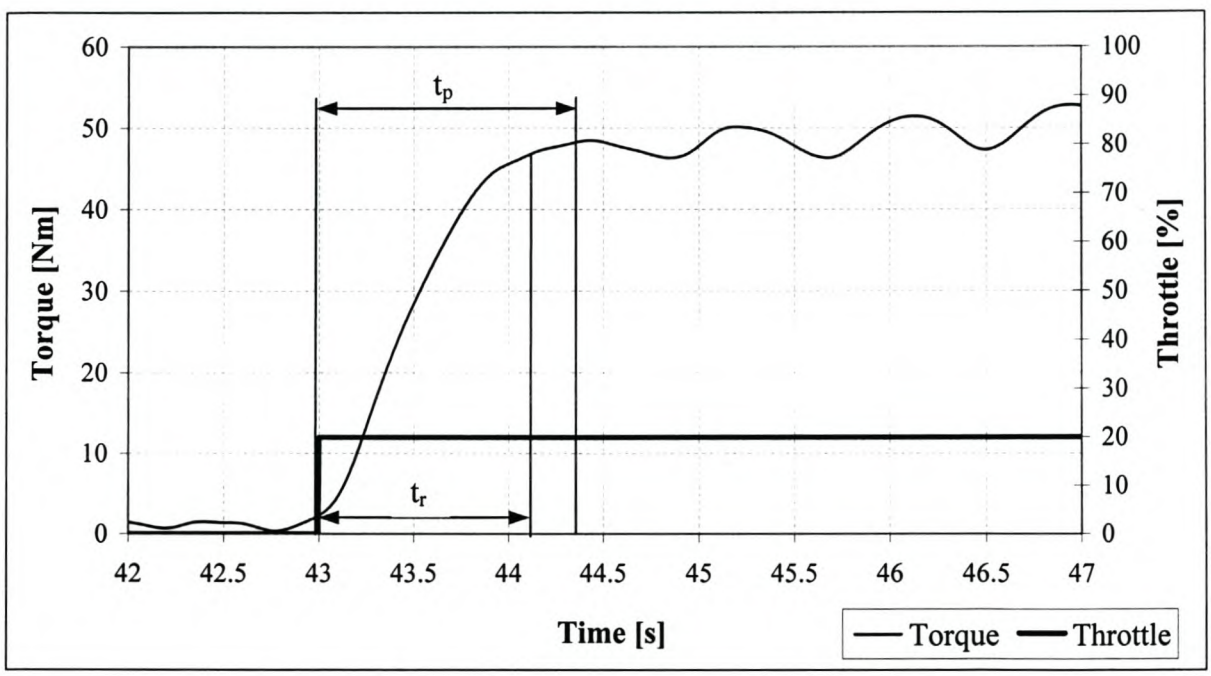

Figure 7.6. Engine response to step-input of throttle demand

Although it was difficult to determine accurately from the data sample above, values for the two parameters t_p and t_r were approximated to be:

$t_p \approx 1.5\,s$

$t_r \approx 1.2\,s$

These values would give one an idea of the transient characteristics of the system from which the bandwidth can be approximated.

From equation (7.5),

$$\omega_d = \frac{\pi}{t_p} = \frac{\pi}{1.5} = 2.094 \text{ rad/s}$$

From the data it is also seen that the system torque response was slightly under-damped. The damping ratio was thus initially taken to be approximately $\zeta \approx 0.9$. Similar damping ratios were found to apply for engines tested by Tuken et al. (1990). After some experimentation and model adaptations, a value of $\zeta \approx 0.8$ was found to correlate well with the observed data during the transition period. Figure 7.7 illustrates both modelled and actual engine data.

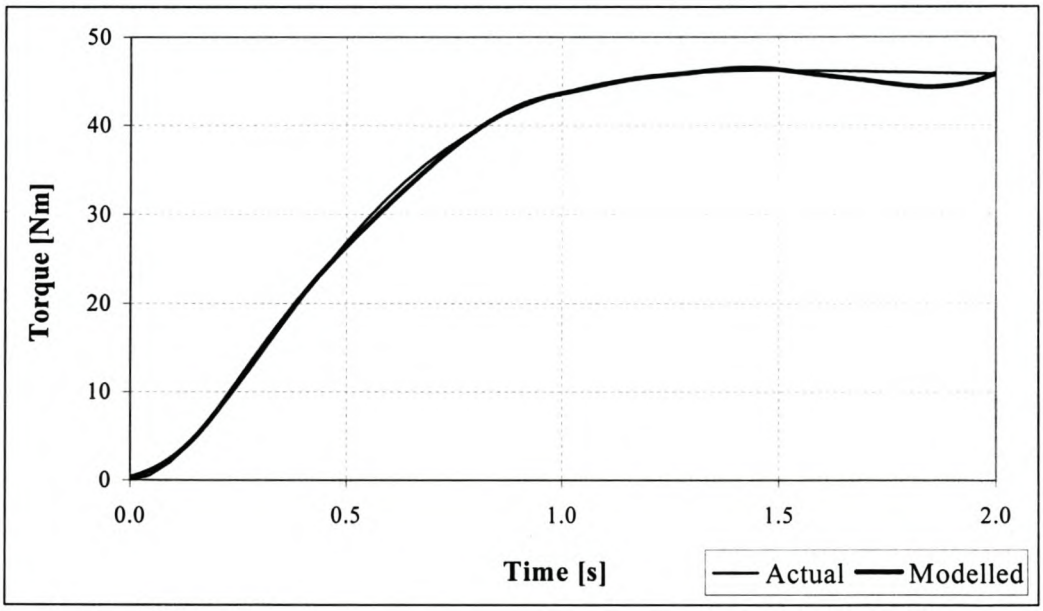

Figure 7.7. Actual versus modelled torque-throttle data

The natural frequency of the system was calculated from equation (7.4) to be:

$$\omega_n = \frac{\omega_d}{\sqrt{1-\zeta^2}}$$
$$= \frac{2.094}{\sqrt{1-0.8^2}}$$
$$= 3.491 \text{ rad/s}$$

With the natural frequency and damping ratio known, the bandwidth of the transfer function $G_{11}(s)$, sub-system #1 was calculated to be:

$$\begin{aligned}\omega_b &= \omega_n\left(1-2\zeta^2+\sqrt{4\zeta^4-4\zeta^2+2}\right)^{1/2} \\ &= 3.491\left(1-2\times0.8^2+\sqrt{4\times0.8^4-4\times0.8^2+2}\right)^{1/2} \\ &= 3.040 \text{ rad/s} \\ &= 0.484 \text{ Hz}\end{aligned} \tag{7.7}$$

$G_{11}(s)$ can thus be written in the form of equation (7.2) as:

$$G_{11}(s) = \frac{K\cdot 12.187}{s^2+5.586s+12.187}$$

$$\text{where the gain } K = \frac{45.5}{20} = 2.275$$

$$\text{thus } G_{11}(s) = \frac{27.725}{s^2+5.586s+12.187}$$

The maximum bandwidth of transfer function $G_{22}(s)$ in sub-system #2 was determined in Section 5.3.1 to be approximately 5.30 Hz for small oscillations and low speeds. Although it is plausible that the bandwidth of $G_{11}(s)$ may increase slightly with speed due to higher manifold gas speeds, it is clearly seen that the dynamometer bandwidth was the determining factor in choosing the sampling frequency. Ideally, a sampling frequency of between about 25 Hz and 50 Hz would be suitable for the specific system. In practice it was, however, found that an "in-the-loop" frequency limit of 20 Hz could be used for the sampling and writing out of data. By first sampling at 200 Hz and then re-sampling in-the-loop at 20 Hz, adequate resolution was obtained. The structure of these sampling loops will be discussed in full in Section 8.

7.3. ANTI-ALIASING FILTER

The importance of including anti-aliasing filters in any sampling process was discussed in Section 7.1. The design and evaluation of such a set of filters is now discussed.

7.3.1. Filter Design

The anti-aliasing filter is a low-pass analogue filter through which data is sampled prior to being digitised. The basic concept is to attenuate frequencies above the *Nyquist* frequency, thus allowing to pass through only signals with frequency content below half the sampling frequency. According to *Shannon's Sampling Theorem* these signals can then be uniquely determined and reconstructed by a digitisation process.

The filter design process was realised using Burr-Brown universal active filters (Burr Brown Corporation, 1993), which can be configured for a wide range of low-pass, high-pass, and band-pass filters. A DOS-compatible filter design programme was used for the implementation of the required filter type. It was decided to use 4^{th} order Butterworth filters for the attenuation of frequencies above 100Hz, half the sampling frequency of 200Hz. These filters provide the flattest possible pass-band magnitude response, with an attenuation of –3dB at the design cut-off frequency. Attenuation above the cut-off frequency is a moderately steep -80dB/decade/pole. The pulse response of the Butterworth filter has moderate overshoot and ringing.

The following parameters were chosen for the filter:

- Type : Butterworth
- Response : Low-pass
- Order : 4^{th}
- Cut-off frequency : 18 Hz (allowing for complete (99.9 %) attenuation at 100Hz)

Figure 7.8 shows the filter design programme's predicted filter performance in terms of gain and phase response. At the *Nyquist frequency* (100Hz) the attenuation is approximately –60dB. This means that the signal amplitude will be 0.1% of the original at that frequency, in practice prohibiting any frequency below the *Nyquist* frequency from passing through it. At the same time, the phase response at 100Hz is equal to –346.49°. This means that a sinusoidal input signal will be out of phase by nearly one whole

wavelength. Signals with a frequency of 18Hz are attenuated with –3dB, their amplitudes thus being 70.7% of the original. Below 18Hz signals are virtually unaffected, falling within the pass-band region of the filter. A schematic diagram of the filter and its power-supply layout can be found in APPENDIX C. The filter was next evaluated to determine whether it did indeed perform as was expected.

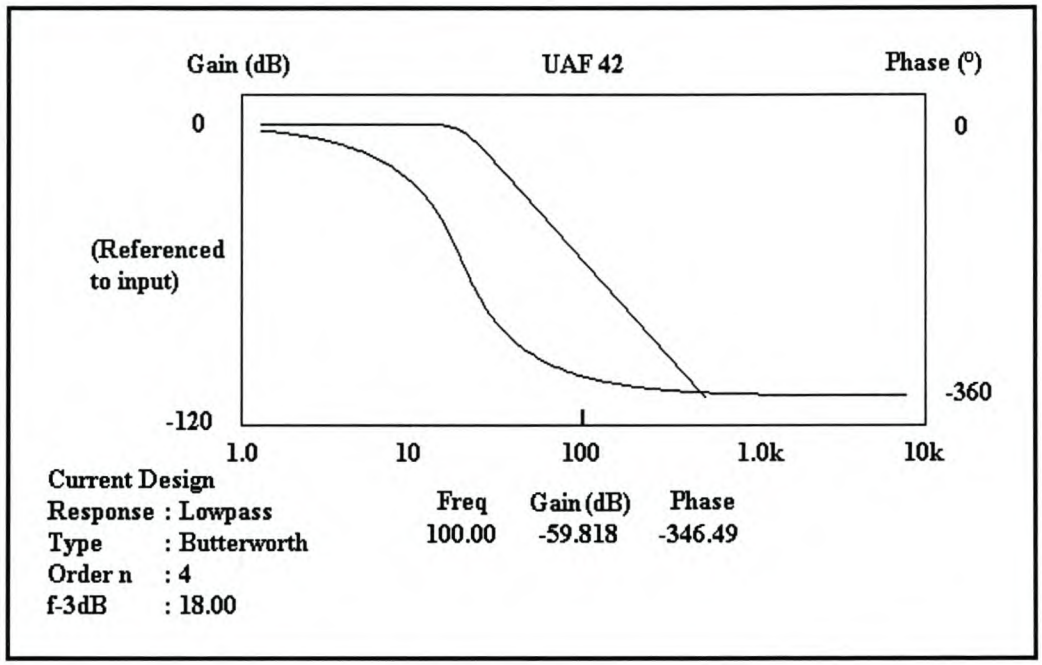

Figure 7.8. Anti-aliasing filter design parameters

7.3.2. Filter Evaluation

Evaluation of the anti-aliasing filter was performed to determine whether signals were attenuated with the required amount at the respective frequencies. The tests consisted of generating sinusoidal input signals of increasing frequency, while measuring the output signals. Input frequencies were swept between 0Hz and 500Hz while signals were recorded at 1 kHz using the Eagle Electronics board described in Section 5.5.1. Fast Fourier Transforms were performed on both input and output signals and amplitudes displayed on a decibel scale. The results of one such a sweep are shown in Figure 7.9.

Here it is seen that the filter did indeed have a cut-off frequency (-3dB) at approximately 18Hz, allowing any signal contents below this frequency to pass through the filter unaffected. It is seen that the attenuation increased steadily up to 100Hz, where it can be seen to be approximately -50dB, meaning that the output amplitude is about 0.3% of that

of the input. Although filter performance was not precisely as was designed for (partly due to the inaccuracy of the signal generated at higher frequencies), it did attenuate signals adequately at frequencies above the Nyquist frequency, thus preventing, or at least minimising, the occurrence of signal aliasing.

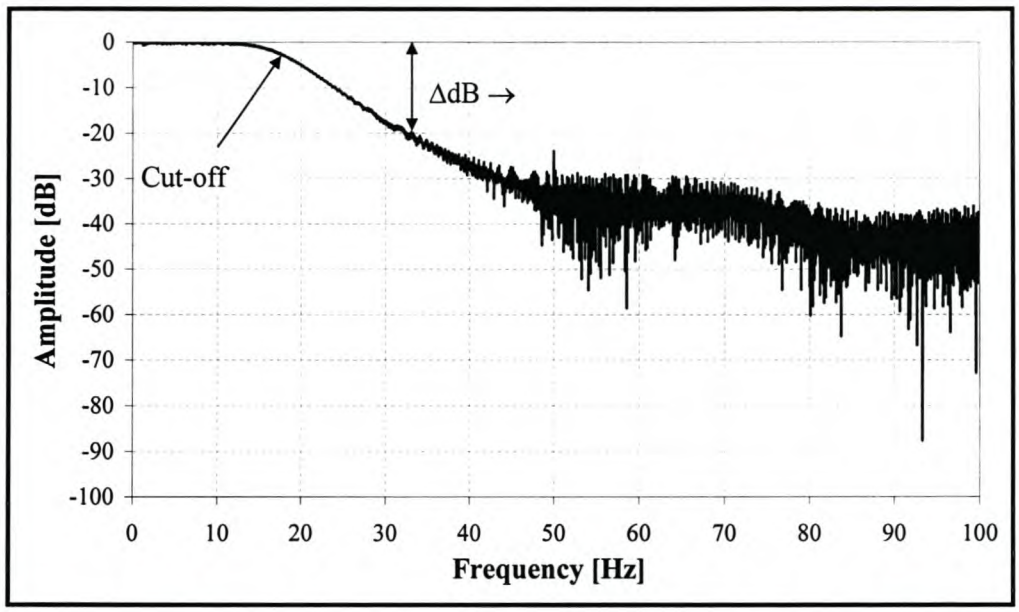

Figure 7.9. Dynamic response data of anti-aliasing filter

7.4. TORQUE SIGNAL ANALYSIS

Two signals were available from the test-bed, namely engine torque and dynamometer speed. Torque signal quality was an important consideration for the success of the project, as it determined the accuracy and repeatability of the simulation process. In order to determine the quality of the available torque signals, raw unfiltered torque data was obtained from a load-cell via a bridge amplifier by sampling at a frequency of 1kHz. At this sampling rate, all required information would be included in the sampled data, as was discussed previously. These signals were then analysed using Matlab (Version 5.1., The MathWorks Inc, 1997).

Figure 7.10 shows a typical torque signal recorded over 4096 samples. In this case the dynamometer was powered on but not turning, while the cooling fan was running. This sample in a way represented the nominal torque quality available from the system. The data set shown was de-trended, meaning that the sample mean, or average DC offset, was

subtracted from all the data points. This was done so that the DC component would not appear in the Fourier Transform, as this would only serve to confuse interpretation. The Fourier transform of the sample is seen in Figure 7.11. Here a dominant frequency can be clearly seen. An enlargement of the graph reveals it to lie at about 24.5Hz (see Figure 7.12).

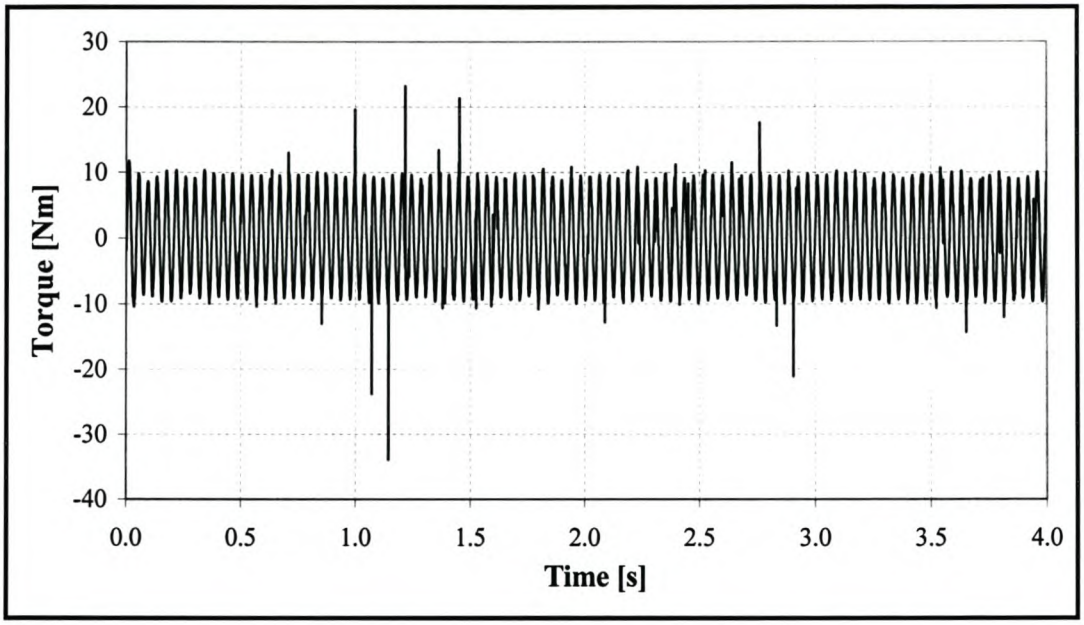

Figure 7.10. Torque sample – Dynamometer on, cooling fan on

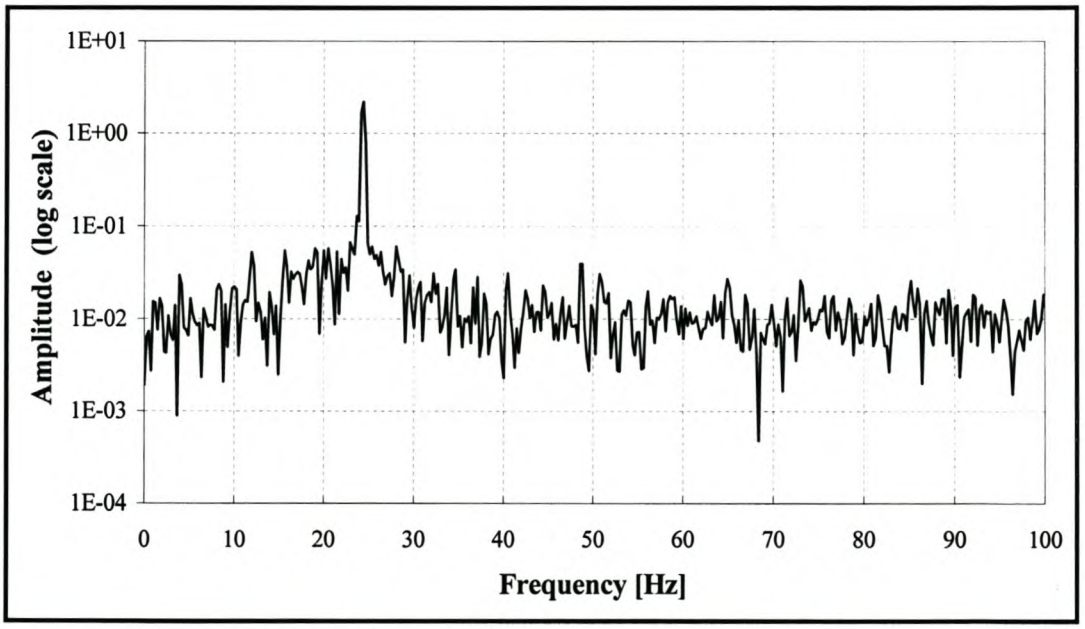

Figure 7.11. Fourier transform of torque sample

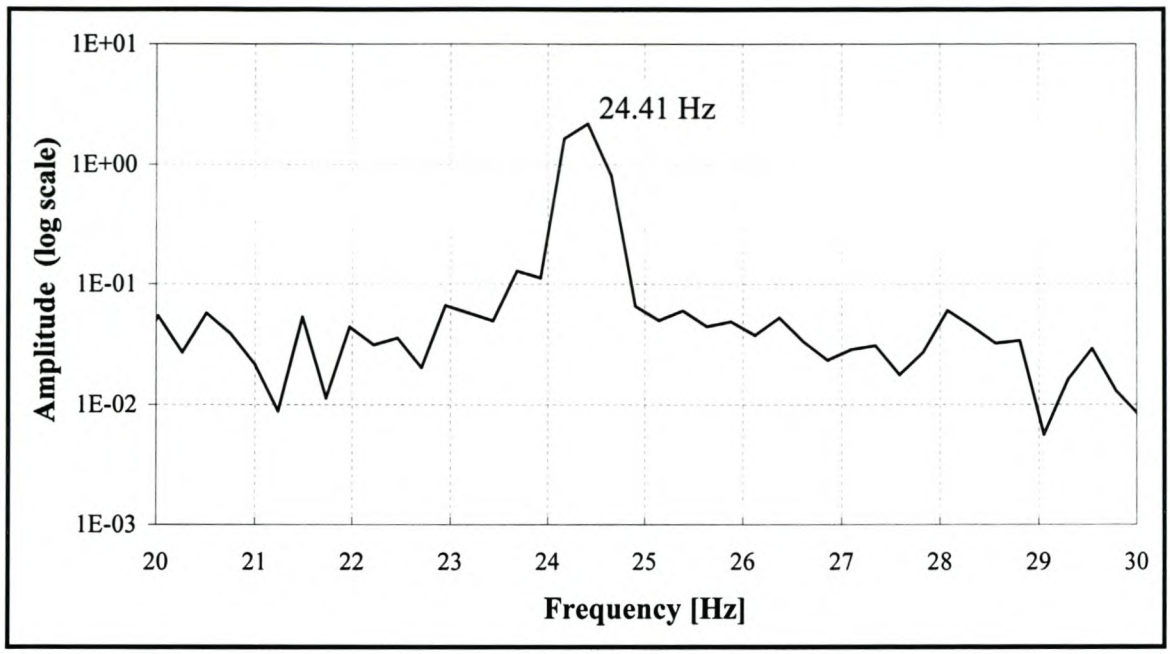

Figure 7.12. Fourier transform of torque sample (enlarged)

This dominant frequency content in the torque signal is clearly seen in an expanded view of the sample, as shown below in Figure 7.13. The standard deviation of this sample was 6.7383 Nm.

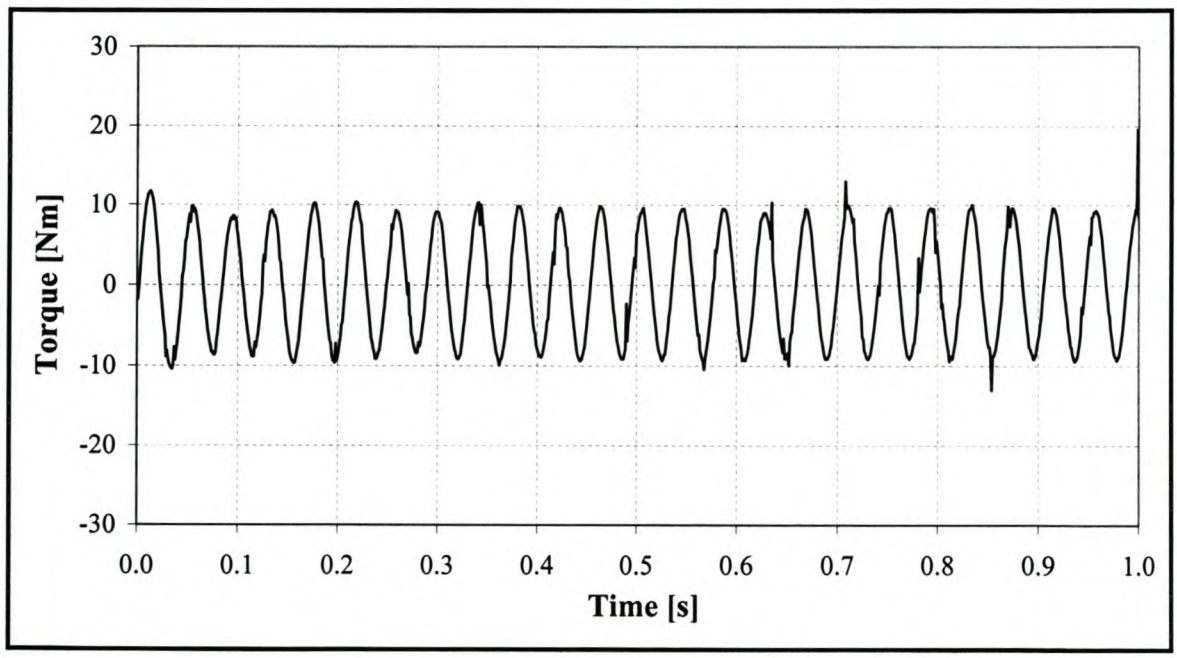

Figure 7.13. Expanded view of torque sample, showing dominant frequency content

This noise source was investigated and the cooling was identified as being the origin of the mechanical noise. This was further confirmed by the fact that the rated cooling fan speed of 1470 rpm ($\frac{1470\,\text{rpm}}{60} = 24.5\,\text{Hz}$) perfectly matched the detected sinusoidal torque frequency. Having established this, corrective action was taken. This involved the physical separation of the cooling fan from the dynamometer, using a rubber coupling to duct air into the motor frame, thus isolating the load-cell from the source of vibration. After having done this, the torque signal was already much cleaner. The absence of a dominant sinusoidal signal is seen in Figure 7.14, where the sample has a standard deviation of 0.5729 Nm.

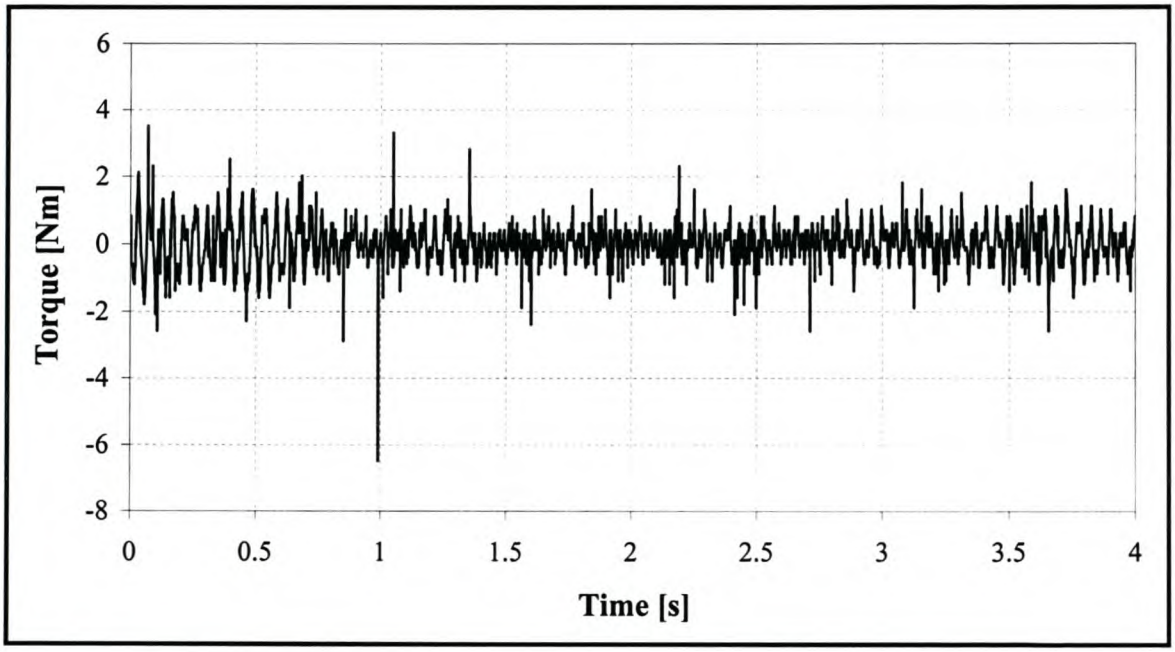

Figure 7.14. Torque sample with cooling fan on, but separated from the motor

An FFT taken of the signal, shown in Figure 7.15, indicates the presence of two dominant frequencies. These are seen to lie at about 22 Hz and just above 51 Hz (see Figure 7.16). They are both of much smaller magnitudes than was seen previously. The higher frequency content was probably due to the power supply to either the data card or the bridge amplifier, having a carrier frequency of 50 Hz. From this analysis it is seen that the torque signal quality was improved substantially by physically distancing the cooling fan from the DC motor.

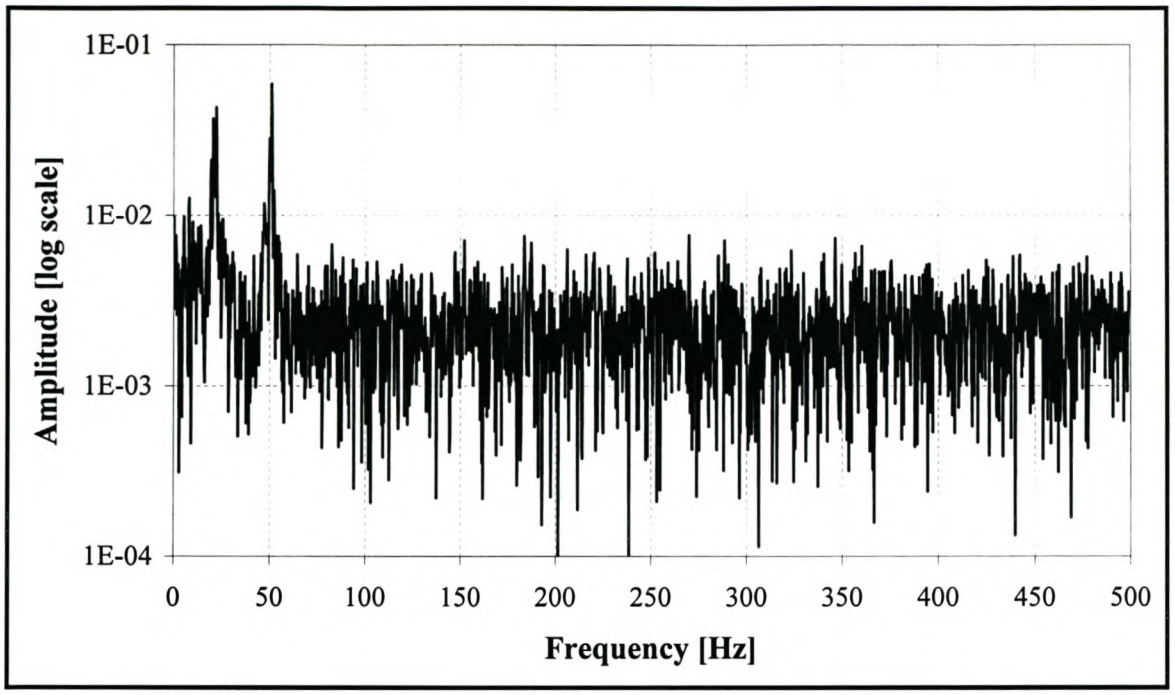

Figure 7.15. FFT of torque sample with cooling fan on, but separated from the motor

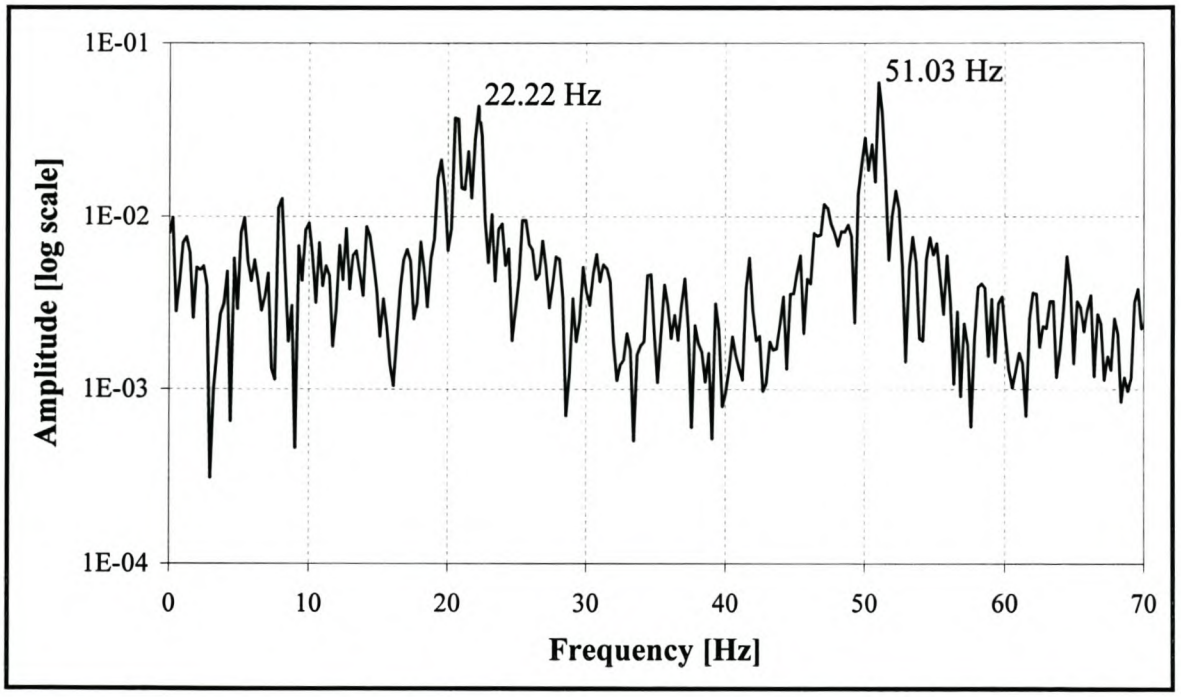

Figure 7.16. FFT of torque sample with cooling fan on, but separated from the motor (enlarged)

7.5. TORQUE CORRECTION AND SIGNAL DIFFERENTIATION

As was mentioned in Section 4.2.3, torque readings obtained from the load-cell did not represent shaft torque, but a combination of shaft torque and dynamometer reaction torque. This meant that the load-cell torque could not be used without modification for vehicle simulation purposes, but had to be dynamically corrected. This process is now described referring to Figure 7.17.

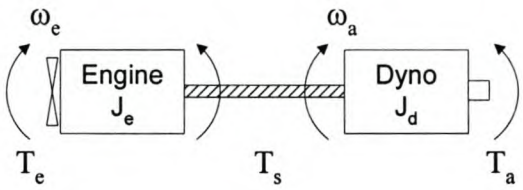

Figure 7.17. Torques relevant to dynamometer system

From Newton's Second law:

$$T_s - T_a = J_d \dot{\omega}_a$$

therefore

$$T_s = T_a + J_d \dot{\omega}_a \tag{7.8}$$

It is seen that the dynamically correct shaft torque can be calculated by equation (7.8). This torque would then represent the torque experienced by the shaft without being influenced by the dynamometer inertia during transient periods of operation. This torque correction process called for differentiation of the speed signal. Differentiation, by nature, amplifies high frequency signal contents, and thus also noise. This is clearly seen by looking at the frequency response curve of an ideal differentiator, shown in Figure 7.18. The amplitude of the differentiated signal is linearly proportional to the frequency of the signal content. Since noise usually contains high frequencies, once differentiated it leads to very high amplitudes of the resulting signal.

A means of keeping this amplification property of differentiation in place had to be investigated if signals of any practical value were to be obtained. Two of the more

common differentiating schemes were considered, together with another more unconventional approach.

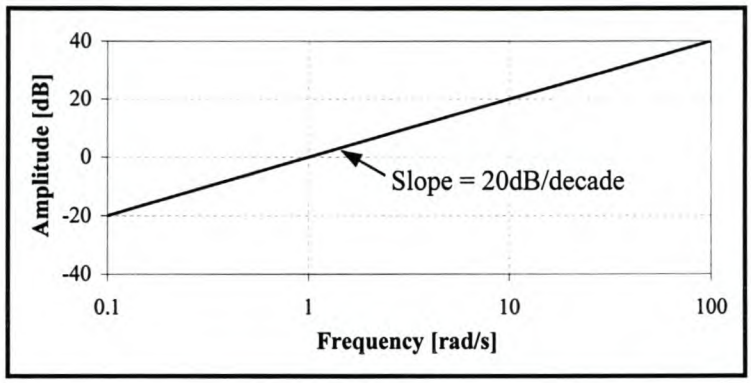

Figure 7.18. Frequency response of ideal differentiator

The most common approach to finding the derivative of a signal is to approximate the signal with an interpolating polynomial, the slope of which is then used as an approximation of the derivative of the original function (Gerald & Wheatly, 1989). In following this approach, the most basic method is to simply connect two adjacent points with a straight line, the slope of which yields the differential at that point. For the case when the derivative is required in real-time and only historic data is available, the derivative obtained by means of this process can be referred to as a *backward difference approximation*, and is given by:

$$f'(x_1) = \frac{f_1 - f_0}{h} + O(h) \tag{7.9}$$

in which h represents the time interval between two successive data points. The error is seen to be of the order $O(h)$, meaning that there exists some constant $K \neq 0$, such that if h is "small enough" and $h > 0$, then $|\text{Error}| \leq Kh^n$. The expression $O(h)^n$ is read "order of h to the n^{th} power". A further improvement to this method is called the *central-difference approximation*, in which a difference across three data points is used. The derivative obtained using this approach is given by:

$$f'(x_1) = \frac{f_2 - f_0}{2h} + O(h^2) \tag{7.10}$$

In this case it is seen that the error coefficient generated using this approach is also significantly smaller than that obtained using the backward difference method. Central-difference formulas are decidedly superior in calculating values for derivatives.

A third, more unconventional approach, was developed by Benedict and Bordner (1962) and was also investigated. In their approach, performance measures were described which realistically reflected both the noise-reduction and manoeuvre -following capabilities of a radar track-while-scan (TWS) system. Illustrations were given which compared various smoothing equations on the basis of the described performance measures. A set of position-and-velocity tracking equations were synthesised by a calculus-of-variations technique. The synthesised set is optimum for both position and velocity tracking within the given performance sense, in the class of all fixed parameter, linear tracking equations. The resulting optimally synthesised set characterises the commonly termed "α–β" tracker, with the important proviso that $\beta = \alpha^2/(2-\alpha)$.

The design necessarily compromises between the conflicting requirements of good noise-smoothing (heavy filtering, sluggish system, long time-constant, or narrow bandwidth) and of good manoeuvre-following or transient capability (light filtering, fast system, short time-constant, or wide bandwidth). The smoothing equations were constructed to give the "best" compromise between these requirements, with one *free parameter* left for adjusting the compromise. For every value of that parameter, noise smoothing is maximum for the given transient capability, and vice versa. The development described above led to the following set of optimal TWS smoothing equations:

$$\begin{aligned} \bar{x}_n &= x_{pn} + \alpha(x_n - x_{pn}) \\ \bar{\dot{x}}_n &= \bar{\dot{x}}_{n-1} + \frac{\alpha^2}{(2-\alpha)\Gamma}(x_n - x_{pn}) \\ x_{pn+1} &= \bar{x}_n + \Gamma\bar{\dot{x}}_n \end{aligned} \qquad (7.11)$$

In the above analysis, the optimum value of the single remaining parameter α is not specified, as this would be impossible. The choice of α is essentially one of bandwidth and must depend upon the system application. It can be shown that equation (7.12) reduces to the form of equation (7.9) for α=1.

The three methods discussed above were analysed and compared with one another based on sample data generated in Matlab. Normally distributed random noise was superimposed on a sinusoidal signal of increasing frequency up to the system bandwidth.

This signal was used for evaluating the differentiation techniques discussed above. This input signal is shown in Figure 7.19.

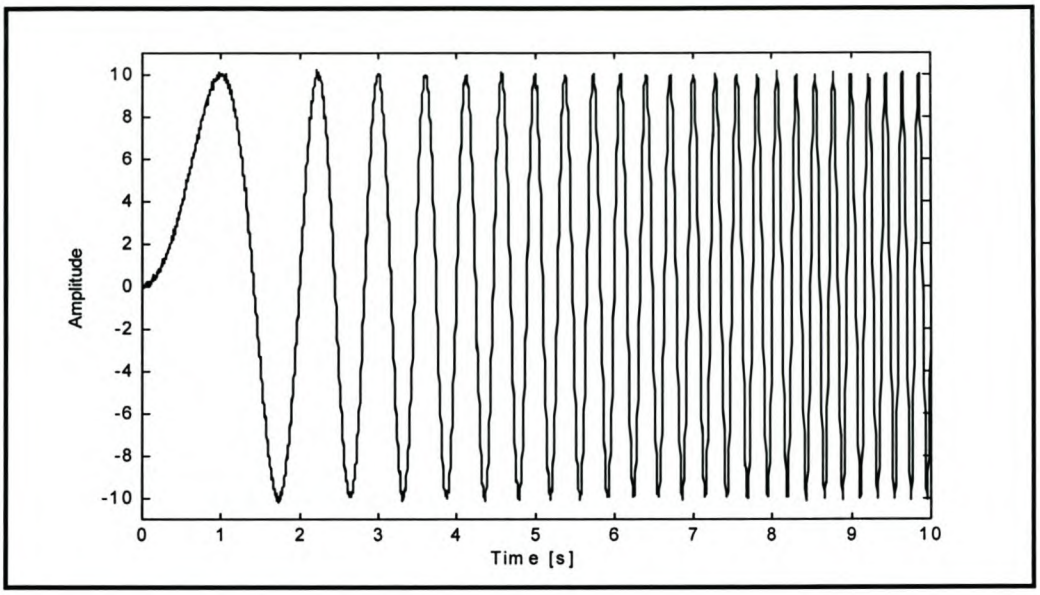

Figure 7.19. Sample signal used for differential evaluation purposes

The differentials obtained of the above signal, using the three methods described, can be seen in Figure 7.20. The free parameter (α) was chosen in such a way as to minimise the difference between the mathematical and numerical derivatives. These differences are shown in Figure 7.21.

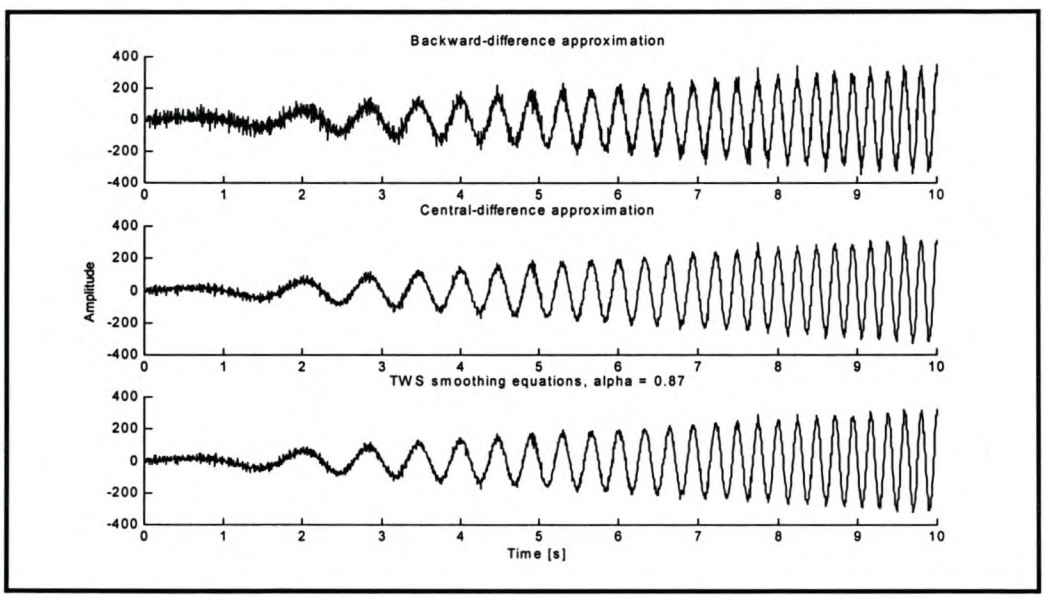

Figure 7.20. Differentials of sample signal using three methods

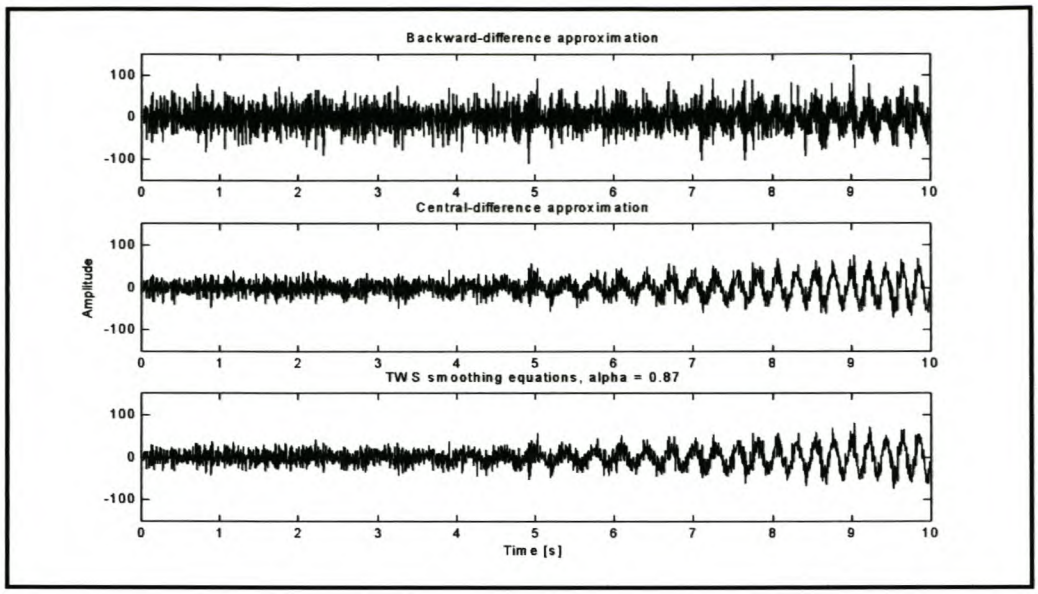

Figure 7.21. Differences between mathematical and numerical derivatives

Standard deviations of these differences, obtained using the three methods described, are shown below in Table 7.1.

Table 7.1. Standard deviations obtained using different differentiation methods

Method	Backward-difference	Central-difference	TWS smoothing equation ($\alpha = 0.87$)
Standard deviation	29.814	21.543	20.973

It is seen that both the central-difference method and TWS smoothing equations yielded far superior results to the backward-difference method, although the last two methods produced very similar results. This fact can also clearly be seen from Figure 7.21. The damping of the TWS method can be increased by decreasing the value of α. This will yield more accurate results at lower frequencies, but adds undesirable phase lag at higher frequencies, resulting in other difficulties during the torque correction process. For the system at hand it was decided to use the TWS smoothing equations approach for calculating signal derivatives, with an α–parameter equal to 0.87.

8. SOFTWARE DEVELOPMENT

In Section 2.3 of this document, system needs were identified and project objectives stipulated. These needs were further refined and developed in Section 3 using the functional analysis approach proposed by Blanchard and Fabrycky (1998). Knowledge gained during this process served as basis for the development of the software necessary to operate the system. With this in mind, the system was designed to perform two main categories of testing:

- To perform virtual-vehicle acceleration runs using different engine configurations, providing researchers with a real-time system using actual engine torque developed to do comparative studies on the effects of fuels, ignition timing, calibrations, exhaust back-pressure, etc.;
- To provide researchers with a driving cycle simulation system using manual throttle control to maintain the speed of a virtual-vehicle within the specified tolerances bands of a standard driving cycle.

In Section 5.5.3 the benefits of working in a Windows environment were highlighted. Windows NT was used because of its operational robustness and system integrity. Delphi 4.0 was chosen as programming language, mainly due to its ease of use and the author's familiarity with Borland Pascal, to which it is closely related. The programme developed for operating the system, *DynaSim*, can be subdivided into two main parts: that which did not occur in real-time (off-line processing), and that which did. Main programme structures and some of the more significant features are now discussed.

8.1. OFF-LINE PROCESSING

These elements of the programme consisted of blocks [1.0] and [12.0]-[15.0] as described by the functional analysis. Block [1.0] was concerned with the setup and configuration of the cycle to be run as well as the that of the virtual vehicle. Referring to Figure A.1.0 (APPENDIX A) the user was given the opportunity to load an existing cycle (block [1.2]) or to create a new cycle by entering new vehicle speed-versus-time node points (block [1.3]). When saving the new cycle, an algorithm interpolated between these node points,

determining demanded vehicle speeds at each point in time. These values were stored in a memory block record created for that point. Allowance was also made for entering information as specified in Section 3.1. The *DynaSim* cycle setup screen can be seen in Figure 8.1.

Tolerance bands were also calculated at each point (block [1.5]). These were based on the standard format specified by most regulating bodies and are necessary since human (or computer) driven vehicles cannot possibly follow a given speed profile exactly. Tolerances specified by the Economic Commission for Europe (ECE) are shown in Figure 8.2. From the figure it is seen that the vehicle speed to be achieved at any particular time t seconds has to be within 2 km/h of at least one of the speeds indicated for t-1, t, and t+1 seconds. In America and Australia, the FTP 75 Test cycle is used, and similar tolerance bands are defined, except that they allow for 3.2 km/h error margins while speed variations outside the prescribed tolerance are permitted provided that their duration is less than 2 seconds. Speeds lower than those prescribed are permitted provided that the vehicle is being operated at maximum available power.

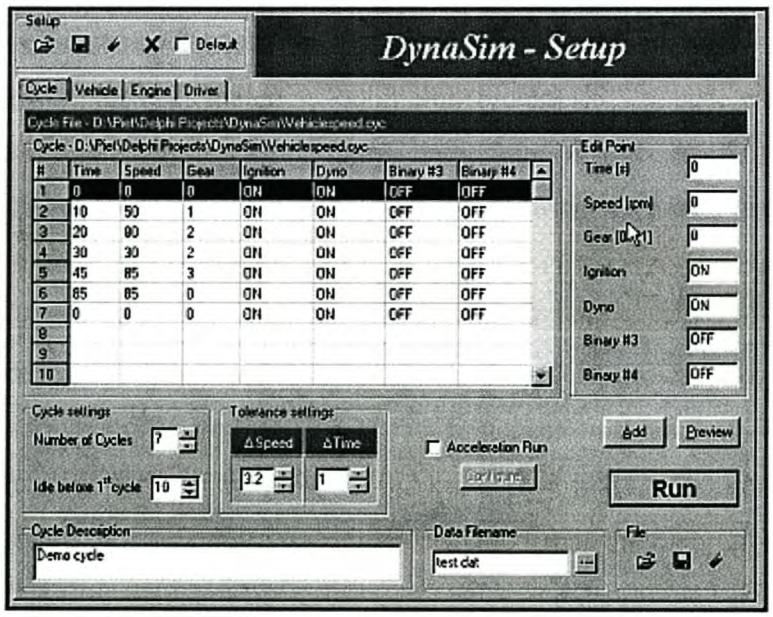

Figure 8.1. *DynaSim* cycle setup screen

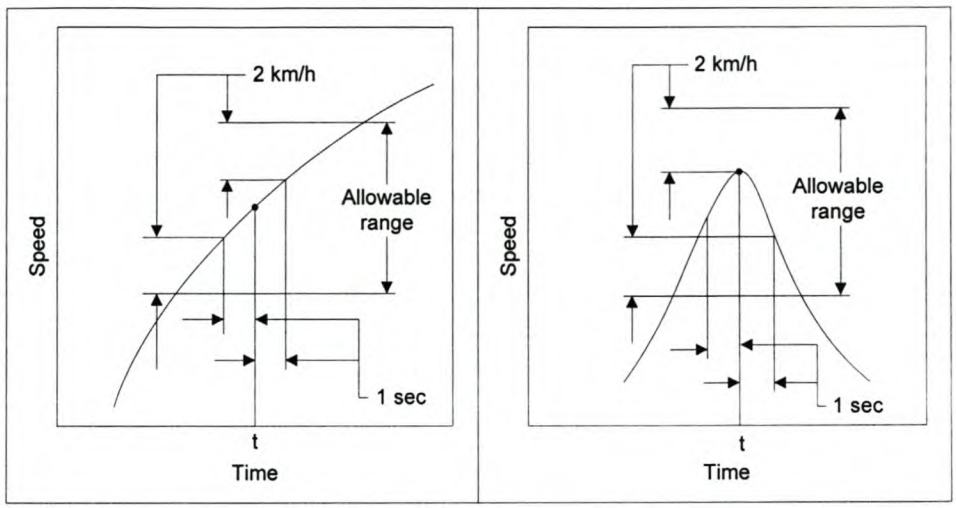

Figure 8.2. Cycle tolerances as specified by the ECE

Vehicle settings (block [1.6]) could be retrieved from a previously created file, created by editing an existing file, or created in its entirety. Allowance was made for entering all items specified in Section 3.1.1. of the functional analysis. Figure 8.3 shows the *DynaSim* vehicle setup screen in which the gear ratio editing page is seen. On the right hand side of the screen a graph visualised gear ratios by plotting vehicle speed versus engine speed. This made it easier to quickly see what effect changing a gear ratio would have on vehicle performance. Allowance was made for the entering of 21 gear ratios, thereby allowing for the simulation of large trucks.

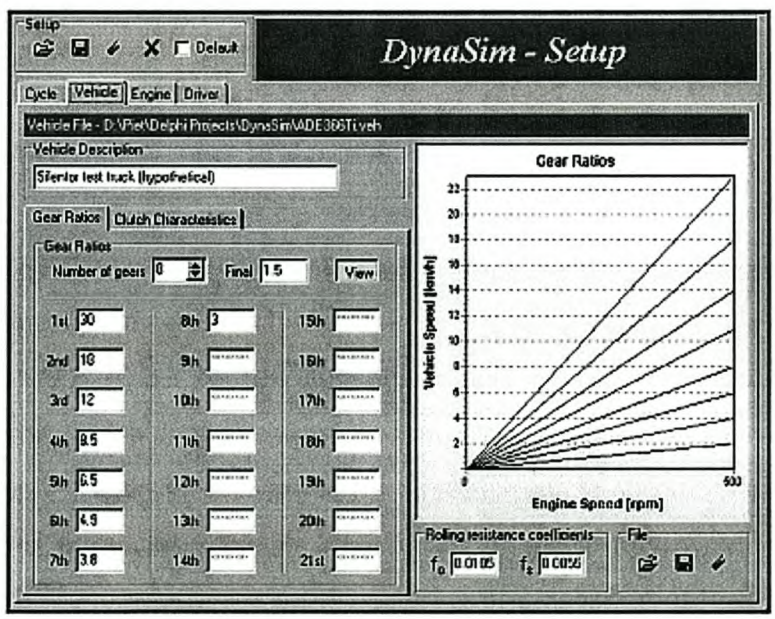

Figure 8.3. *DynaSim* vehicle setup screen: gear ratios

As part of setting up clutch characteristics, maximum positive and negative clutch torques had to be entered by the user. These torques were used to calculate the clutch torque transmitted during periods of clutch slip such as pull-away, gear shifts, and down-shifting. A characteristic clutch torque profile also had to be adjusted to suit engine and driver behaviours. By means of experimentation, it was found that the clutch torque profile during periods of engagement could be modelled satisfactorily by the following function:

$$T_c = \frac{C(e^{C\times x.xx})}{100(e^{100\times x.xx})} T_{cmax} \tag{8.1}$$

where C = percentage clutch travel.

The clutch setup screen, together with the clutch torque profile for with profile coefficient x.xx = 0.02 is seen in Figure 8.4.

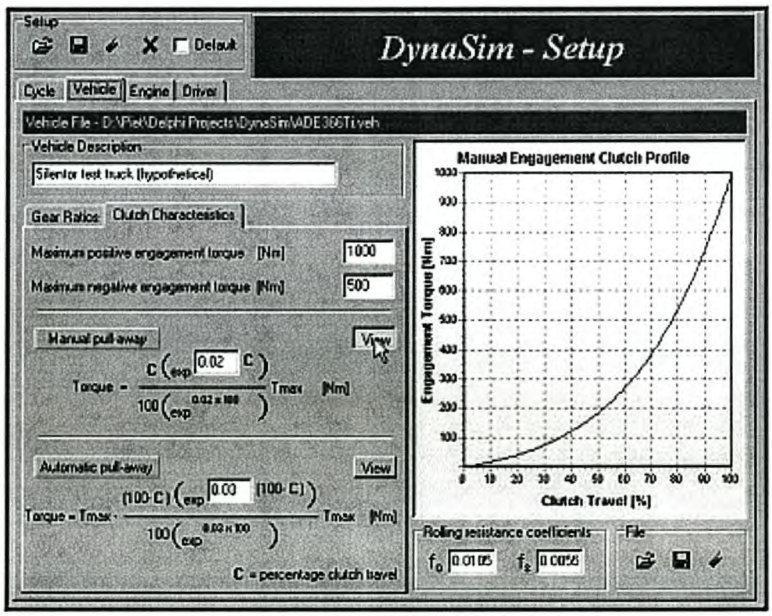

Figure 8.4. *DynaSim* vehicle setup screen: clutch characteristics

The engine setup section (block [1.7]) allowed for the opening, editing or creating of engine setup files. Allowance was made for the parameters specified in Section 3.1.1. Engine inertia was required for solving the dynamic equations of the simulation and was determined using the method discussed in Section 6.1. Maximum engine speed was required to ensure that the user could not accidentally over-speed the engine. This was realised by simply clipping the engine speed demand if it was above the maximum

allowable speed. Idle speed was required for motoring purposes after start-up, before the ignition was turned on and the cycle commenced.

The last of the setup pages allowed for setting up driver parameters (block [1.8]). Parameters allowed for are specified in Section 3.1.1. Manual and automatic gear shifting mode options were available. In manual mode, the driver determined in what gear the vehicle was at any given time. When in automatic mode, gear selection was determined by the gear selections programmed into the cycle (*cycle-mode*), or by the engine speed when operating in *free-style* mode. This feature, for example, allowed for the repeatable execution of acceleration runs with gear changes programmed to occur at specific engine speeds such as those where the engine develops its maximum torque or power.

An automatic pull-away option was included, configuration of which required of the user to enter the engine speed at which engagement was to commence, and the time over which the clutch would be fully released. This feature was intended to allow for repeatable pull-aways during the execution of acceleration runs, ensuring that data sets could be compared on an equal basis. Lastly, shifting times between individual gears had to be entered, both for up and down-shifting of gears. By entering these times between engagements, users could have some control over the way in which gear shifts would be conducted.

The above paragraphs described some of the off-line features of *DynaSim,* required before any real-time operations, described next, could be performed.

8.2. REAL-TIME VIRTUAL VEHICLE ENGINE

This section of the programme is what was referred to as the virtual vehicle simulation *engine* in Section 2.2 and consisted of blocks [2.0] to [11.0] of the functional analysis. Main tasks of this engine included the acquisition and conditioning of required input data, the manipulation of data and solving of equations, and providing output to the relevant subsystems of the facility. Providing this loop with an accurate time base initially proved to be quite difficult. The Windows system timer available to Delphi proved to be very inaccurate and inconsistent. This is due to the multi-tasking nature of Windows as the CPU has to share its resources between all menial operating system tasks, as well as any other running applications. Depending on the CPU load at any given time, the system

timer would vary greatly in its ability to provide an accurate time base from which to work. Another strategy had to be engineered as timing accuracy was important for such computations as the filtering, differentiation and integration of signals.

The decision was made to make use of the I/O board's onboard counters for this purpose. A polling strategy was used, by which a high-speed (2 MHz) counter's reading was obtained every time an outer loop was executed. This reading was compared with the previous reading in order to determine whether or not one sampling period (chosen as 0.05s, see Section 7.2) had expired since the last reading was taken. If this was the case, a high-frequency loop was entered into. If not, outer loop execution resumed at the maximum speed of which the computer was capable.

Using the above strategy, a more accurate time base could be established than was possible using the available system timer. Using this time base, program execution could repeatedly be redirected into a lower-frequency loop after a fixed period of time had elapsed. This polling strategy is illustrated in Figure 8.5.

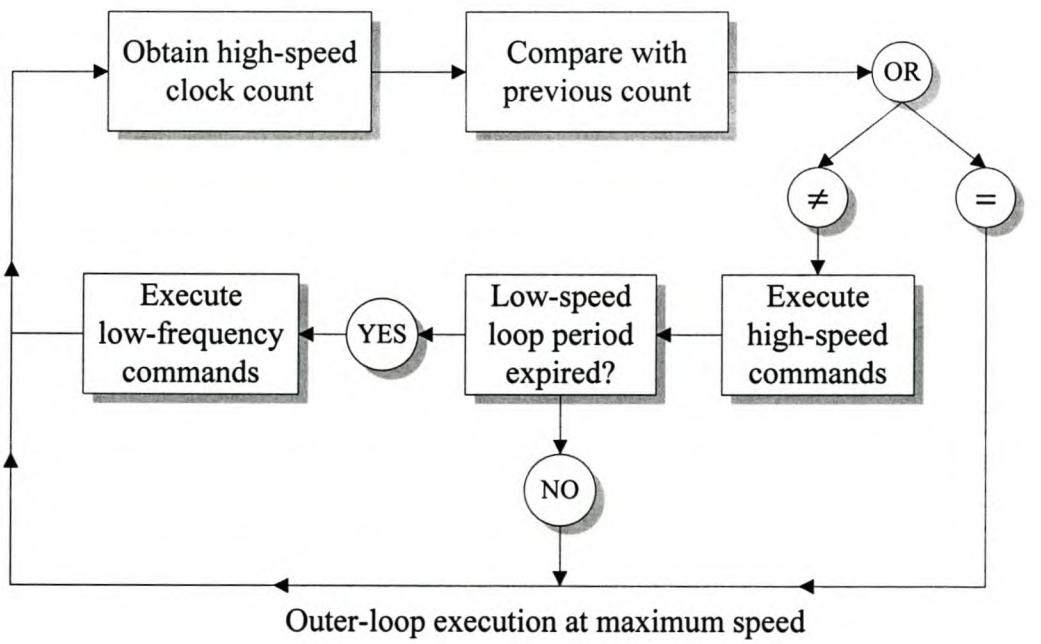

Figure 8.5. Polling strategy used as time-base

8.2.1. High-frequency commands

Having established the above structure, a sequence of high-frequency commands were executed each time the most recently obtained clock count reading differed from the previous one indicating that another clock period had expired. The following high-speed operations were executed consecutively inside the loop:

- Calculation of the total sampling time. This time was used in deciding whether to enter the low-frequency (20Hz) loop (see next section).
- Updating of clock count variable
- Obtaining the high-frequency speed and torque reading from the PC30GA
- Calculating the "exact" time period that has elapsed since the last clock counter reading was taken. This was achieved by obtaining the elapsed counter readings of a high-speed (8MHz) counter on the PC14B card and calculating the time by multiplying this reading by the known clock period. This period was used for differential calculation purposes.
- Implementation of digital filtering of the speed and torque signals. Once again Butterworth filters were used for these purposes because of the qualities mentioned previously. Digital implementation of the filter was realised using the following transfer function:

$$H(z) = \frac{B(z)}{A(z)} = \frac{b(1) + b(2)z^{-1} + ... + b(n+1)z^{-n}}{1 + a(2)z^{-1} + ... + a(n+1)z^{-n}} \tag{8.2}$$

  where vectors b and a were determined using the Matlab function *butter.m.* By rewriting equation (8.3) the following linear difference equation was obtained which could be readily incorporated into the computer algorithm:

$$y(t) = b(1)u(t) + b(2)u(t-1) + ... + b(n+1)u(t-n) - a(2)y(t-1) - ... - a(n+1)y(t-n) \tag{8.4}$$

- Implementation of the TWS filter on the speed signal (see Section 7.5).
- Updating of TWS and Butterworth filter variables.
- Performing of torque correction calculations (see Section 7.5).
- Recording of high-speed readings for analysis purposes.

8.2.2. Low-frequency commands

With the total sampling time known with the completion of every high-frequency loop, a decision could be made regarding when the lower- frequency loop was to be entered into. All data acquisition, manipulation and command generation calculations were performed in this loop at a rate of 20Hz. In order of execution these included:

- Advancing the time at which the low- frequency loop was to be triggered.
- Displaying the elapsed time in the status bar.
- Monitoring of the "END SAMPLING" button for cycle termination.
- Reading of the estimated dynamometer thyristor temperature for safety reasons.
- Reading accelerator, brake and clutch pedal inputs.
- Filter of the above inputs.
- Shifting of filter variables.
- Reading of "gearbox" buttons and determining requested gear.
- Display gear and clutch status on screen.
- Determination of rolling resistance.
- Determination of aerodynamic drag.
- Determination of braking torque.
- Calculation of vehicle load torque.
- Calculation of effective vehicle inertia (see Section 6.5).
- Calculation of vehicle response, depending on clutch mode. This process is described in Section 6.5.
- Creation/allocation of memory block depending on cycle mode (see Figure A.4.0).
- Updating memory block with latest information.
- Output throttle and speed demands.
- Output dynamometer temperature reading to screen.
- Updating of engine and vehicle speed, throttle, brake and clutch positions to screen.
- Updating of graph.

9. POSSIBLE CONTROL STRATEGIES INVESTIGATED

Included in the system requirements specification was the need to operate the system under complete computer control during the execution of standard emission cycles (indicated as block [7.0] in Figure A.0.). Various dynamic test-bed control schemes have been developed and implemented over the last two decades, some with more success than others. These range from the most common type, namely, PID control, to state-of-the-art robust multivariable control as described by Bunker et al. (1997). These attempted to independently control engine speed and torque in such a way as to simulate load conditions as would be experienced on the road. The reason for the inclusion of this section is to investigate control approaches that had been developed by various authors and implemented with varying success in similar test systems, the intention being the future implementation of a suitable control strategy in the system under.

When developing a control system there are various aspects to consider. These include what type of controller to implement and how this is to be achieved. The type and complexity of the system that is to be controlled plays a major part in determining how to solve the control problem. If the system is such that a mathematical model of it can be derived from first principles, or obtained using a *"black box"*, or system identification method, it is possible to employ any one of a number of well established design techniques in designing a controller for the system. Controller parameters can then be calculated to meet the transient and steady-state specifications required by the customer. If, however, the system is too complex for a model to be readily obtained, an analytical approach to the design of a controller is not possible. Various experimental techniques have been developed to deal with such cases.

9.1. PID CONTROL

Proportional-plus-integral-plus-derivative (PID) controllers are by far the most common types of controllers used in industry. This is partly due to their suitability to many control applications, their low cost, and the ease with which they can be configured. These controllers combine the actions of proportional, integral and derivative control and have

the advantages of each of these three control actions. The control actions are briefly described below.

For a controller with ***proportional control action***, the relationship between the output of the controller u(t) and the actuating error signal e(t) is

$$u(t) = K_p e(t) \tag{9.1}$$

or, in Laplace-transformed quantities,

$$\frac{U(s)}{E(s)} = K_p \tag{9.2}$$

where K_p is termed the *proportional gain.* The proportional controller is essentially an amplifier with an adjustable gain.

In a controller with ***integral control action***, the value of the controller output u(t) is changed at a rate proportional to the actuating error signal e(t). That is,

$$\frac{du(t)}{dt} = K_i e(t) \tag{9.3}$$

or

$$u(t) = K_i \int_0^t e(t)dt \tag{9.4}$$

where K_i is an adjustable constant. The transfer function of the integral controller is

$$\frac{U(s)}{E(s)} = \frac{K_i}{s} \tag{9.5}$$

If the value of e(t) is doubled, the value of u(t) varies twice as fast. For zero actuating error, the value of u(t) remains stationary. The integral control action is sometimes called *reset control.*

In a controller using ***derivative control action***, sometimes referred to as *rate control*, the magnitude of the controller output u(t) is proportional to the rate of change of the actuating error signal e(t). That is,

$$u(t) = T_d \frac{de(t)}{dt} \tag{9.6}$$

or in Laplace-transformed quantities

$$\frac{U(s)}{E(s)} = T_d s \tag{9.7}$$

Here T_d is an adjustable constant called the *derivative time*. The derivative time T_d is the time interval by which the rate action advances the effect of the proportional control action. The derivative control action has an anticipatory character. As a matter of course, however, derivative control action can never anticipate any action that has not yet taken place. While derivative control action has the advantage of being anticipatory, it has the disadvantage that it amplifies noise signals and may cause a saturation effect in the actuator. Also note that derivative control action can never be used by itself because this control action is effective only during transient periods.

Proportional-plus-integral-plus-derivative control action combines the above types of controllers. The equation of a controller with this combined action is given by

$$u(t) = K_p e(t) + \frac{K_p}{T_i}\int_0^t e(t)dt + K_p T_d \frac{de(t)}{dt} \tag{9.8}$$

the transfer function given by

$$\frac{U(s)}{E(s)} = K_p\left(1 + \frac{1}{T_i s} + T_d s\right) \tag{9.9}$$

where K_p is the proportional gain, T_i is the integral time, and T_d is the derivative time. The block diagram of the proportional-plus-integral-plus-derivative controller is shown in Figure 9.1, while the controller response to a unit input can be seen in Figure 9.2.

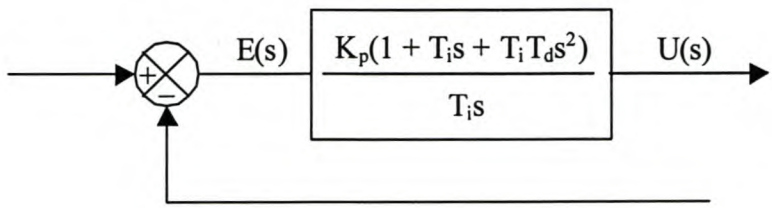

Figure 9.1. Block diagram of the PID controller as part of a system

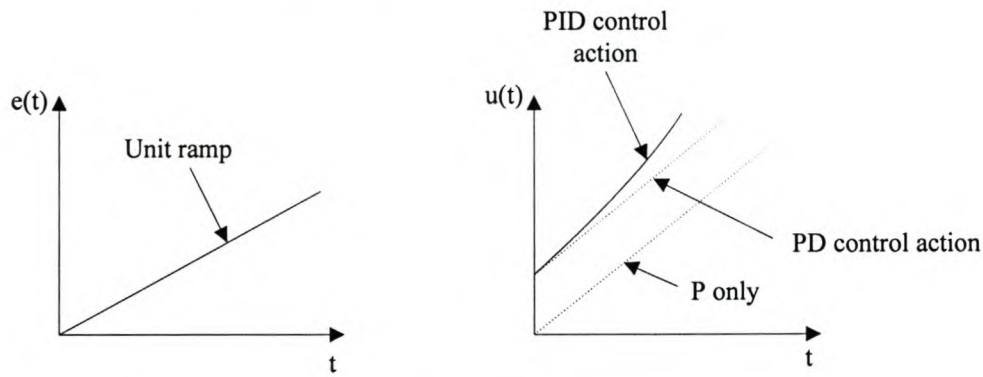

Figure 9.2. Unit ramp input and PID controller output

For systems of which mathematical models can be derived, it is possible to apply various design techniques for determining parameters of the controller that will meet the transient and steady-state specifications of the close-loop system. If, however, the plant is so complicated that a mathematical model for it cannot be obtained, then an analytical approach to the design of a PID controller is not possible. In these cases one must resort to experimental approaches to the design of PID controllers. This process of selecting controller parameters to meet given performance specifications is known as *controller tuning*. One such method, the *Ziegler-Nichols rules for tuning PID controllers* (Ziegler & Nichols, 1942), is widely used in industry and can be implemented on site by engineers. It is based on experimental step responses or based on the value of K_p that results in marginal stability with only the proportional control action being used. *Ziegler-Nichols rules* are very convenient when mathematical models of plants are not known, but can also be applied to the design of systems with known mathematical models. The reader is referred to Ogata (1990) for a discussion of the theory and application of the *Ziegler-Nichols rules*.

Germane and Heaton (1980) have successfully applied the discrete equivalent of the continuous PID controller for the independent control of speed and torque of a bench-mounted internal combustion engine. Their reasoning for choosing this type of controller was that an adequately detailed model of their engine-dynamometer was not available (and would be extremely complex had it been) and that the chosen controller required little knowledge of the dynamic characteristics of the process under control. True adaptive control was accomplished by recognising the non-linearities of the engine-dynamometer system and performing the necessary control scheme modifications. A block diagram of the system is shown in Figure 9.3.

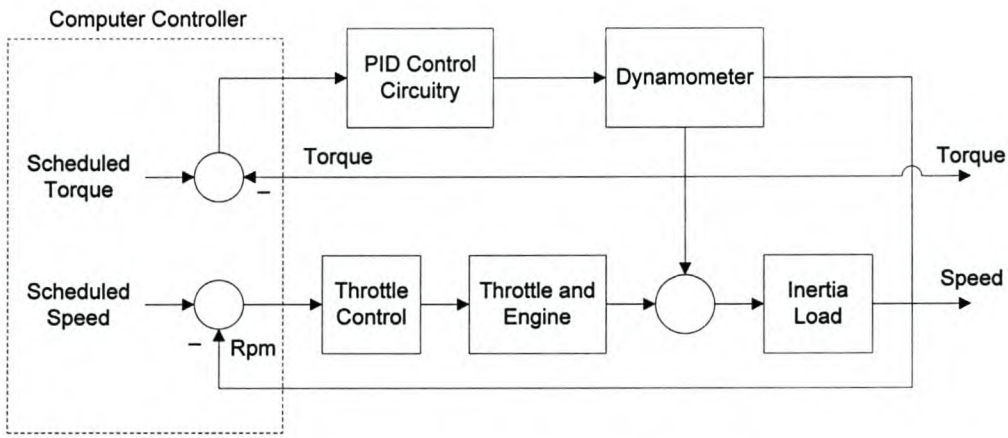

Figure 9.3. Block diagram of PID controlled test-bed (Germane & Heaton, 1980)

Monk and Comfort (1970) identified the internal combustion engine as a first order system with a time delay, and found the time delay to be inversely proportional to the engine speed. The authors ran several tests on the engine at various dynamometer loads to determine its response to a step input in throttle position, and at various speeds to observe the response to a step change in dynamometer command. The system appeared to be of the first order with a time delay, but a functional relationship of the time delay in terms of dynamometer setting and the throttle actuator signals could not be determined. Also, the slope of the response curve, which is a tuning parameter according to the *Ziegler-Nichols* analysis, could not be correlated to the dynamometer load and engine throttle position.

These facts prompted them to use a simplified technique (Roberts et al., 1974) for single parameter tuning of discrete PID control algorithms, which combines that of Ziegler and

Nichols with others. This technique can be used for direct digital control with the following difference equation:

$$C_n = C_{n-1} + K_c(2.45e_n - 3.50e_{n-1} + 1.25e_{n-2}) \tag{9.10}$$

where C_n is the new command signal for the throttle or dynamometer controller, C_{n-1} is the previous command signal, K_c is the proportional throttle or dynamometer gain constant ($K_{c(th)}$ for the throttle controller and $K_{c(dy)}$ for the dynamometer controller), and e_n, e_{n-1} and e_{n-2} are the differences between engine speed and desired speed, or dynamometer torque and desired torque, for two previous time steps. Only the proportional gain constants need to be determined on line. These constants were experimentally determined for both the throttle position and the dynamometer current control. The authors obtained their best results with a throttle and dynamometer constant which were based on the rate of change of the scheduled speed and torque, and the actual speed of the engine.

Since a first order system lags a ramp input by one time constant, the authors added a feed-forward element to the scheme by implementing the adjustment in throttle gain up to four seconds prior to a ramp input. Also, a modified integral control was added whereby an additional throttle correction ΔC_n was made which was proportional to the sum of the present and past errors:

$$\Delta C_n = K_i(e_n + e_{n-1} + e_{n-2}) \tag{9.11}$$

where K_i is an integral gain constant which was experimentally determined ($K_{i(th)}$ for the throttle controller and $K_{i(dy)}$ for the dynamometer controller) for the throttle and dynamometer controller. The actual command signal was that value from equation (9.10) plus the contribution from the additional integral control from equation (9.11).

The determination of the PID proportional and integral gain constants for the throttle and dynamometer controller took the form now described. Initially, the approximate value of the PID constants were found experimentally. The system was operated under proportional control, and the preliminary value was determined for a one-half second delay between control demands. In their particular case it was found that, at low engine speeds, the system was more sensitive to throttle and dynamometer command changes. The system required additional gain to follow a ramp input, and the required gain was roughly

proportional to the slope of the speed or torque schedule. The speed effect together with the slope were implemented to calculate the throttle and dynamometer PID gain constants.

For throttle control, the relationship was found to be

$$K_{c(th)} = 0.02 + 0.025(\text{rpm} - 1000)/700 + (0.00005)(\text{slope})$$

where *slope* had the units of rpm per second.

For dynamometer control, the relationship was

$$K_{c(dy)} = 0.3 + 0.5(\text{rpm} - 1000)/700 + (0.1)(\text{slope})$$

where *slope* had the units of foot-pound per second.

The integral gain constants were calculated simply as a function of the slope:

$$K_{i(th)} = 0.09 + (0.00001)(\text{slope})$$

for the throttle controller, and

$$K_{i(dy)} = 0.25 + (0.008)(\text{slope})$$

for the dynamometer controller.

These gain constants were calculated and updated prior to each calculation and output of the control commands to the throttle and dynamometer, which occurred every one-half second during a test run. Throttle and torque controller performances were evaluated with both modifications (feed forward and integral) implemented. A test cycle, including abrupt changes in engine speed, was run. The effects of both modifications to the throttle control brought the engine speed to within an average of 2% of the scheduled value.

Further tests were conducted in which the engine was operated with sinusoidal torque and speed schedules of a range of amplitudes and frequencies. Generally the amplitude ratio increased from unity for the higher frequencies used, but only slight phase shifts could be detected. For the torque variations used, the actual torque followed the desired torque within 2% of the scheduled values. The throttle control for these tests caused the engine to operate within 30 rpm of the 2000 rpm set point for each cycle.

9.2. PDT_L CONTROL

As part of their research, Pfeiffer and Isermann (1993) developed a strategy for controlling the simulated road speed of a virtual vehicle powered by a physical engine mounted on a dynamic testing facility. This contrasts with the strategy discussed above in which the aim was to independently control engine speed and torque. The system now being described was very much targeted towards the execution of standard emission cycles, the objective being to follow a prescribed vehicle speed profile, and thereby indirectly control engine speed and torque. A block diagram of the closed-loop vehicle speed control concept is illustrated in Figure 9.4.

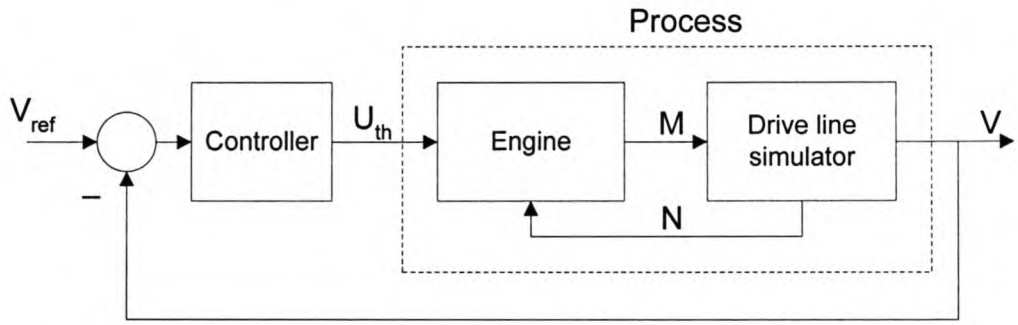

Figure 9.4. Vehicle speed control concept

For the cycle under consideration the controller input was the difference between the reference and the simulated value of vehicle velocity, the controller output being throttle position. This was the case no matter whether velocity control was achieved using a human driver or computer. In designing a feedback velocity controller, it was necessary to obtain a parametric model of the system, consisting of the real engine and the drive line simulation. The authors observed that the transfer-function of this process (G_s), with the accelerator pedal as input and vehicle velocity as output value, generally had an integral behaviour. Differences between linear integral behaviour and that observed was attributed to the non-linearity of the diesel engine being considered, the governor playing a dominant role at higher engine speeds. In the Laplace-domain, the process was approximately given by:

$$G_s(s) = \frac{K_i}{s} \qquad (9.12)$$

in which the process parameter K_i could be determined from the linear part of the step response, and depended on the transmission ratio. The following performance criteria were defined for the closed-loop controller:

- no control difference at steady-state
- fast operation of the controller by variation of the reference velocity
- smooth changes of the manipulated variable (accelerator pedal)

In order to avoid a permanent control difference at steady-state conditions, an control system must contain an integrator in the loop. The integral behaviour of the system at hand was considered to be sufficient to avoid such a permanent control difference. Fast controller action can be achieved if a differential (D) component is included in the control algorithm. Pfeiffer and Isermann considered a PD control algorithm to be insufficient as a driver simulator because of limited controller output. This motivated them to design and implement a PD control algorithm incorporating a time lag T_l component (PDT_l controller). In the Laplace-domain, the PDT_l control algorithm was given by

$$G_c(s) = K_c\left(1+\frac{T_d s}{1+T_l s}\right) \tag{9.13}$$

The process parameters K_c and lag times T_l obtained for a four-speed passenger vehicle are shown in Table 9.1.

Table 9.1. Process parameters for PDT_l controller (Pfeiffer & Isermann, 1993)

gear	K_c	T_l
1	9.28	0.1077
2	5.58	0.1792
3	3.68	0.2717
4	2.54	0.3932

Stability conditions for the controller were determined from the root locus by looking at the characteristic polynomial of the closed-loop

$$D(z) = z^2 + d_1 z + d_0 = 0 \tag{9.14}$$

from which the poles could be determined to lie at

$$z_{1/2} = -\frac{d_1}{2} \pm \sqrt{\left(\frac{d_1}{2}\right)^2 - d_0} \tag{9.15}$$

Constrained by the discrete-time closed-loop stability criterion

$$|z| \leq 1 \tag{9.16}$$

the stability conditions for the controller parameters were given by

$$K_c \geq 0 \tag{9.17}$$

$$K_c \leq \frac{2}{T_0/T_1} \tag{9.18}$$

$$\frac{T_D}{T_1} \leq \frac{2}{K_c \cdot T_0/T_1} \tag{9.19}$$

where T_0 is the sampling time.

These conditions resulted in a stability area of the velocity closed-loop controller, as shown in Figure 9.5. The critical controller gain was determined by the ratio T_0/T_1. A variation of the sampling time T_0 also resulted in a reduction or expansion of the stability area.

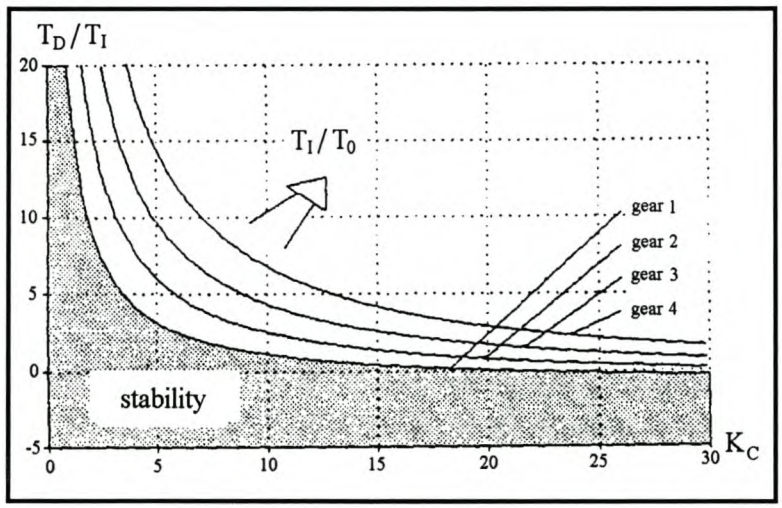

Figure 9.5. Stability area of the velocity control loop with PDT_1 controller (Pfeiffer & Isermann, 1993)

Theoretically, the closed loop was to reach the limit of stability for a ratio $T_D/T_1 = 1.0$ ($T_D/T_0 = 10.7$) at $K_c = 0.955$, but practically the limit of stability was reached at $K_c = 2.0$, see Figure 9.6.

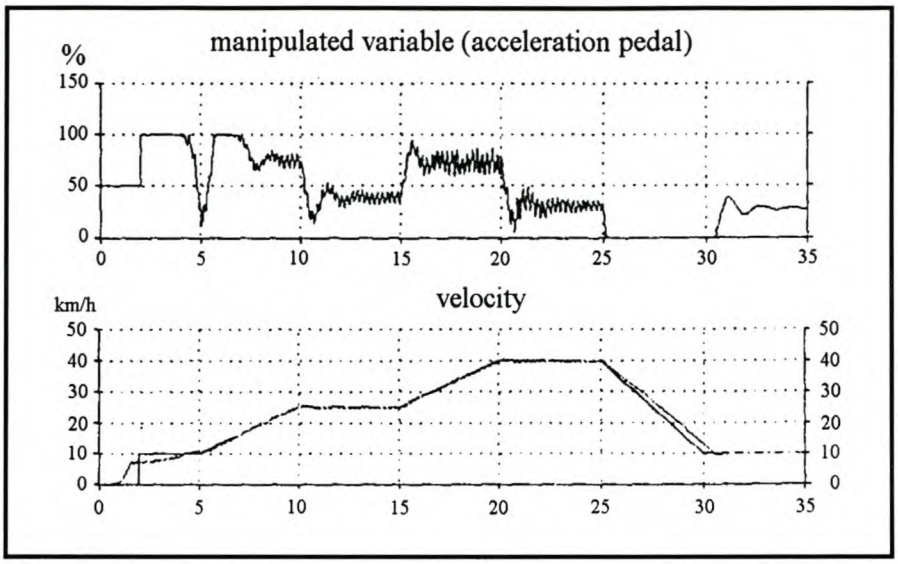

Figure 9.6. PDT_1 controller with $K_c = 2$ at stability limit (Pfeiffer & Isermann, 1993)

The difference between the theoretical and practical stability of the closed loop was ascribed to the inexact identification of the process parameter T_1. It was found that to obtain a stable system, the margin between the controller gain K_C and the stability limit had to be significant. A suitable value for the controller gain was reached at $K_C = 1.0$. The controller behaviour using this setting is seen in Figure 9.7. The reference following behaviour is seen to have been reasonably good, a variation of the reference signal nevertheless provoking an oscillatory operation of the manipulated variable. These oscillations are seen to be asymptotic stable.

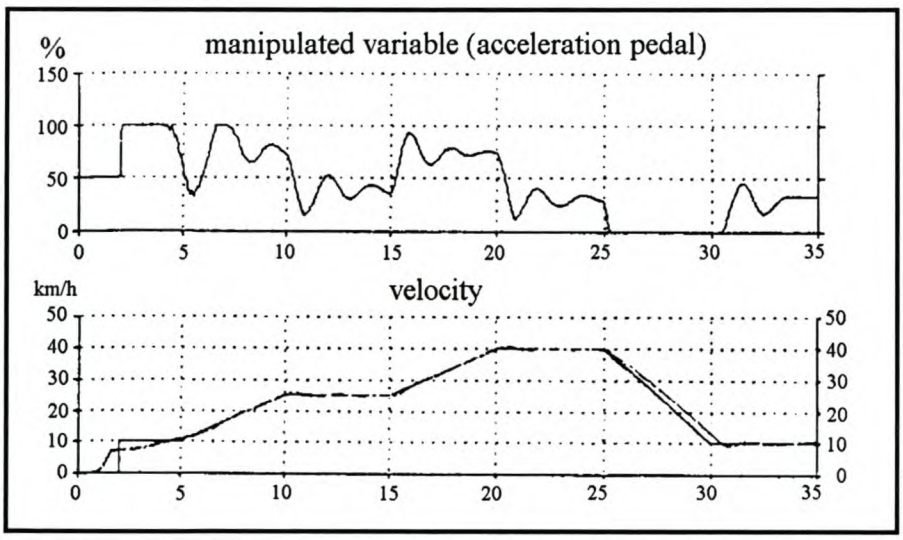

Figure 9.7. PDT_1 controller with $K_c = 1.0$ (optimised controller parameters) (Pfeiffer & Isermann, 1993)

Pfeiffer and Isermann considered the above controller to be unsuitable as a driver simulation for exhaust emission tests since it provoked abnormally high exhaust emissions due to the oscillatory nature of the accelerator pedal. It was concluded that the PDT_1 controller would have to be modified so that the manipulated variable trend would be damped. A normal human driver who is not trained in driving exhaust emission cycles, needs much practice to drive these test cycles with the required degree of control performance. It is more difficult for humans to follow "synthetic" velocity profiles than to follow the daily traffic. Human drivers have the advantage of a more *a priori* knowledge regarding future reference velocity values than the presented PDTl controller. Therefore a trained human driver brings about a smoother operation of the manipulated variable than the presented controller. The operation of a trained human driver is seen in Figure 9.8.

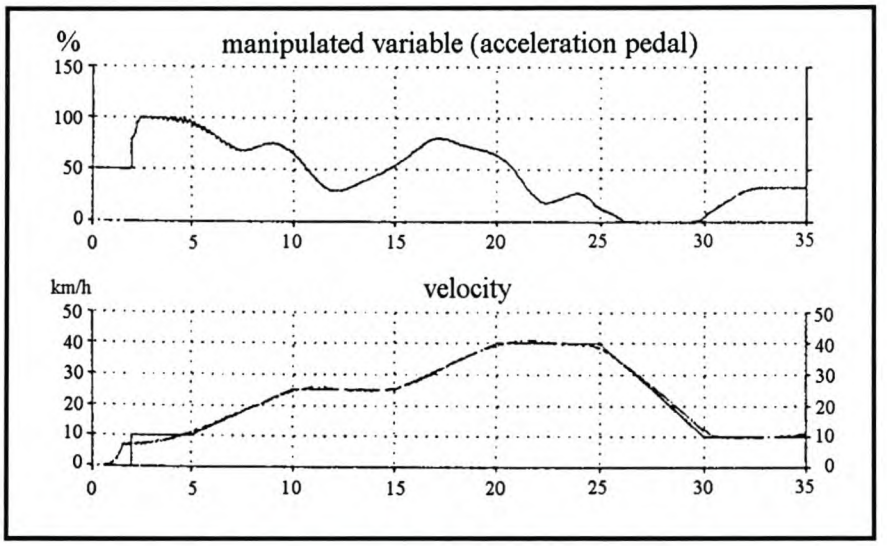

Figure 9.8. Vehicle velocity profile obtained by a human driver (Pfeiffer & Isermann, 1993)

The authors concluded that a smoother behaviour of the manipulated variable could be obtained by:

- predictive filtering of the reference value for an optimised PDT_1 controller
- predictive control concepts
- other control concepts with neural networks or fuzzy logic

It was also noted that a proper feedback controller for the brake pedal as second manipulated variable needed to be designed in order to make the driver simulation as intelligent as a trained human driver.

9.3. POLE ASSIGNMENT & PREDICTOR

Tuken et al. (1990) developed a digital controller capable of following the EPA transient test cycle using a turbo-charged diesel engine direct-current dynamometer testing facility. A simplified mathematical model for the throttle-torque system was developed, while off-line parameter identification algorithms were used to find the model parameters. The controller design was carried out using a closed-loop *pole assignment* technique. Since the model included a time delay, a *Smith predictor* control scheme was included in the design. Feed-forward control was added to the Smith predictor to counteract load disturbances caused by speed variations of the engine. Transient engine tests showed that the Smith predictor with feed-forward disturbance rejection gave transient cycle performance well within the specifications of the EPA. Main elements of their research will now be discussed.

As an initial step in their research, Tuken et al. developed mathematical models for the throttle-torque system, as this would tell them how the engine would react to throttle changes. In order to do this they developed model structures of the individual sub-components of the system, i.e. the electro-mechanical actuator, the governor, and the engine combustion dynamics. By using input-output data obtained from open-loop step response tests, model parameters could be estimated using a parameter identification method. Previous research performed by Kuo (1979), in which he detailed the dynamic modelling of a permanent-magnet motor, resulted in him developing a third-order non-linear dynamic model to describe the input-output relation of the step motor. After linearisation and performing Laplace transforms, it was discovered that a linear third-order dynamic model plus a time delay, due to the microprocessor and driver unit, adequately approximated the step-motor performance. Mathematical modelling of the governor revealed that, in the constant speed case, a second order dynamic model represents the relationship between fuel rack position and the fuel rate that goes into the engine. The transfer function for the engine combustion system was found as:

$$\frac{G_e(s)}{q(s)} = K_e e^{-T_F s} \tag{9.20}$$

in which $G_e(s)$ was the engine combustion output, $q(s)$ the fuelling rate, K_e a combustion constant and T_F the firing delay.

The input-output relationships of the above sub-systems were all shown to be non-linear. However, around some operation conditions, these equations could be linearised by Taylor series expansion and written in the familiar Laplace transformed forms. As a result, the open-loop system representation could be depicted as shown in Figure 9.9.

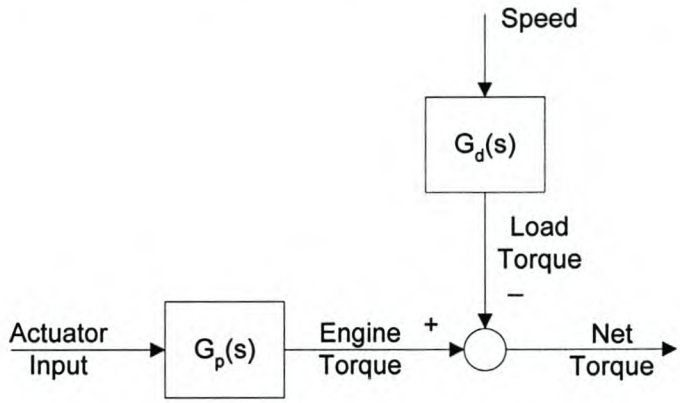

Figure 9.9. Simplified open-loop representation of the throttle torque system (Tuken et al., 1990)

In Figure 9.9, the transfer function $G_p(s)$ represents the fifth-order dynamics of the plant, consisting of the actuator, governor, and combustion process. The transfer function $G_d(s)$ represents the second-order dynamics caused by the speed controller and the dynamometer. To find the parameters of the overall linearised plant and disturbance transfer functions shown in Figure 9.9, the authors performed extensive step response tests over all operating conditions were performed. Two groups of tests were conducted. In the first group, the engine speed was held constant by the dynamometer controller, while the response of the system to a step input of the throttle actuator was observed. This test was repeated for ten different speed regions to see the variations of the system parameters. In the second group of tests, the throttle position was held constant while the system response to a change in speed was observed. This test was also performed for ten different throttle positions to investigate the parameters variations.

Tests in the first group gave rise to the parameters of the throttle-torque system when no load disturbance was present. Tests in the second group provided the parameters of the interactive speed-torque disturbance system. An off-line continuous-time parameter identification algorithm employing the *Poisson Moment Functional* (PMF) approach was used to find the parameters of the open-loop plant and the disturbance transfer functions.

The following average pole locations over the operating range of the engine were found for open-loop plant and disturbance transfer functions (TF) by the PMF method:

Plant TF Poles	Disturbance TF Poles
$s_1 = -1.88 + 0.89j$	$s_1 = -1.86 + 1.45j$
$s_2 = -1.88 - 0.89j$	$s_2 = -1.86 - 1.45j$
$s_3 = -9.3 + 0.4j$	
$s_4 = -9.3 - 0.4j$	
$s_5 = -12.4$	

From the parameter identification, the authors found that that only s_1 and s_2 were dominant in the system response, and therefore, for simplicity, the plant model was estimated by second-order dynamics plus a time delay transfer function. The parameters of the reduced order transfer functions were found thus:

$$\hat{G}_P(s) = \frac{8.4e^{-0.4s}}{s^2 + 3.76s + 4.34} \tag{9.21}$$

$$\hat{G}_d(s) = \frac{1.3e^{-0.4s}}{s^2 + 3.73s + 5.60} \tag{9.22}$$

Since the system was actually non-linear, the parameters of the plant and disturbance transfer functions varied depending on the operation conditions. These variations are shown in Table 9.2.

Table 9.2. Pole locations for variations of plant and disturbance transfer function

Plant TF	Disturbance TF
$(s_{1-2})_{max} = -2.02 \pm 0.60j$	$(s_{1-2})_{max} = -2.08 \pm 1.61j$
$(s_{1-2})_{min} = -1.61 \pm 1.06j$	$(s_{1-2})_{min} = -1.46 \pm 1.40j$
$Gain_{max} = 8.7$	$Gain_{max} = 1.41$
$Gain_{min} = 7.9$	$Gain_{min} = 1.08$
$Time\ delay_{max} = 0.5$	$Time\ delay_{max} = 0.5$
$Time\ delay_{min} = 0.3$	$Time\ delay_{min} = 0.3$

In systems having significant time delays, conventional delay-free control methods may not lead to satisfactory performance. In these cases, Smith's method has some powerful advantages. A block diagram representation of Smith's method is shown in Figure 9.10.

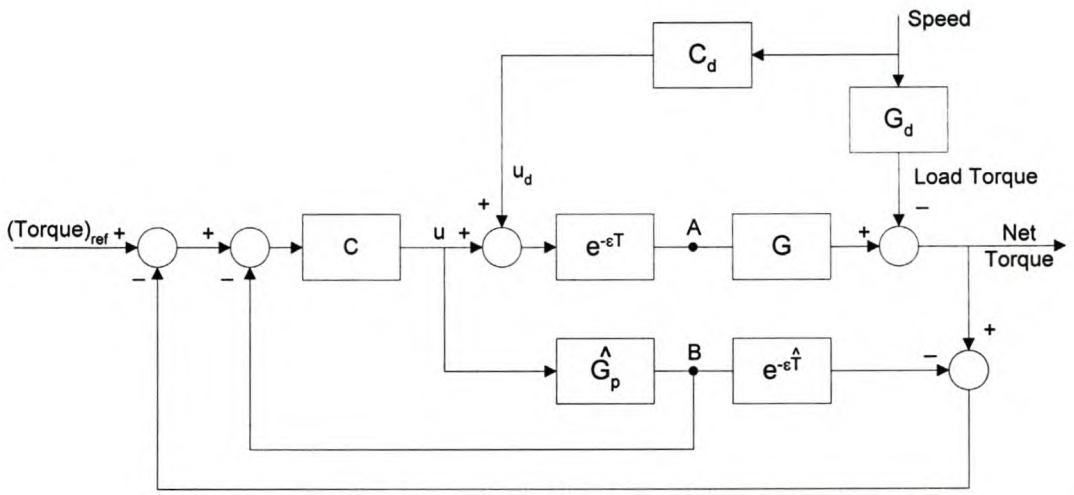

Figure 9.10. Smith predictor for diesel engine torque control (Tuken et al., 1990)

In this figure, C is the delay free controller, C_d is the disturbance compensator, G an G_d are the delay free parts of the plant and disturbance transfer functions, and T is the time delay. The models of G_p and T are shown as $\hat{G}_p$ and $\hat{T}$. The control signal u is delayed by T seconds before it affects the output. During this initial period of time, the controller cannot influence the output. However, the point B, a predicted version of the output signal, can be used as a feedback signal. Thus, controller design can be carried out using classical methods for delay-free systems. Therefore, specifications of system performance can be given in the familiar delay-free terms.

The second outer loop is included because of the possible mismatch between G and $\hat{G}$, and T and $\hat{T}$. Removal of the outer loop gives open-loop control, which makes no use of output information and can lead to inferior performance in practice. Since load disturbance does not appear explicitly in Smith's method, a feed-forward compensator, C_d, was added to the Smith design. In order to meet the EPA's performance specifications, the following time-domain specifications were established:

- Settling time equal to or less than 1 second since reference torque values were specified with 1-second intervals.
- Little or no overshoot
- Zero or minimum steady-state error.

Controller design was carried out in the discrete-time domain. Using a sampling frequency of 5 Hz, the plant and disturbance transfer functions were first converted to discrete time transfer functions using the Z-transform. This yielded process yielded the following results:

$$\hat{G}_p(z) = \frac{0.17z + 0.12}{z^2 - 1.22z + 0.39} \tag{9.23}$$

$$\hat{G}_d(z) = \frac{0.02z + 0.02}{z^2 - 1.71z + 0.74} \tag{9.24}$$

Tuken et al. made use of a lead-lag controller in order to meet the time-domain performance specifications. The lag controller was designed with a pole at unity, providing for integral action, as this would ensure zero steady-state error for a constant reference torque input. The controller transfer function was:

$$C(z) = \frac{az^2 + bz + c}{(z + d)(z - 1)} \tag{9.25}$$

Taking advantage of the properties of the Smith predictor, both the feed-forward and feedback controller were designed without including the time delay. Figure 9.11 shows the closed loop system for the Smith predictor.

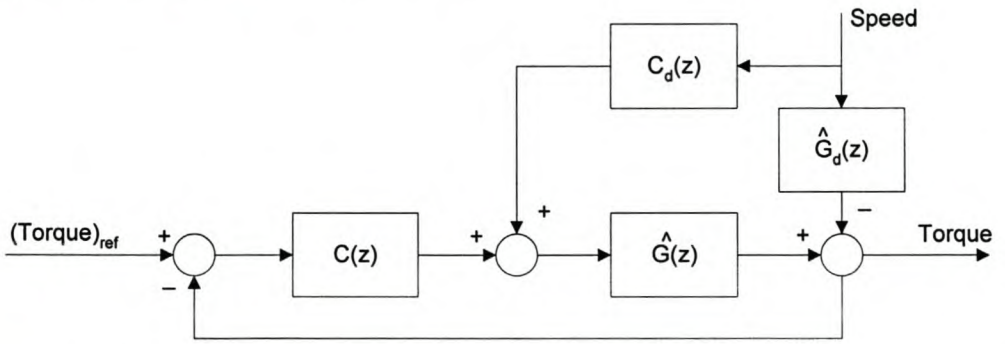

Figure 9.11. Closed-loop Smith predictor for the design of delay-free controller (Tuken et al., 1990)

The parameters a, b, c, and d of the controller transfer function were determined by using a closed-loop pole assignment technique. Load disturbance was also compensated for via a feed-forward controller. In order to cancel the disturbance dynamics of the closed-loop system, the feed-forward controller was selected as:

$$C_d(z) = \frac{\hat{G}_d(z)}{\hat{G}(z)} \tag{9.26}$$

In order to evaluate their research, the controller described above was implemented and 24 transient engine test cycles carried out over a period of three days by Tuken et al. Reference and observed values obtained during one such cycle are shown in Figure 9.12.

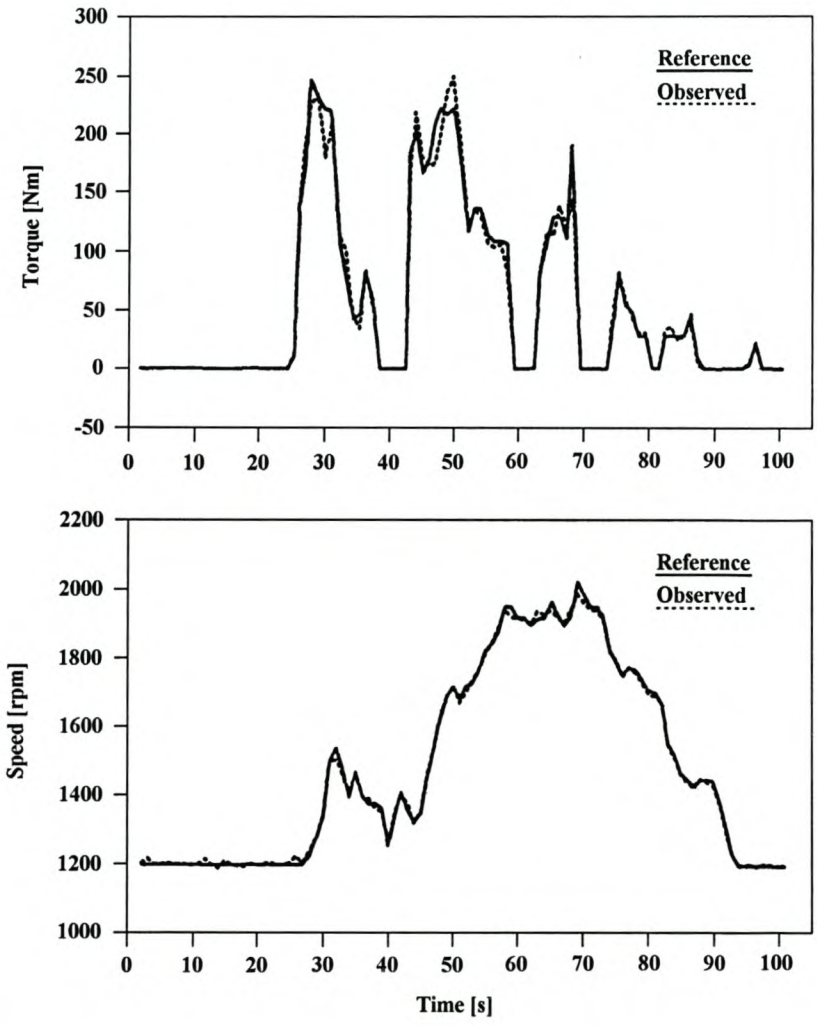

Figure 9.12. Comparison of actual speed and torque values vs. reference values (Tuken et al., 1990)

The authors observed that actual torque values followed reference values closely, with some offsets during acceleration and deceleration. Since the disturbance was compensated for with a fixed feed-forward controller, there was a mismatch between plant and disturbance transfer function model coefficients and their actual time-varying values. This was what gave rise to offsets in the transient response. Of the 24 tests that were conducted, 22 were found to be valid according to EPA specifications. The authors concluded that the transient test cycles showed that the digital controller with a Smith predictor performed acceptably over a wide range of operating conditions and met the test validity criteria specified by the EPA. Possibilities for future studies were mentioned by the authors and will be the next topic of discussion.

9.4. ADAPTIVE CONTROL

As part of their research into transient engine, Fullmer et al., (1992) applied adaptive control techniques to the problem of diesel engine torque control. Three strategies were tested and compared with one another: self-tuning control with one-shot parameter identification and controller design, self tuning gain-scheduling control, and self-tuning control with continuous adaptation of system and controller parameters. A continuous-time parameter identification approach, the Poisson moment function (PMF) method, was employed because of its superior noise rejection characteristics. In order to ensure the applicability of time-delay systems, the Smith predictor design method was employed, while the controller design was implemented by using a new pole-zero placement algorithm to ensure closed-loop stability. Comparisons with constant parameter controllers revealed that adaptive control provided equal or better torque control. The results of the transient cycle tests also proved that the self-tuning control could be applied successfully to system with dramatically different dynamic characteristics, hence showing the versatility of the self-tuning adaptive control method.

In the *first approach* the complete system identification , parameter estimation, and controller design were carried out on-line during a brief test period prior to the transient test cycle. The throttle-speed-torque system was considered as a multiple-input-single-output (MISO) system with two inputs and one output as depicted in Figure 9.13.

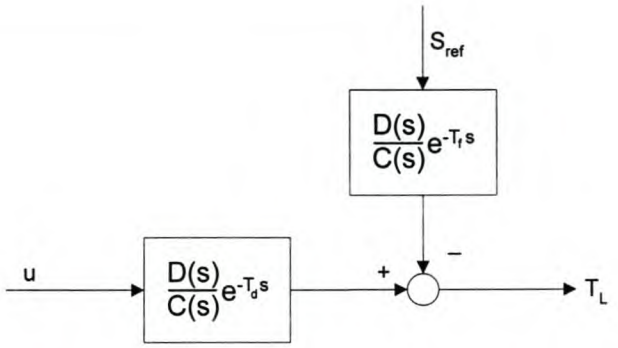

Figure 9.13. Throttle-speed-torque MISO system (Fullmer et al., 1992)

However, for one-shot system identification purposes, two separate single-input-single-output (SISO) system identification problems were solved in their research to avoid problems associated with the MISO system identification, such as the complexity of estimating two time delays and the convergence problems that come from the increased system order. To find the orders and parameters of B(s) and A(s) and the time delay T_f, the researchers held the speed reference command constant and applied a step input to the throttle command, while sampling load torque signals at a rate of 50 Hz. Similarly, to find the parameters of C(s) and D(s) and the time delay T_d, they held the throttle command constant and applied a step input to the speed reference command. Again, load torque signals were sampled at a rate of 50 Hz. Since there was no *a priori* knowledge assumed about the system, various models and time delays were considered, the parameters of each model were determined, and the model that described the system best found by using an error minimisation algorithm.

The *second approach* used by Fullmer et al. was similar to the first one, but included gain-scheduling control that was implemented based on measurements of engine speeds. Operating conditions of the engine were divided into five regions according to the engine speed: 1200-1400 rpm, 1400-1600 rpm, 1600-1800 rpm, 1800-2000 rpm and 2000-2200 rpm. For each speed, the parameter and system identification process described earlier was repeated on-line during a short period prior to the test cycle by employing the multiple one-shot parameter estimation algorithms. During test cycle execution, the controller parameters were changed as a function of operating conditions on the basis of the known parameters of the system for each speed range. Again, as in the first approach, no prior knowledge about the system was assumed.

The *third method* used by Fullmer et al. was different from the first two and employed continuous parameter estimation and controller parameter update during the transient test cycle. This is what is traditionally understood as an adaptive controller. Prior knowledge about the system, however, was required for this approach. If controller parameters were to be changed in a recursive fashion on the basis of system parameters, the time-delay, system model, and estimates of the model parameters had to be determined off-line prior to the test cycle. The purpose of this algorithm was to track time-varying parameters of the system caused by operating conditions and, hence, obtain better tracking of the reference speed and torque trajectories. Higher-order models are not suitable in a recursive parameter-estimation algorithm, since the parameter convergence will be very slow and more severe, and persistent excitement conditions on the input signals will be required. This led the authors to fit a lower-order model to the experimental data.

The following second-order MISO model was found to adequately represent the throttle-speed-torque system:

$$G_L = \frac{5.55}{s^2 + 3.76s + 4.34} e^{-0.4s} u + \frac{4.15}{s^2 + 3.76s + 4.34} e^{-0.4s} S_{ref} \tag{9.27}$$

Figure 9.15 compares the actual load torque output with the estimated load torque values when step inputs shown in Figure 9.14 were applied to the system. It is seen from Figure 9.15 that the second order model shown in equation (9.27) was a good approximation of the overall open-loop throttle-speed-torque system.

Since the closed-loop response specifications, as laid down by the EPA, were in the time domain, the pole-zero assignment algorithm was chosen as the most suitable controller design method. Consider the closed-loop torque control system shown schematically in Figure 9.16. T_r represents the reference torque trajectory, T_a is the actual torque output, and u is the control signal. The process model is specified by B(z)/A(z). Since a Smith predictor was used in the final design, the time delay was excluded from the process model for controller design purposes. The desired closed-loop system response was specified by $B_m(z)/A_m(z)$.

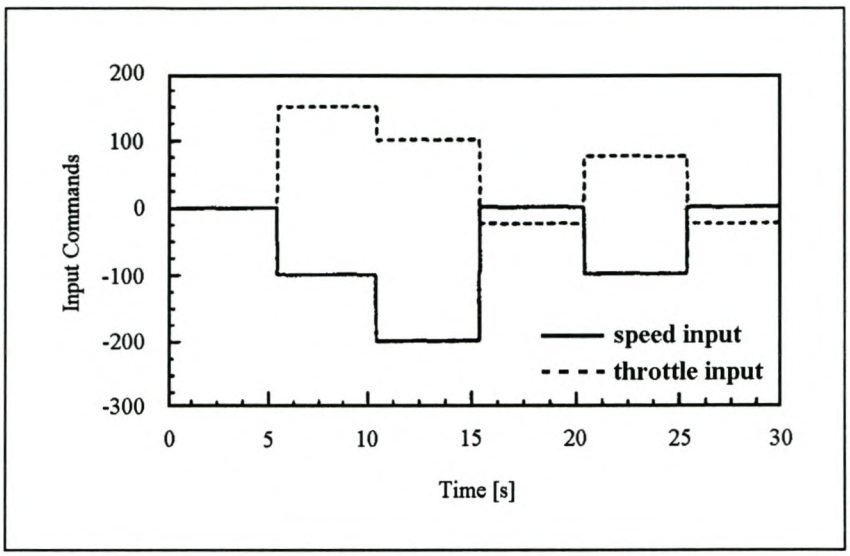

Figure 9.14. Step inputs of throttle valve and speed reference commands (Fullmer et al., 1992)

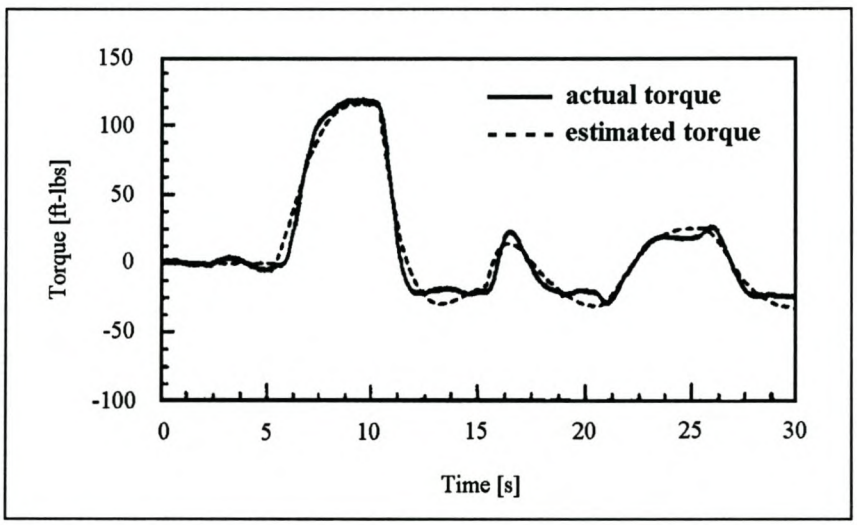

Figure 9.15. Comparison of estimated and actual load torques values (Fullmer et al., 1992)

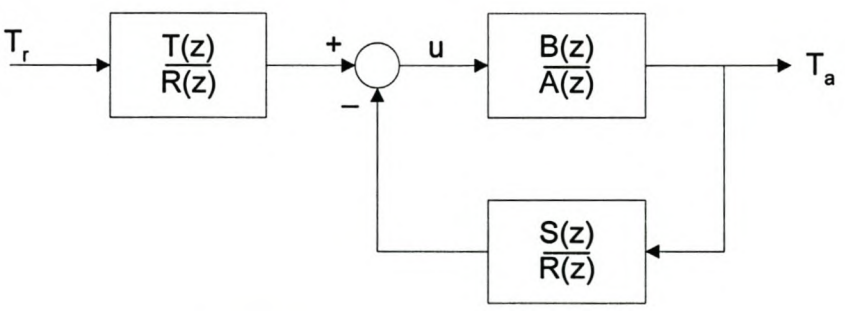

Figure 9.16. Block diagram of the pole assignment control law (Fullmer et al., 1992)

The control signal u was calculated by $R(z)u = T(z)T_r - S(z)T_a$, as seen in Figure 9.16. The pole-zero placement problem then became the determination of polynomials R(z), S(z), and T(z), such that the closed-loop system transfer function would be equal to the desired closed-loop transfer function, $B_m(z)/A_m(z)$. In the case of no-process zero cancellation, the solution was given by the following steps:

1). R(z) and S(z) was solved from the following diophantine equation:

$$A(z)R(z) + B(z)S(z) = A_0(z)A_m(z) \tag{9.28}$$

2). T(z) was found from

$$T(z) = \frac{A_0 B_m(z)}{B(z)} \tag{9.29}$$

3). The control signal u was then calculated from

$$u = \frac{T(z)}{R(z)}T_r - \frac{S(z)}{R(z)}T_a \tag{9.30}$$

In order to avoid complexity, the researchers chose the order of the closed-loop reference model to be equal to the order of the open-loop process model. All the poles of the desired closed-loop transfer function were set to $z = e^{-T/\tau}$, where T was the sampling period, and τ the desired time constant for the closed-loop system. The EPA specifications suggested that the closed-loop system should reach its steady-state value, to a given reference step input, in 1 second or less since torque and speed trajectories were given in seconds. Therefore, the desired time constant τ was set to 0.25 sec, since a closed-loop system will reach 98% of its steady-state value to a given step-input in four time constants.

In the pole-zero assignment algorithm of Astrom and Wittenmark (1987), the observer polynomial $A_0(z)$ was selected somewhat arbitrarily. The only condition imposed on the observer polynomial was to restrict all the zeros of the observer polynomial to lie inside the unit circle in the z-plane. However, during actual transient test cycles, it was found that arbitrary selection of the observer polynomial resulted in a R(z) controller polynomial whose zeros were outside the unit circle. This resulted in unstable closed-loop operation. To overcome the limitations of the above-mentioned pole-zero assignment method

required a new modified pole-zero assignment algorithm (Tuken & Van Gerpen, 1990). All the zero locations of the R(z) polynomial were projected inside the unit circle in the proposed algorithm by changing the zero locations of the observer polynomial in a systematic way. This process is discussed in detail in the reference given above.

Because of the time delay inherent in internal combustion engines, and the control problems resulting from this, Smith's method was again used to extend the application of adaptive control systems to time-delay processes. A block diagram representation of the Smith predictor configuration used by Fullmer et al., can be seen Figure 9.17. In this figure T(z), R(z) and S(z) represent the delay-free controller, B(z)/A(z) is the delay-free part of the process transfer function, k*T is the time delay of the system where T is the sampling period, and $\hat{B}(z)/\hat{A}(z)$ and $\hat{k}$*T are the estimates of the process transfer function and time delay, respectively.

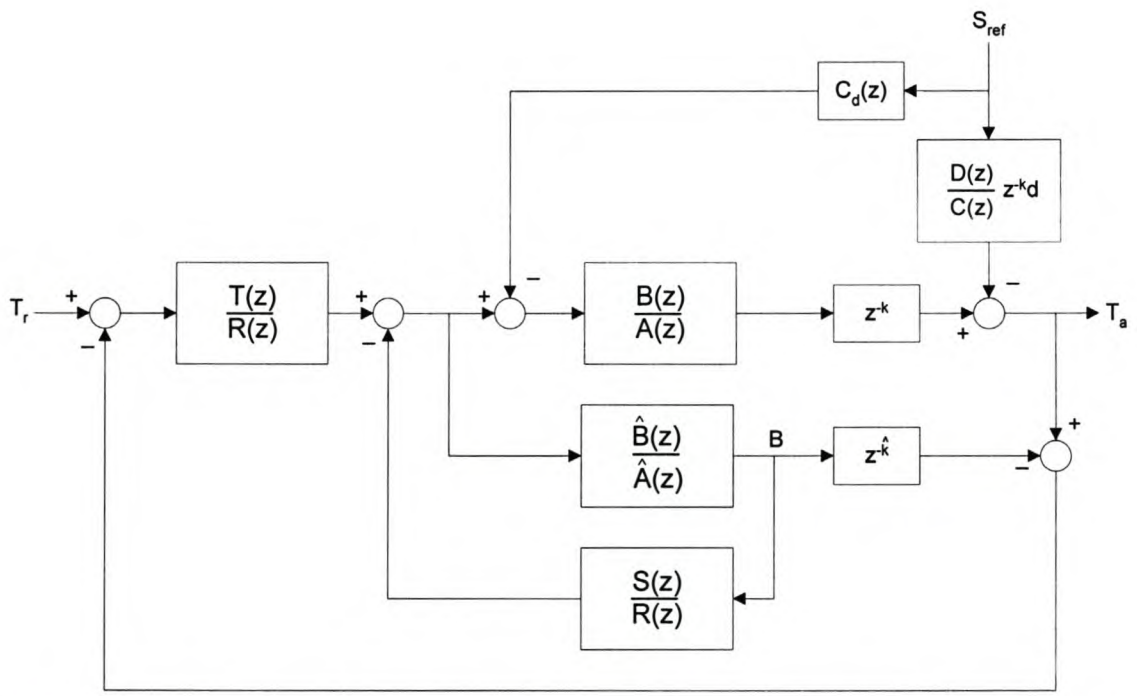

Figure 9.17. Smith predictor with feed-forward compensation (Fullmer et al., 1992)

The control signal u, is delayed by k*T seconds before it effects the output. During this initial period of time, the control cannot influence the output. The signal shown on Figure 9.17 at point B, however, is a predicted version of the output signal and can be used as a feedback signal. Thus, the controller design can be carried out by using classical methods

for delay-free systems. Therefore, the specifications of system performance can be given in familiar delay-free terms. The second outer loop in Figure 9.17 was included because of the possible mismatch between actual and estimated system parameters. Removal of the outer loop gives open-loop control, which makes no use of actual output information, and can lead to inferior performance in practice.

Any variation of the speed reference command causes a load disturbance to the throttle-torque system. Since the load disturbance does not appear explicitly in Smith's method, a feed-forward compensator, $C_d(z)$, was added to the Smith predictor. $D(z)\cdot z^{-k_d}/C(z)$ in Figure 9.17 represents the speed-torque transfer function. As feed-forward does not affect stability of the control loop, the feed-forward control system was added after the design of the controller system. For an ideal feed-forward control, $C_d(z)$ was calculated by

$$C_d(z) = \frac{G_d(z)z^{-k_d}}{G_p(z)z^{-k}} \tag{9.31}$$

where $G_p(z) = B(z)/A(z)$, $G_d(z) = D(z)/C(z)$ and $\hat{(\,)}$ represents the estimated quantities of actual variables. If the above feed-forward control is stable, the influence of the disturbance S_{ref} on the output torque T_a is completely eliminated.

Fullmer et al. (1992) implemented the three proposed control algorithms on a Zenith-386 microcomputer. Ten transient test cycles were run with each algorithm in order to validate the statistical properties of the results. By implementing the *first approach*, self-tuning control with one-shot parameter estimation and controller design, the results of all ten tests performed were found to be valid according to the EPA specifications. Parameter estimation algorithms revealed that a third-order model with first-order numerator dynamics gave the minimum sum of squared errors for both the speed-torque and throttle-torque sub-systems. It was also shown in all experiments using the one-shot parameter estimation algorithm that parameter convergence was fast.

Using the *second approach*, the parameter identification and controller design were carried out for five different speed ranges. It was found that the steady-state gain and natural frequency of both sub-systems increased with increasing engine speed. The damping ratio decreased with increasing engine speed in the throttle-torque system while it increased with increasing speed in the speed-torque system. All ten tests performed using this

approach satisfied the EPA regression line specifications and were declared to be valid. In nine of the tests a second-order model was found to be the best fit, and in the remaining test a third-order model was selected. Results obtained with the two approaches above were compared using statistical measures. Improvements of up to 35% were observed for the parameters of the torque and brake horsepower regression lines. The researchers concluded that the gain-scheduling self-tuning controller resulted in values closer to the EPA specifications than did the one-shot self-tuning controller.

As was explained earlier, a second-order model with a time delay of 0.40 seconds was selected for both systems of the adaptive controller with continuous update of process and controller parameters. Of the ten transient tests performed, only six satisfied the EPA specifications. Several factors were thought to have led to the deteriorated performance of the adaptive regulator. Whereas process parameters were determined from well-designed, on-line, open-loop tests in the gain-scheduling control, for adaptive control they were determined in closed-loop tests where there was no guarantee of the stability and convergence of the estimated parameters. Adaptive regulators also require a minimum order system description for best parameter convergence, the majority of successful adaptive regulators reported in the literature employing first-order systems as a process model. In their research, the authors found that a first-order model did not adequately describe the system behaviour, and therefore employed at least a second-order model system to describe their system. This fact was mentioned as another possible reason for the adaptive regulator not performing well. Lastly it was pointed out that adaptive regulators require for the time-delay of the system to be known and to be constant over the operating range for better parameter estimation and better closed-loop control. However, in the throttle-torque system studied in their research, the actual time-delay varied based on operating condition, although it was assumed to be constant in the estimation algorithm.

Finally, Fullmer et al. (1992) concluded that the gain-scheduling self-tuning control gave the best results among all three adaptive control approaches studied in their research. One-shot self-tuning control also gave good results and had the advantage of being computationally less complex than a gain-scheduling self-tuning control approach. However, the authors did not recommended the application of full adaptive regulators for the torque control of diesel engines operating over transient test cycles.

9.5. GENERALISED PREDICTIVE CONTROL (GPC)

In their paper, *Predictive Control Engineering to Transient Engine Test-beds*, Noble et al. (1988) described the application of a modern control technique, Generalised Predictive Control (GPC), to the problem of dynamically controlling engine speed and torque on the test-bed. By using system identification, coupled with the GPC design algorithm, the controller could automatically be tuned by a computer, ensuring that the best performance could be obtained for each engine test-bed installation. Their results showed that, on a test-bed equipped with a standard eddy-current dynamometer, tight control of the transient speed and torque could be achieved using these techniques.

Conventionally, three-term or proportional-integral-derivative (PID) feedback controllers are used for test-bed control (see Section 9.1). However, their performance is poor compared to that of a modern control algorithm implemented in hardware of comparable cost. Their tuning is difficult and does not necessarily lead to optimal or even satisfactory performance under all operating conditions. This is mainly so because engines often involve significant non-linearities. This problem is aggravated for speed and torque controllers operating in a research and development environment where many types of engines are tested and their characteristics are constantly being modified. In order to maintain accurate control, the controllers must be tuned for each particular engine configuration. Compromises are often made, with the controllers deliberately tuned to have a slow but safe response, therefore not requiring frequent re-tuning. Although the current practice of using PID controllers is acceptable for most steady-state engine testing requirements, their performance under transient conditions is inferior compared with the potential of more advanced theories. It is for these reasons that researchers have investigated modern test-bed control techniques.

As their first step, it was necessary to model the system before a controller for the process could be designed. The modelling of complex dynamical processes is a difficult and demanding discipline. Where the physical properties of a system are known, it may be possible to derive models from first principles by analysing the dynamics of the individual system elements. These models are, however, usually specific to one class of system (e.g. eddy-current dynamometer or D.C. motor) and may not be directly suited to control system design. An alternative approach is to regard the system as a "black box" with

mathematical relationship (typically differential or difference equations) between the inputs and outputs, no significance being attached to any internal parameters. The modelling then reduces to finding the parameters of this mathematical relationship from experimental data and is therefore valid for many different types of systems. Noble et al. adopted this second approach, known as "system identification", for their work.

They considered the test-bed as a two-input, two-output system with the input variables being throttle position demand and dynamometer excitation current demand, and engine speed and dynamometer torque output variables to be controlled. The system was represented in discrete time as a two by two transfer function matrix relating the inputs to the outputs with a two by two transfer function matrix to model random processes, such as measurement noise and variations in combustion. The system was described by the equation:

$$\begin{bmatrix}\Delta\omega(t)\\ \Delta\tau(t)\end{bmatrix}=\begin{bmatrix} z^{-k_{11}}\dfrac{B_{11}}{A_1} & z^{-k_{12}}\dfrac{B_{12}}{A_1}\\ z^{-k_{21}}\dfrac{B_{21}}{A_2} & z^{-k_{22}}\dfrac{B_{22}}{A_2}\end{bmatrix}\begin{bmatrix}\Delta\theta(t)\\ \Delta\iota(t)\end{bmatrix}+\begin{bmatrix}C_1 & 0\\ 0 & C_2\end{bmatrix}\begin{bmatrix}\zeta_1(t)\\ \zeta_2(t)\end{bmatrix} \tag{9.32}$$

where

$\Delta\omega(t)$ is the change in engine speed

$\Delta\tau(t)$ is the change in dynamometer torque

$\Delta\theta(t)$ is the change in throttle position demand

$\Delta\iota(t)$ is the change in excitation current demand

$\zeta_1(t)$ and $\zeta_2(t)$ are independent white noise processes

z is the discrete time operator ($zx(t) = x(t+1)$)

k_{11}, k_{12}, k_{21} and k_{22} are integer delays, and

B_{11}, B_{12}, B_{21}, B_{22}, A_1, A_2, C_1 and C_2 are polynomials in z^{-1}

It can be shown, by multiplying out the matrix equation, that the speed and torque responses can be regarded as separate two input, one output processes represented by *controlled autoregressive integrated moving average* (CARIMA) models of the form:

$$A\Delta y(t) = B_1\Delta u_1(t-k_1) + B_2\Delta u_2(t-k_2) + C\zeta(t) \tag{9.33}$$

The system could therefore be identified as independent models of speed and torque response with the above representation. The identification process consisted of three stages. An experiment was performed on the plant by perturbing the inputs and measuring the response of the outputs. The experimental data was then used by an identification algorithm to produce a model which was then validated. In their experiment, the inputs were perturbed with two independent *pseudo random binary sequences* (PRBS) about a nominal operating condition. PRBS excitation was used as it is simple to generate on a computer, maximises the signal power of a given amplitude and contains a wide spread of frequencies with which to excite the plant dynamics. The identification algorithm used the *prediction error method* of Ljung (1993) from the MATLAB identification toolbox. This procedure uses a Gauss-Newton minimisation procedure which is repeatedly applied until the norm of the Gauss-Newton vector is less than a specified tolerance Ljung (1987).

Predictive speed and torque control differs from conventional feedback control in a variety of ways. With a conventional controller, the inputs are calculated from the current and previous errors (the difference between the desired and achieved outputs). In a predictive control law, the inputs are calculated from future predicted errors. This means that conventional controllers can therefore only react to set-point changes and disturbances after they have occurred. Significant errors are unavoidable unless additional measures such as feed-forward are employed. A predictive controller can effectively compensate for errors before they occur. This is especially applicable when the speed and torque must follow a predefined cycle (such as the ECE15 test cycle) where future set-points are known. The predictive controller can make natural use of the information to drive the speed and torque along their desired trajectories.

Generalised predictive control is an optimal control law with a finite receding prediction horizon. The control law is optimal in that it is the solution for u(t) which minimises the cost function:

$$J = \sum_{j=n_1}^{n_2}\left[w(t+j) - \hat{y}(t+j) \right]^2 + \sum_{i=n_1}^{n_2} \lambda\left[\Delta u(t+i)\right]^2 \qquad (9.34)$$

under the constraint:

$$\Delta u(t+i) = 0 \text{ for } i \geq n_u$$

where

$w(t+j)$ is the set-point at time $t+j$ ($j = n_1$ to n_2)

$\hat{y}(t+j)$ is the predicted output at time $t+j$

$\Delta u(t+i)$ is the change in input at time $t+i$ ($i = 0$ to n_u-1)

λ is the user chosen control weighting, and

n_1, n_2 and n_u are user chosen design parameters; the starting point for prediction, the prediction horizon and the control horizon respectively.

The prediction horizon is receding in that, at each sample time (t), it advances one time step to $t+n_2$.

From a CARIMA model, the optimal control law is given by:

$$\Delta u(t) = g^{-T}[W(t) - F(t)] \tag{9.35}$$

where

$W(t)$ is a vector of future set-points

i.e. $W(t) = [w(t+n_1)\ w(t+n_1+1) \ldots w(t+n_2)]^T$

$F(t)$ is a vector of predicted outputs

i.e. $F(t) = [\hat{y}(t+n_1)\ \hat{y}(t+n_1+1) \ldots \hat{y}(t+n_2)]$

and g^{-T} is a vector of control parameters, calculated from the solution of the cost function.

The controller can also include dynamic feed-forward compensation and model following. Feed-forward was used in their application to compensate for the cross-coupling between the speed and torque loops. The input to the second loop is regarded as a disturbance acting on the first loop, and vice-versa. Modern control algorithms permit compromises to be made between speed response, robustness, actuator wear and computational requirements in the design of the controller. In their application, the control design parameters were chosen by experimentation until a satisfactory compromise was achieved. Having established a set of GPC design parameters for the system, the computer automatically calculated the controller from each identified model.

The ability of the algorithm to independently control speed and torque is shown in Figure 9.18. The controller maintained the engine speed to within 1.2 rev/s of the speed set-point

of 29 rev/s, whilst stepping the torque between 25 and 31 Nm. With the engine speed changing from 25 to 31 rev/s, the load torque was held to within 0.6 Nm of the set-point of 29 Nm. These results demonstrated that the controller was properly adjusted for that operating point and that the use of dynamic feed-forward compensation effectively decoupled the two loops.

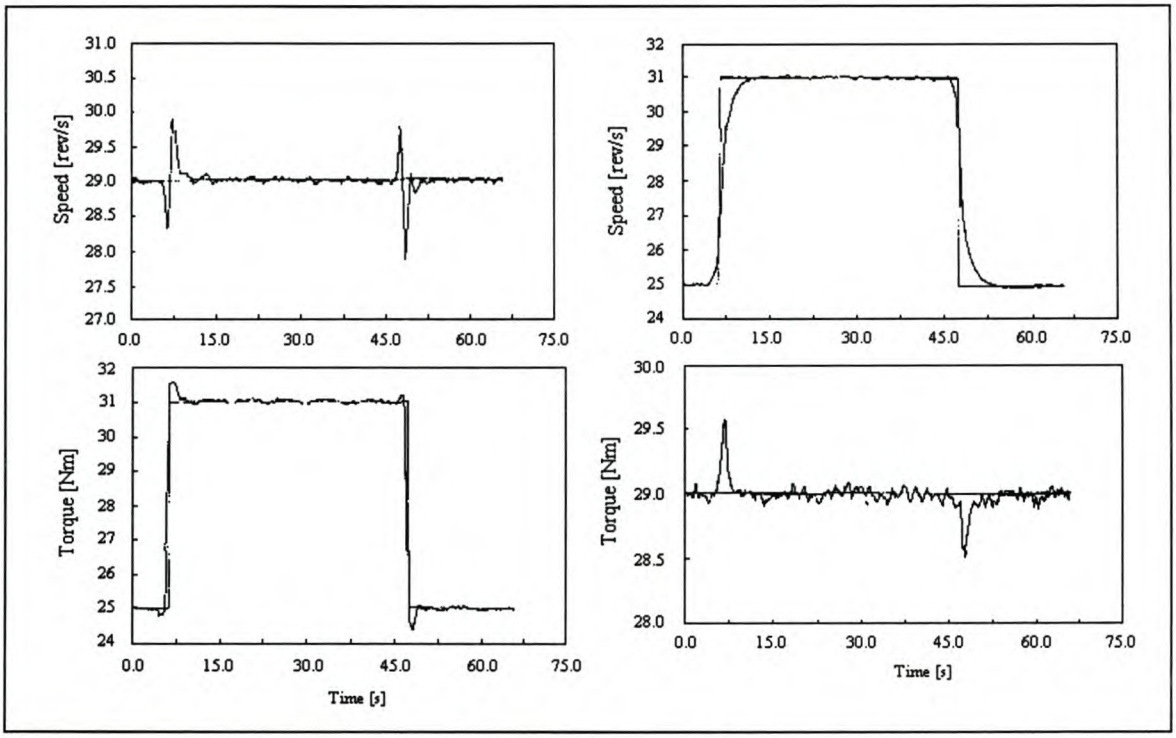

Figure 9.18. Independent control of speed and torque (Noble et al., 1988)

The test-bed was also programmed to execute part of a legislative emissions cycle (ECE15). The test-bed was not capable of simulating overrun (negative torque) as the eddy-current dynamometer could not motor the engine. Under these conditions, the desired load torque was assumed to be zero. Part of this cycle can be seen in Figure 9.19. It is seen that the engine was not accurately controlled at low speeds and during simulated gear changes, partly due to the gross non-linearities in the speed response at low throttle openings and the inherently slow response of the dynamometer. The vehicle speed that was effectively achieved, along with the acceptable tolerance bands, is seen in Figure 9.20. The vehicle speed is not shown during gear changes as there is no direct relationship to engine speed and there are no tolerance bands. The vehicle speed was almost entirely within the acceptable limits for the test.

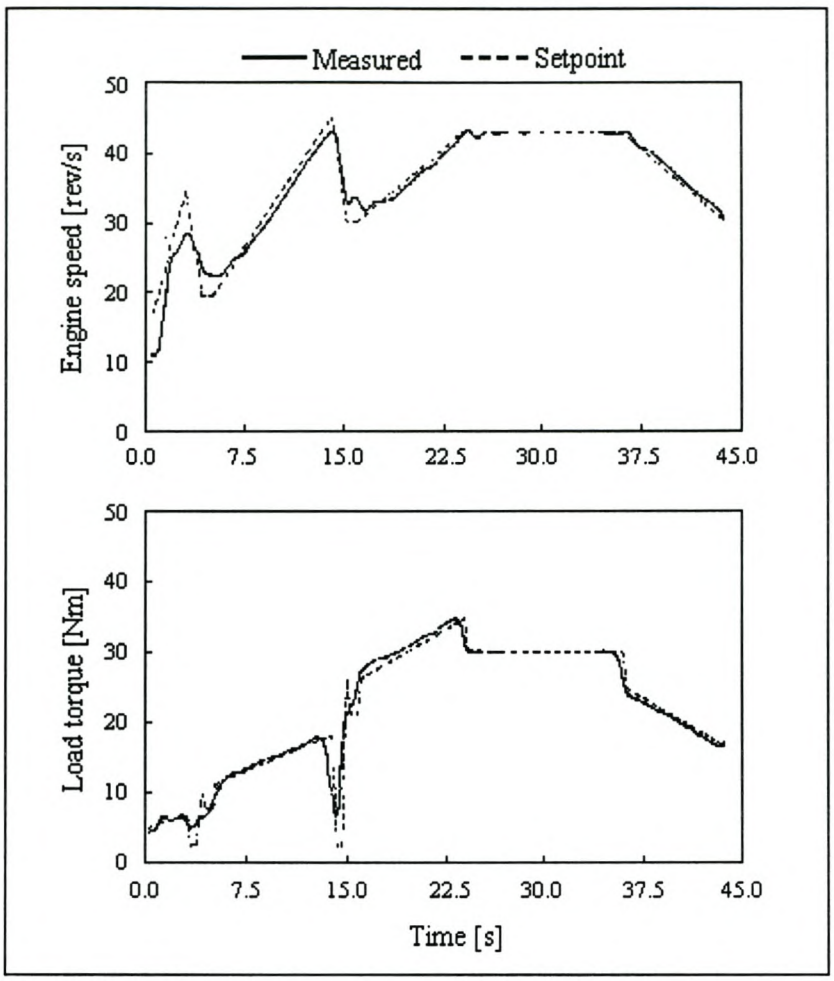

Figure 9.19. ECE15 Emissions cycle - engine speed and load torque (Noble et al., 1988)

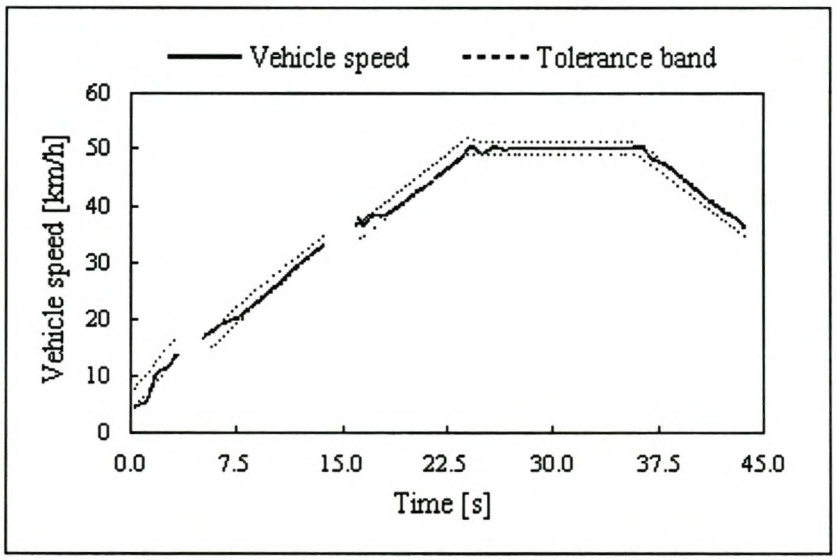

Figure 9.20. ECE15 Emissions cycle – vehicle speed (Noble et al., 1988)

10. SYSTEM EVALUATION AND DISCUSSION

In order to establish the degree to which the system described in this document fulfilled the objectives laid out in Section 2, an evaluation was performed assessing its capabilities. The system evaluation was divided into the following categories:

- system reproducibility
- sensitivity analysis
- tracking accuracy
- simulation accuracy

The evaluation was performed using an ADE366Ti diesel (Euro 1 specifications) engine mounted on the test-bed. Technical specifications for the engine used for testing are given in Table 10.1.

Table 10.1. Technical specifications for ADE366Ti diesel engine

Model	Vertical, in-line with exhaust gas turbo-charger and intercooler
Cooling	Water, re-circulating
Combustion process	4-stroke, diesel, direct injection
Number of cylinders	6
Cylinder bore	97.5 mm
Piston stroke	133 mm
Total piston displacement	5958 cm^3
Compression ratio	17:1
Maximum Power	177 kW @ 2600 rpm
Maximum Torque	750 Nm @ 1600 rpm

10.1. EVALUATION PROCEDURE

System evaluation was carried out by performing vehicle acceleration simulations. This method of evaluation was chosen mainly because it allowed for the generation of all information necessary to draw meaningful conclusions regarding system performance.

The *Dynasim* programme was configured to simulate a medium-sized truck (15 ton). Gear ratios were chosen in such a way that realistic acceleration runs would result. Care was taken to evenly distribute the ratios so that similar engine speed drops would occur at each gear change. The following ratios yielded satisfactory acceleration results:

Table 10.2. Gear ratios used during truck acceleration simulations

Gear	Ratio
1st	30.0
2nd	18.0
3rd	12.0
4th	8.5
5th	6.5
6th	4.9
7th	3.8
8th	3.0
final	1.5

The following sequence of events was followed with the execution of each acceleration run:

1). The engine was warmed up thoroughly according to standard warm-up procedures until oil and water temperatures had stabilised. This was done to ensure that each set of acceleration runs was started with the engine under the same thermal condition.

2). First gear was engaged and pull-away initiated. This was not taken to be part of the acceleration run, as repeatable pull-aways were difficult to achieve.

3). The vehicle was run in an engaged state with the engine idling until its speed had reached steady-state conditions. The speed-controlled governor ensured that the engine did not stall under these conditions.

4). With the simulation programme configured to automatically change gears at 2400 rpm, the acceleration run was started with the governor rack position maintained at a maximum setting. Due to torque absorption limitations of the dynamometer, the vehicle was accelerated to a speed of just above 60/70 km/h, during which gears were changed from first to sixth.

5). At this time the vehicle was allowed to coast down, while still engaged in the last gear selected, until a specified engine speed had been reached, at which time neutral was selected and the vehicle brought to a standstill. This procedure was repeated three times for every vehicle configuration.

The above procedure was used during the execution of acceleration cycles since it was essential to ensure that data sets could be compared with one another on an equal basis.

10.2. SYSTEM REPRODUCIBILITY

A fundamental prerequisite for testing engines under research and development conditions is for data to be reproducible when all other parameters remain unchanged. It is this quality that enables researchers to make comparisons between engines and/or engine components during the course of research and development work. It was thus important to determine to what degree the CAE dynamic test-bed could reproduce results given identical input conditions. This was achieved by executing three acceleration runs performed according to the procedure described above, and analysing the data generated. The results of one such a set of acceleration runs are shown in Figure 10.1.

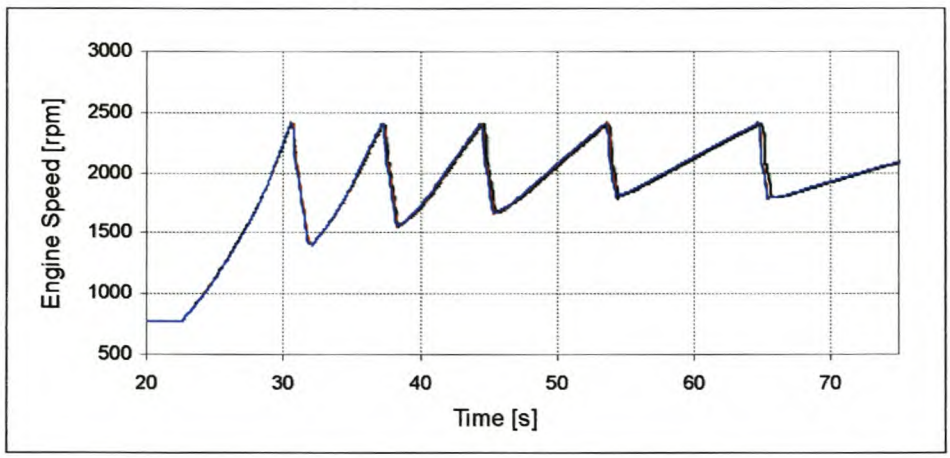

Figure 10.1. Evaluation results: Reproducibility of complete system

In the case shown above the complete system was considered, inputs being accelerator pedal position and gear selection and outputs, engine and vehicle speed. The transfer function thus included the entire virtual vehicle simulation process as well as the physical engine response to these inputs.

Maximum differences between runs were found to occur during gear changes due to the events not being initiated at exactly the same times. As these events were triggered automatically based on engine speed, the accuracy with which the speed signal was resolved could have influenced the initiation of these automated events. Two of these transition periods are shown enlarged in Figure 10.2.

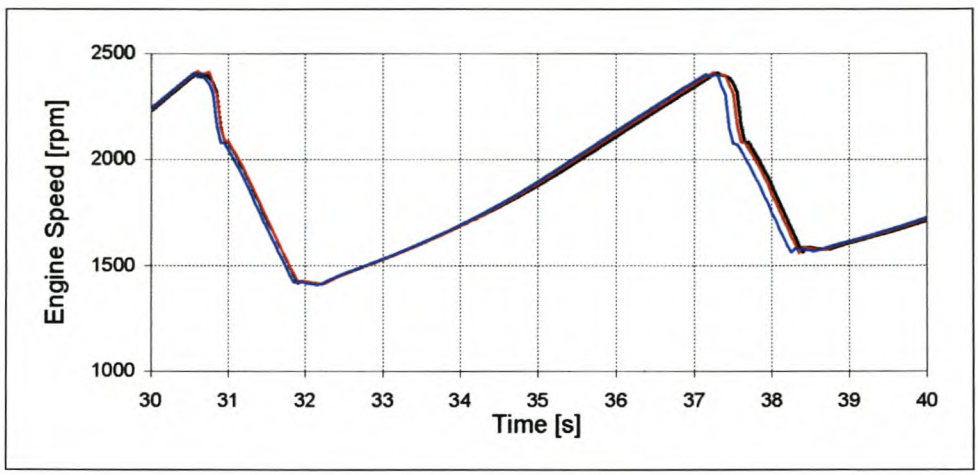

Figure 10.2. Evaluation results: Reproducibility during gear transitions

During previous research performed by the author (Conradie, 1995), the ability of the dynamometer to track a speed profile was examined. A section of the ECE15.04 emission cycle was executed by demanding a pre-calculated speed profile from the DC dynamometer. Three test runs were executed, the results of which are shown in Figure 10.3.

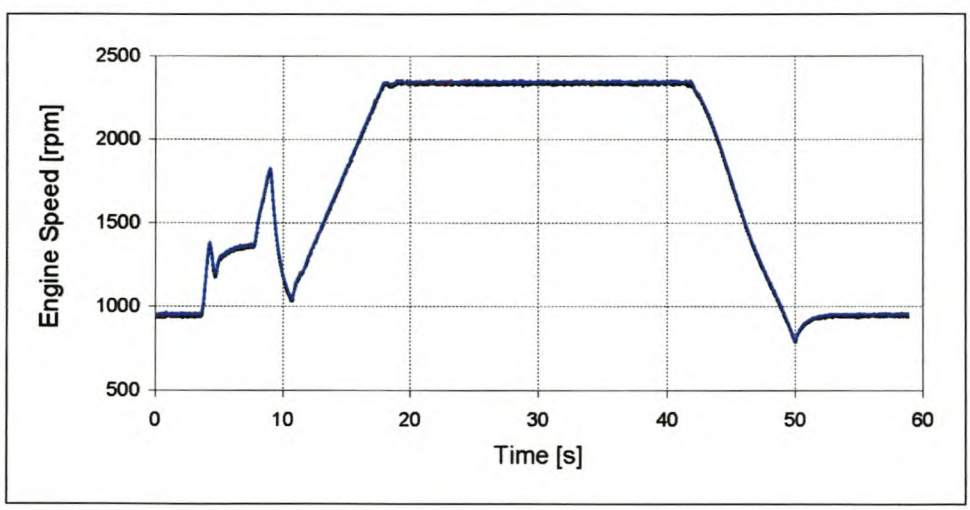

Figure 10.3. Evaluation results: Reproducibility of dynamometer (Conradie, 1995),

The maximum speed differences between the runs were calculated at each sampling instant and yielded an average value of 12.64 rpm with a maximum value of 34.87 rpm. These differences were mainly due to maximum time delays between signals of approximately 0.1s. The standard deviation from the average speed value was found to be 5.00 rpm, indicating that the Siemens speed controller was able to follow demanded speed values with a high degree of reproducibility.

10.3. SENSITIVITY ANALYSIS

Another important aspect that needed to be evaluated, was that of the system's sensitivity to parameter changes. Apart from the dynamic nature of the testing facility, it also used real-time engine output (i.e. torque and speed) to compute virtual vehicle behaviour. This fact makes the system very useful for analysing complete vehicle configurations while only the engine was available for testing. It was therefore possible for vehicle performance to be analysed with various changes made to engine and vehicle parameters. In order to determine the system's sensitivity, the effects of engine and vehicle parameter changes on simulated vehicle performance were analysed.

10.3.1. Engine effects

The engine is probably the one component that has the greatest effect on the performance of a vehicle. The output of an engine is its torque, which is what overcomes the various resistances to accelerate the vehicle. Any changes made to the engine that affect the torque output logically have to affect the rest of the vehicle system and thus also the way in which it will perform. The CAE test-bed's ability to respond to changes made to engine parameters was tested by adjusting the back pressure of the previously described ADE366Ti diesel engine and then performing acceleration runs according the procedure specified in Section 10.1. All other parameters were kept constant during these test runs.

Back pressure strongly influences turbo-charged engines in that it affects turbo-charger wind-up and the consequent build-up of boost pressure. This in turn affects the engine's ability to generate torque and determines, not only the maximum value generated, but also the lag resulting due to the various induction processes. Three sets of acceleration runs were executed, the first with the engine's nominal exhaust back pressure (set with engine

operating at full power @ 2600 rpm) set to 3 kPa, the second with a nominal back pressure set to 10 kPa, and the third with a nominal back pressure set to 20 kPa. Engine speeds obtained during these three test runs are shown in Figure 10.4 and the corresponding vehicle speeds obtained in Figure 10.5.

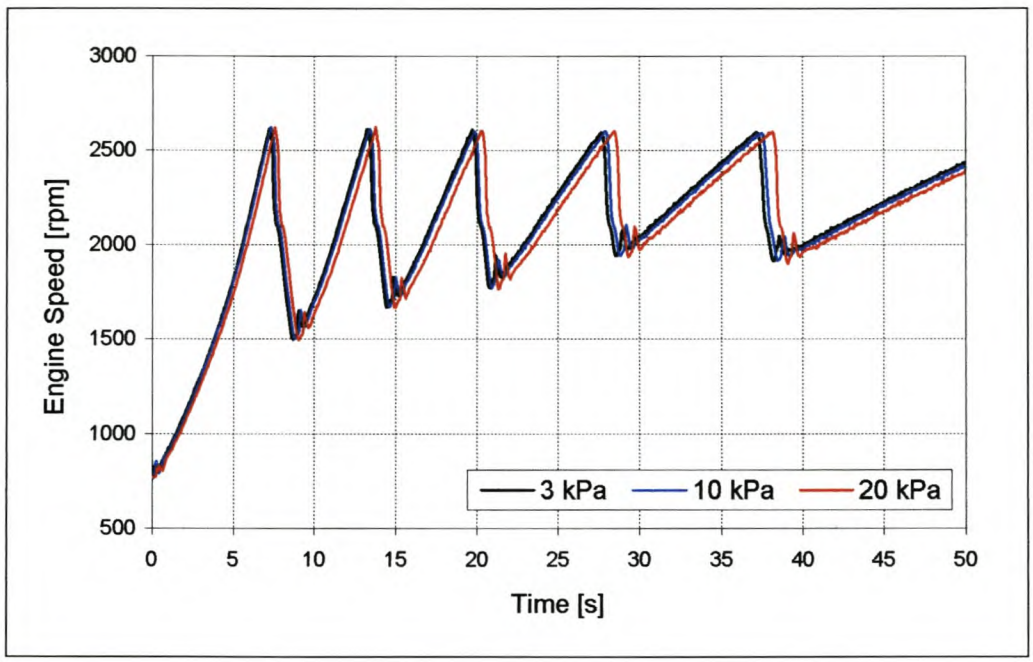

Figure 10.4. Sensitivity analysis: Engine speeds with varying back pressures

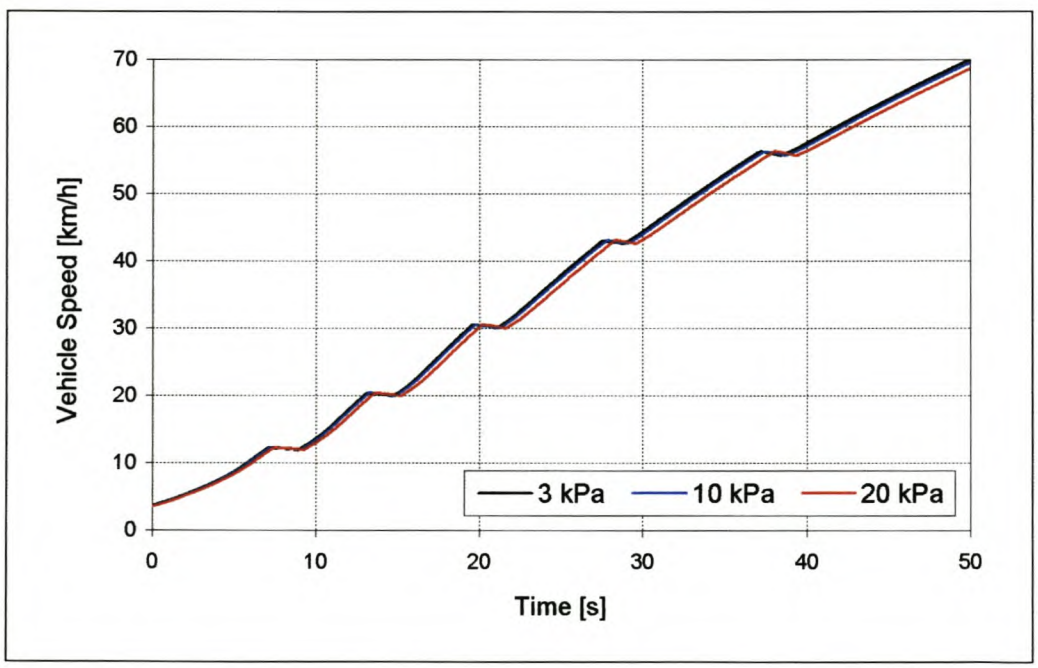

Figure 10.5. Sensitivity analysis: Vehicle speeds with varying back pressures

Actual exhaust back pressures measured during these acceleration runs are shown in Figure 10.6, while Figure 10.7 shows the turbo-boost pressures obtained during the three acceleration runs. The correlation between exhaust back pressure and turbo-boost pressure is quite clear: it is seen that the turbo-charger boost developed with a lower back pressure setting was substantially higher than with a higher back pressure. This is due to a higher pressure differential over the turbine. Final values obtained are indicated, the difference between highest and lowest being 24.1 kPa (19%). These simulations suggested "time-to-60 km/h" acceleration variations due to back pressure, of up to 2.38%.

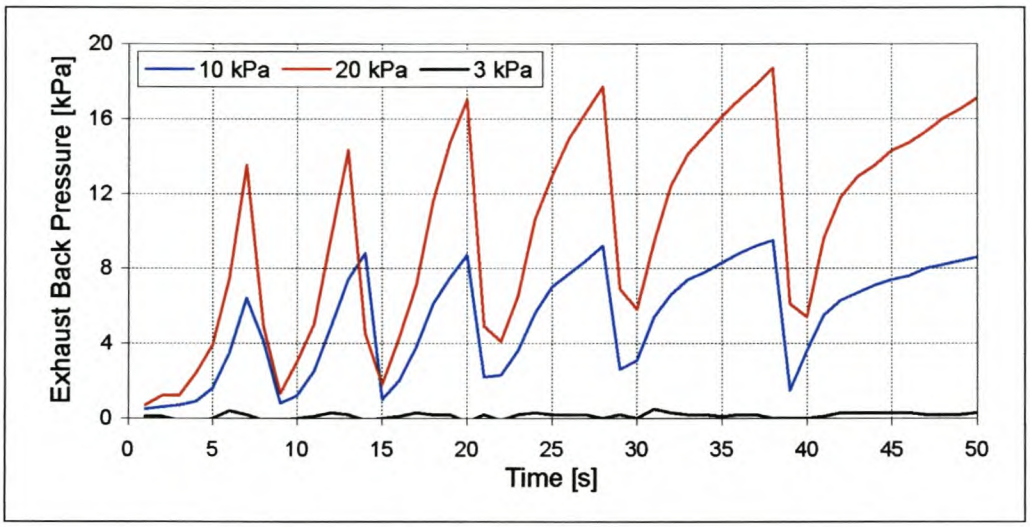

Figure 10.6. Sensitivity analysis: Exhaust back pressures obtained during acceleration runs

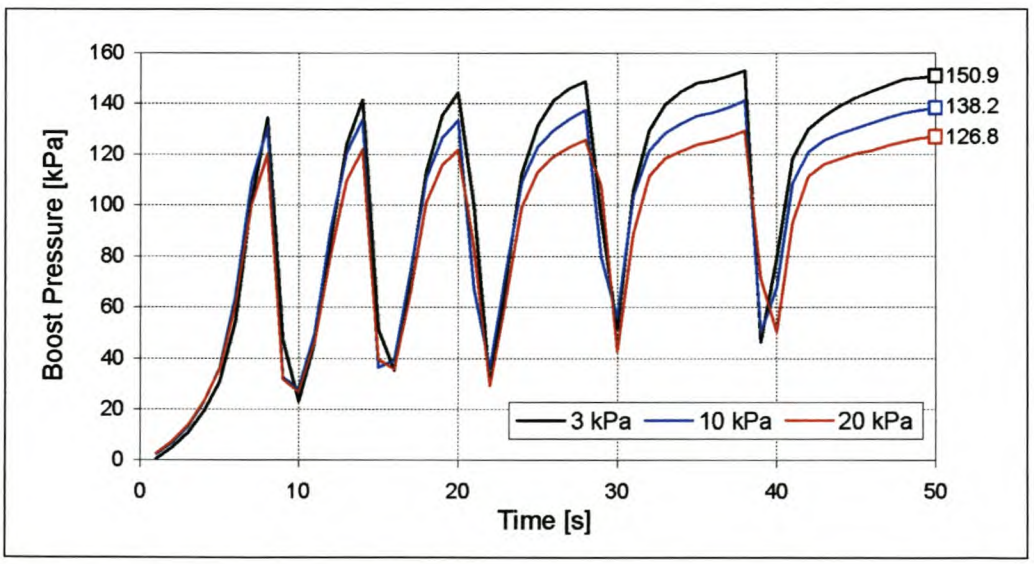

Figure 10.7. Sensitivity analysis: Turbo-boost pressures obtained with varying back pressures

Engine torques measured during the acceleration runs are shown in Figure 10.8.

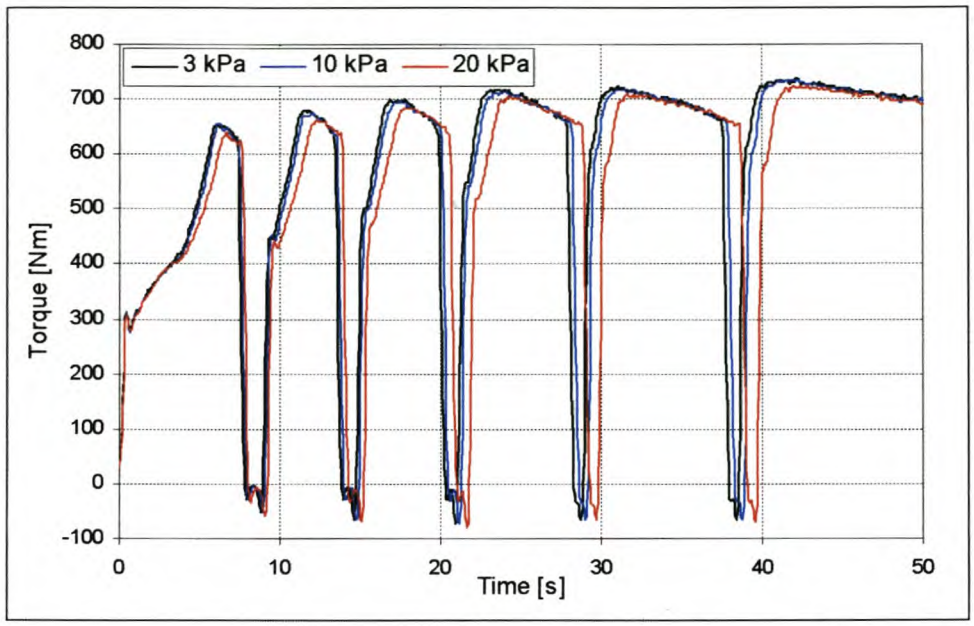

Figure 10.8. Sensitivity analysis: Engine torques measured during acceleration runs

These results show the affects of varying exhaust back pressures on the engine torque developed. Most noticeable are the torque build-up delays experienced following gear changes. The maximum torque developed in each gear is also seen to be affected by back pressure. This can be attributed to the differential pressure across the turbine of the turbo-charger being affected by the back pressure, which in turn affected the boost developed and therefore the quantity of air supplied to the engine. A very direct correlation can be seen to exist between exhaust back pressure and torque, increasing back-pressure having a negative effect on both torque build-up and maximum torque developed. The significance of this is further illustrated in Figure 10.9.

The graph shows integrated torque curves for the acceleration run for each back pressure setting. A resemblance to the vehicle speed profiles (see Figure 10.5) is noted and can be explained by the fact that a vehicle is merely a torque integrator. The difference between the maximum (3 kPa setting) and minimum torque integrals (20 kPa setting) is also shown. A maximum difference of 865.9 Nm.s is noted. This can be interpreted as an average torque difference of 17.3 Nm over the 50 second acceleration run. This is of great significance and the effects are clearly seen in the truck's simulated acceleration performance.

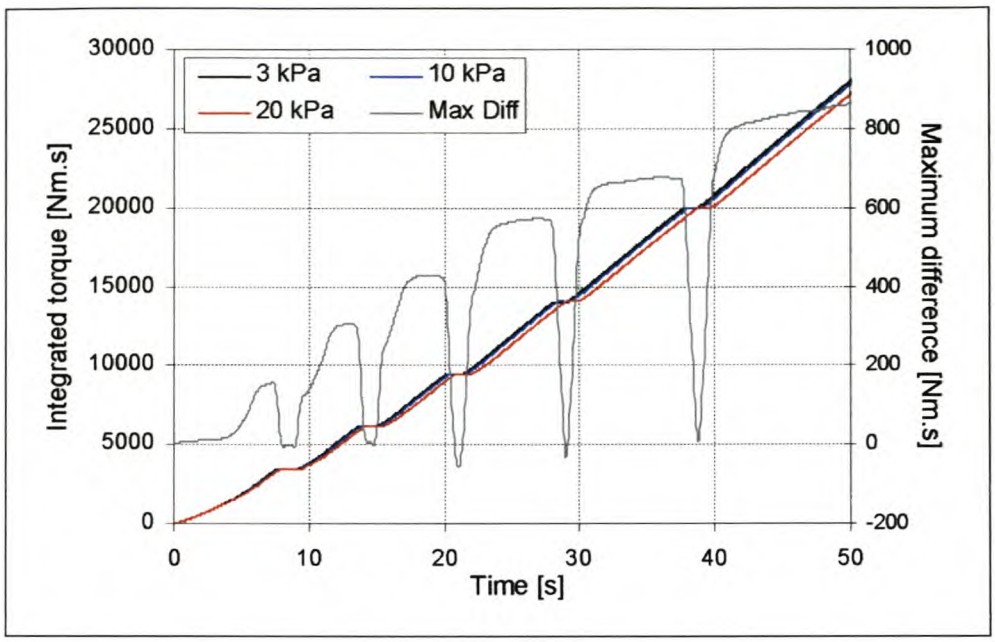

Figure 10.9. Sensitivity analysis: Integrated torque with different back pressures

The results described above could only have been obtained using a dynamic test-bed such as was described in this document. This is because of the nature of the facility, and because of a direct relationship between the internal workings of the engine and the outcome of the simulation results. The actual transient torque developed by the engine was used during these simulations, meaning that changes made to the engine (such as the back-pressure variations described) were translated directly into observable changes in vehicle response. Referring to Figure 10.8 one can clearly see the difference in engine torque developed while accelerating in 1st gear versus that developed while accelerating in 5th gear. This fact can be attributed to the fact that less time was spent accelerating in 1st gear than in 5th gear, allowing less time for engine heat to be generated and lower boost pressures to develop (see Figure 10.7). These thermal effects are also reflected in Figure 10.6 which shows the exhaust back-pressures developed during this acceleration run. It is seen that higher exhaust back-pressures result, given longer acceleration times, due to more heat being generated by the engine.

Obtaining similar results using conventional testing facilities would have been impossible, since they are not designed for this type of work, but operate under steady-state conditions. The above results illustrated the test-bed sensitivity to changes made to engine parameters and the effects it had on the simulated vehicle response. The CAE dynamic test-bed has

been successfully used to conduct investigations into the effects of specialised silencers on diesel engine performance. System sensitivity to vehicle parameter changes, and the effects of these on performance, will be the next topic under discussion.

10.3.2. Vehicle effects

In order to evaluate the effect of vehicle parameters, as set in the simulation programme, two acceleration runs were conducted using different vehicle mass settings. In the first simulation, an acceleration run was performed of a 20 000kg truck, with all other parameters as was set for the simulations described in the previous section. A second acceleration run was performed with only the vehicle mass changed to 10 000kg, all others parameters remaining unchanged. Again terminal vehicle speeds were limited, this time to 60 km/h, due to dynamometer torque limitations over extended periods of time. Engine speeds obtained during these tests can be seen in Figure 10.10, with corresponding vehicle speeds obtained shown in Figure 10.11.

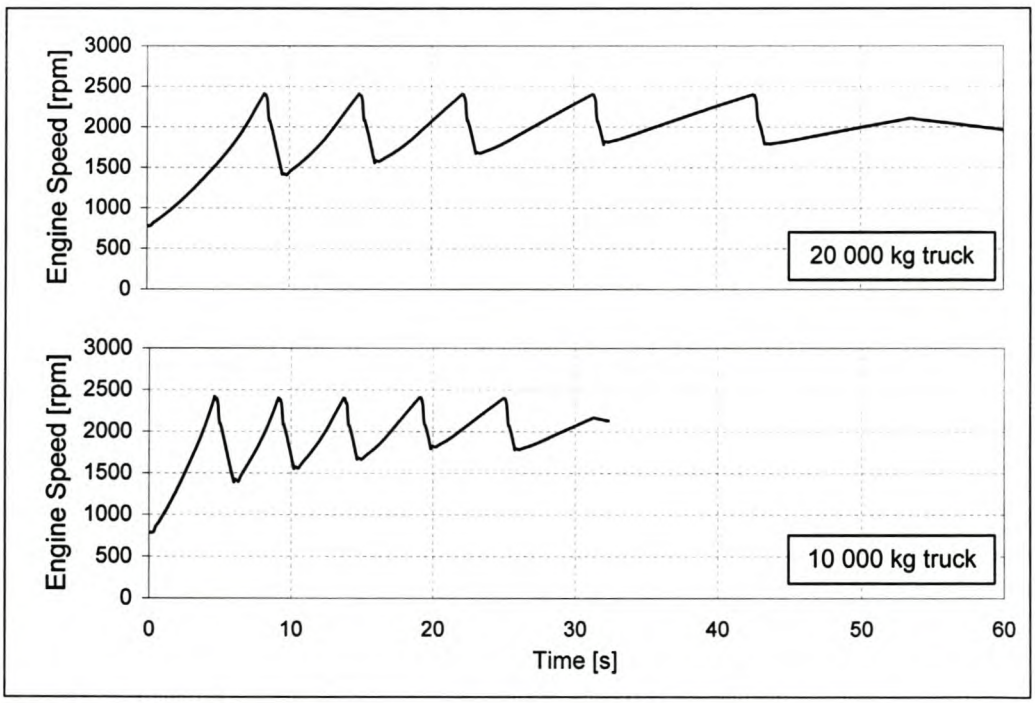

Figure 10.10. Sensitivity analysis: Engine speeds obtained using two different truck masses

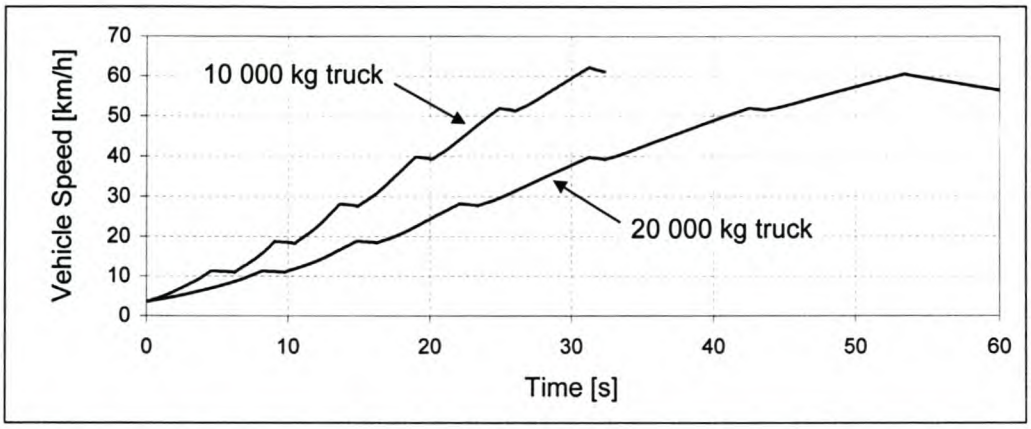

Figure 10.11. Sensitivity analysis: Vehicle speeds obtained using two different truck masses

The data indicates how the lighter truck accelerates a lot quicker than the heavier truck. The 10 000kg truck reached a speed of 60 km/h after 30.25 sec, whereas the 20 000kg truck reached the same speed only after 52.85 sec. A doubling of the vehicle mass thus resulted in the "time-to-60 km/h" acceleration being extended by 74.7%. The reason for this time not doubling, as did the vehicle mass, was that the aerodynamic drag and drive-train efficiency remained the same in both cases, with only the vehicle inertia and rolling resistance changing. Acceleration time is therefore not proportional to vehicle mass, but is a function of all forces acting on the vehicle and its subsystems. Using the dynamic test-bed in this way aided the researchers by providing them with a better understanding of how changing these parameters would have influenced an actual truck on the road. The test data indicated that the testing facility was sensitive not only to changes made to engine parameters, but also to parameter changes made to the virtual vehicle being simulated.

10.4. TRACKING ACCURACY

In Section 5.3.1, the response characteristics of the dynamometer used were quantified. This was carried out in order to gain a better understanding of how well the system would be able to follow demanded engine speed values. The ability of the system to "track" demand values was important if accurate and realistic simulations were to be obtained. The tracking accuracy of the system was assessed over the simulated acceleration run of a 10 tonne truck during which time five gear transitions were performed.

Figure 10.12 shows the result of a simulated acceleration run. Graph (a) shows the actual versus demanded engine speed values while the differences between the two values are shown in graph (b). It is seen that the dynamometer's ability to track demanded speed values varied according to the speed gradient demanded. From graph (b) it is seen that speed deviations were greatest during gear changes at which time high ramp-rates were demanded. During these phases, the dynamometer was not able to follow the speed demand very accurately as it was limited by its low power-to-mass ratio. With the vehicle in gear, speed deviations were minimal, decreasing further as higher gears were selected which resulted in lower speed-rate changes being demanded.

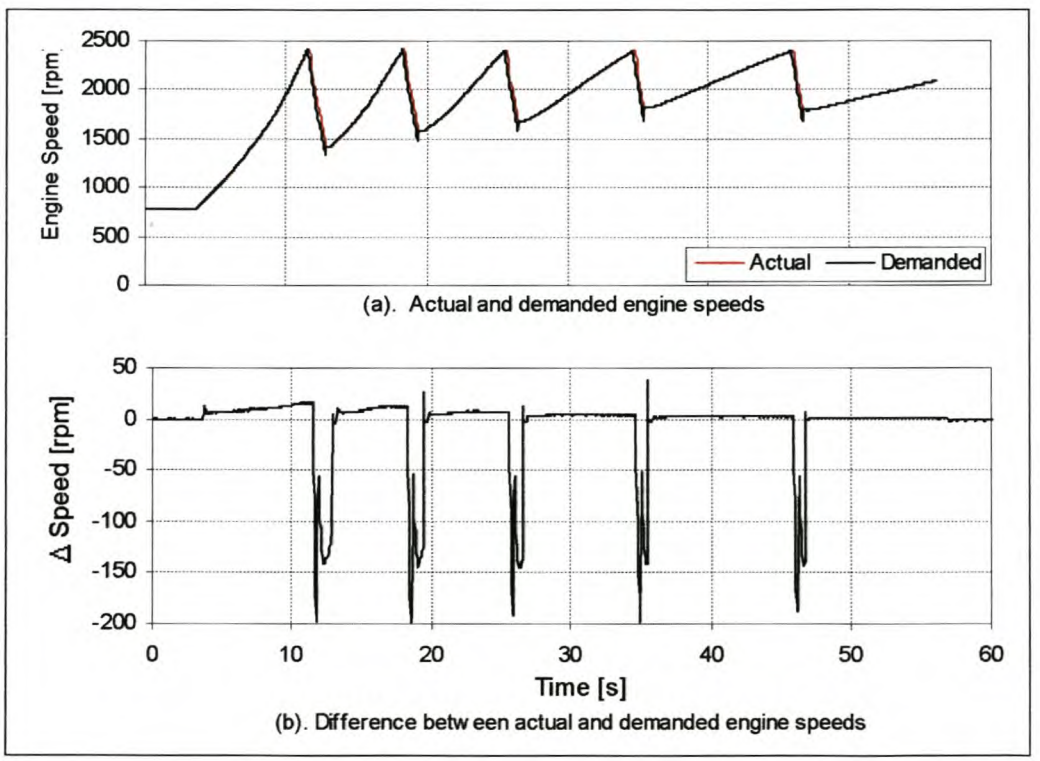

Figure 10.12. Evaluation results: Tracking accuracy during acceleration run

For the acceleration illustrated above, a maximum speed difference of 11 rpm was observed during periods of clutch engagement, while a maximum difference of 200 rpm was noted during gear transition periods. It is conceivable that speed deviations will be greater when lighter vehicle engines are being tested. This is due to the fact that they have less inertia than larger diesel engines, resulting in higher accelerations during gear shifts. These limitations can be overcome only if a more suitable dynamometer with a higher

acceleration-to-power ratio is integrated with the testing facility. This concern is discussed in more detail in Section 12.1.1.

10.5. SIMULATION ACCURACY

The final aspect to be discussed is that of simulation accuracy. In other words, with what degree of accuracy can one reasonably expect the vehicle dynamics and their interaction with external forces to be simulated? In order to answer this question, it is helpful to look at the individual factors influencing the simulation accuracy. These will now be discussed in point form.

10.5.1. Vehicle inertia

Of the three major resisting forces impinging on the vehicle, the vehicle inertia force has by far the largest influence on the way in which the virtual vehicle responds to torque developed by the engine. As was discussed in Section 6.5, the inertia of all rotating parts of the vehicle, together with the translating parts, was considered as a combined mass, the rotational inertia of which was used for calculation purposes. This inertia was obtained using a gear-dependent empirical formula taking into account all these aspects of the vehicle model (equation (6.14)). The accuracy of the vehicle simulation model, therefore, depends to a large degree on the accuracy with which this equation estimates the total equivalent rotational inertia of the vehicle.

Since the equation is used for all types of vehicles, it is likely that some degree of inaccuracy does enter into the model at this point. In order to obtain a more accurate estimate of total vehicle inertia, a more complex vehicle model would have to be developed. Such an approach could be very time consuming and a high level of expertise required to obtain the geometric characteristics needed to compute rotational inertia values for individual drive-line components. Another alternative would be to physically measure the inertial values of each drive-line component or that of the complete drive-line system.

10.5.2. Rolling resistance

Rolling resistance is the second major force impinging on the vehicle, and at low speeds plays a larger role than does the aerodynamic drag. Once again, empirical equations were used to obtain rolling resistance coefficients. Since the model used in the simulation package included only certain aspects that influence rolling resistance (tyre inflation pressure and vehicle speed) and was aimed mainly at giving rough estimates of these values, it is very likely that substantial errors were made in calculating rolling resistance values. If the complete vehicle is available for testing, more accurate rolling resistance coefficients may be obtained using the procedure described in Section 6.3.1.

10.5.3. Aerodynamic drag

Aerodynamic drag is the last of the three major external forces working against the tractive force of the vehicle. It plays a major role at higher vehicle speeds, exceeding that of rolling resistance. This drag force is a function of frontal vehicle area and the drag coefficient which is determined experimentally. As the macro effects of aerodynamic drag are well understood, values of aerodynamic drag can be assumed to be as accurate as are the values available for the drag coefficient, C_D.

10.5.4. Mechanical friction

Mechanical friction can be described as the inability of the drive-line to transmit torque from the engine to the driving wheels. In the simulation model developed, mechanical friction was expressed as a percentage. The torque to be transmitted was then simply multiplied by this percentage in order to simulate the effect mechanical friction has on the drive-line as a whole. As a rule of thumb, efficiencies of about 80% to 90% are typically used to characterise the drive-line (Gillespie T. D., 1992). It is unlikely that this aspect of the vehicle model gave rise to inaccuracies of more than about 5%.

10.5.5. Accuracy of numerical method

The final aspect to be considered as having a possible influence on simulation accuracy is that of the numerical method used in estimating, or predicting, the next vehicle and engine speed demands. Both these speeds were arrived at by the extrapolation of the current speeds using accelerations calculated previously (see equations (6.7) and (6.8)). Extrapolation was performed using the simple Euler method as only previous data was available at each time step. This method also requires a minimum number of calculations and yields predictions which are maximally responsive to preceding derivatives. Other extrapolation techniques (least-squares, cubic-splines) were attempted but resulted in sluggish system response due to the "numerical inertia" associated with them. More accuracy will be obtained if smaller time steps are used; however, the real-time nature of the system, together with processor speed, limited the minimum time-step that could be used without encountering other computational problems.

10.5.6. Final remarks

A number of possible sources of inaccuracies exist within the vehicle simulation system. Some of these have been identified and discussed above. As far as modelling inaccuracies are concerned, simulation accuracy may be increased if reliable vehicle data is available. Numerical accuracy was found to be limited mainly by the time increment used in extrapolating engine and vehicle speeds. Due to the real-time nature of the application, working inside a Windows environment and with a finite processor speed, meant that the time increment had to be limited to 50ms so that all computations could be completed within the required period. The inevitable availability of faster processors will progressively improve this situation.

Depending on the exact application of the vehicle simulator, these inaccuracies will impact on the result to a greater or lesser extent. If the ultimate goal of the system is to simulate standard exhaust emission cycles, accuracy is important and great care will have to be taken to ensure that results obtained from the dynamic test-bed coincide with those acquired using a chassis dynamometer. This will necessarily involve the fine-tuning of vehicle parameters, using as a starting point accurate values obtained from a reliable source. In the case of comparative simulations such as the acceleration tests described in

this document or back-to-back emission cycle testing, it is clearly less important for results to be absolutely accurate. In these cases, more significance is placed on the repeatability and sensitivity of the system. It is therefore not of principal importance for the results to be a 100% accurate portrayal of the actual events. The fact that data sets can be compared with one another and trends observed or recognised, is what is critical in these cases. It was shown in the sensitivity analysis that the system was indeed highly reproducible and capable of discriminating between test results after vehicle configurations were changed. This, in part, is what makes the dynamic test-bed such a powerful tool for research and development in the automotive industry.

11. CONCLUSIONS

The automotive industry has advanced to such an extent that it has become necessary to revise the methods used for the research, design and testing of internal combustion engines. This thesis assessed the current state of engine testing technology and revealed that high-technology testing facilities have become essential tools for the development and optimisation of modern-day engines. The dynamic engine test-bed is regarded as one of the latest and most sophisticated additions to the arsenal of tools used by automotive engineers world-wide in their quest to gain the advantage over their competition. This report documented the development of such a dynamic engine test-bed which will be used at the University of Stellenbosch.

The main project objective laid out in Section 2 of this document, i.e. the design and development of a real-time, engine performance sensitive research tool was achieved to a satisfactory degree. The most difficult obstacle encountered during the development process was that of obtaining an acceptable level of inertia-torque cancellation (see Section 7.5). This proved to be a very problematic task and largely depended on the quality (noise and phase-shift characteristics) of the speed and torque signals. Acceptable results were eventually obtained, but the need for an in-line torque transducer was highlighted. Not all of the project objectives were however achieved; of these, full computer-implemented vehicle speed-control was the most significant. Various control strategies were, however, investigated and assessed in terms of their suitability to the system at hand. Recommendations regarding the future improvement of current system features and the addition of new capabilities were finally made.

Most of the hardware involved in the system was already available in the laboratory. An existing DC-motor and Siemens speed-controller were characterised and the parameters required for further development, obtained. Characterisation results indicated that the dynamometer unit was limited to a bandwidth of less than 5 Hz and could attain maximum ramp-rates of less than 5000 rpm/s. Signals available from the test-bed were conditioned and care was taken to ensure that they could be used by the simulator for further calculations. This involved the design and manufacture of an anti-aliasing filter to ensure that data would not be corrupted by sampling effects and could be trusted for correctness.

It was also necessary to compensate for the dynamometer reaction torque measured by the load-cell. A set of pedals was constructed for the driver to input accelerator, brake and clutch demands. Gear changing was allowed for by means of a hand-held "*tip-tronic*" style selector unit.

A simplified vehicle model was developed that included clutch action, thereby making it possible to simulate vehicle pull-away and gear changing. A rigid drive-shaft was assumed in the current model as the dynamometer unit did not have the response required to simulate vehicle dynamics of higher frequencies. A computer programme was developed that integrated all aspects of the vehicle model to calculate how a virtual vehicle would have responded to the torque currently being developed by the engine. The core of this programme was the *virtual-vehicle-engine* that governed how data was handled and manipulated. It proved to be very difficult to achieve accurately timed programme-loop execution within the Windows NT operating environment, as the system clock proved to be very inaccurate under these circumstances. An elaborate polling technique was eventually used with reasonable success.

The system was evaluated by the simulating of a large truck acceleration, from idle through the first five or six gears. Results showed that the test-bed delivered reproducible data, an important virtue for any scientific piece of equipment. Further evaluation proved the system to be sensitive to both parameter changes to the engine and virtual vehicle, with engine back-pressure and vehicle mass changes reflected in the outcome of acceleration runs.

To conclude, the project undertaken has culminated in a test system that has the ability to perform testing which cannot currently be carried out at any other facility in South Africa. Although the system has not yet been perfected, it has shown great promise and potential for future development. It is envisaged that the system described in this document will result in a powerful tool to aid automotive engineers in their strive to further improve internal combustion engines in an increasingly competitive industry.

12. RECOMMENDATIONS

During the system development period, several shortcomings and limitations were found to exist. These were noted and will now be discussed and recommendations will be made to remove them where applicable.

12.1. HARDWARE ASPECTS

These recommendations pertain to physical items of hardware that will enhance the capabilities of the testing facility. Due to a lack of finances at the time that the system was being developed, these items could not be procured, but should be considered for future implementation.

12.1.1. Low-inertia three-phase AC dynamometer

Section 5 dealt with the characteristics of the DC dynamometer used in developing the CAE testing facility. It was mentioned that the dynamometer inertia, as described by the *mass ratio*, to a large extent determines the dynamic capabilities of the system as a whole. There are a three ways of improving the dynamic capabilities of a dynamometer. The first is to make use of an electric motor with a lower inertia. This would lower the mass ratio and therefore, for a motor with similar power characteristics, increase the system's bandwidth giving it the capability to simulate higher frequency vehicle dynamics. The second, and obvious, method is to use a more powerful motor without increasing its inertia. This would not only improve the system's dynamic capabilities, but allow for the simulation and testing of heavy-duty cycles and larger engines.

Three-phase induction motors are today commonly used in dynamic engine testing facilities, and are even purposefully designed to meet these requirements (Siemens AG, 1999). These motors are available with squirrel-cage rotors specially designed for test operation and can be employed either as motoring or generating machines. The stator lamination core is of self-supporting design and does not require a housing. The advantages of this type of construction include reduced space requirements and reduced noise emissions. The maintenance-free rotor is an extremely compact type of construction

with a particularly low moment of inertia and high torsional stiffness, thus allowing high angular accelerations. These robust induction motors, benefiting from low moments of inertia and high dynamic responses, exhibit a high degree of reliability and require minimum maintenance. In order to illustrate their superiority over the DC motor used in the CAE system (see Table 5.1 and Table 5.3), the technical data of a Siemens 1SR9 316 induction motor of comparable power rating is shown in Table 12.1.

Table 12.1. Technical specifications of Siemens 1SR9 316 induction motor

Shaft power [kW]	300
Basic speed [rpm]	4800
Maximum speed [rpm]	9000
Maximum torque [Nm]	600
Torque at n_{max} [Nm]	320
Rated converter supply voltage [V]	400
Intrinsic acceleration [1)] in basic speed range [rpm/s]	7710
Rated machine current [A]	440
Moment of inertia [kgm^2]	0.73

1) At rated magnetisation, ignoring the overload capacity of the drive

With an inertia of less than half that of the DC motor, double the power, and a resulting ramp rate of more than four times that of the DC motor, it is clear that such a motor would vastly improve the capabilities of the current dynamic testing facility.

A third method commonly used to reduce the negative effects of dynamometer inertia, is to connect the dynamometer and engine via a reduction gearbox or belt system (Pfeiffer & Isermann, 1993, Shafai & Geering, 1989, Voigt, 1991 and Von Thun, 1987). This also serves to match the maximal allowable speeds of the engine and the dynamometer. The main advantage of using this connection scheme is that the effective dynamometer inertia is reduced by a factor of g^2, where g is the reduction ratio. Using this method it is possible to obtain a very low output inertia, thus enhancing the dynamic capabilities of the dynamometer. Flat-bed transmissions often feature the absence of backlash and have very high natural frequencies. As a result, it has been found (Von Thun, 1987) that the dynamometer/engine assembly can be considered to be rigidly connected for control purposes.

12.1.2. Torque measuring hub

As was discussed in Section 7.5, the torque as measured by the load-cell, could not be used directly in any simulation calculations. This was due to the dynamometer inertia influencing the reading during transient operations. To counter this effect, the inertia torque was compensated for by multiplying the dynamometer inertia with a calculated acceleration and adding the result to the load-cell torque. It was also explained that differentiation, especially of a noisy signal, amplifies signal noise tremendously, creating other problems, including the need for extensive filtering. This in turn lowers system bandwidth, negatively affecting the dynamic capabilities of the dynamometer.

One method that effectively overcomes the need for differentiation of the speed signal, is that of using a *torque measuring hub* to obtain dynamically correct torque readings. Torque measuring hubs, also referred to as in-line torque transducers, are connected directly between the dynamometer and engine, and as such are unable to "see" the reaction torque produced because of the dynamometer inertia. Typically, torque is measured in the measuring hub by means of foil strain gauges (FSG) on the basis of a defined torsion of the measuring body. In general, several FSG bridges are connected in a circuit to compensate for the transverse forces and bending moments experienced.

One of two methods can be used to transmit the torque. Slip rings have been used in the past, but these are found to result in noisy signals and are generally limited to a few thousand rpm. Electronic transmission is the preferred method as cleaner signals can be obtained at very high operating speeds. An electronic circuit rotating with the measuring hub converts signals into frequency signals (mV into kHz). In this way, the dynamically correct torque is reliably transmitted to the stator of the measuring hub without the need for slip rings. A downstream evaluation-electronic circuit converts the signal into an analogue DC voltage signal which can readily be acquired using a computer board. Torque measuring hubs specifically designed for engine testing are available and take into account the high alternating and peak torques which occur in internal combustion engines. Calibration is possible by initiating a defined torque with the help of calibrated weights and an attached calibration lever in a manner similar to that employed for cradle dynamometers. In the process, the rotor of the machine is blocked by means of a torque-counteracting support or locking device.

12.2. MODELLING ASPECTS

The following modelling aspects have been identified, either for further research and improvements, or for addition to the system, to improve modelling accuracy or add to the functionality of the testing facility.

12.2.1. Engine cranking simulation

The transient behaviour of internal combustion engines during starting is an important consideration for vehicle manufacturers. Aspects such as the cold-starting ability of engines, and even starter motor matching and design, form integral parts of the vehicle design and optimisation process. A dynamic test-bed with motoring capability has the ability to perform starting simulations under various conditions. This would enable researchers to optimise engine management systems under starting conditions. Computer simulations of engine cranking by a starter motor have been developed by various researchers (Atul & Nitin, 1993 and Miao & Hewko, 1992). It is therefore suggested for further studies to be conducted into the implementation and integration of a suitable starter motor model into the current testing facility as this could be a useful and powerful tool for future research and testing work.

12.2.2. Flexible drive-line model

The vehicle model used in the system described in this document assumed a rigid drive-line mainly due to complexity considerations, but also because the dynamometer system was incapable of simulating these higher drive-line dynamics. It is envisaged that these models will in future include more complex elements of the drive-line, enabling the simulation of complicated drive-line dynamics. This recommendation does, however, also necessitate a more suitable, high-dynamic dynamometer. More complex drive-train equations have been developed by numerous authors (Leonhardt et al., 1992, Shafai & Geering, 1989 and Von Thun, 1987), and included elements such as driveline flexibility and damping. This development will make possible the investigation of drivability and vibration phenomena often associated with drive-line flexibility and damping, such as drive-train ringing caused by improper engine/transmission matching, and may also lead to insight being gained in the designing and placing of engine mounting rubbers. This type of

research is difficult to conduct, since realistic road conditions are difficult to simulate in a controlled laboratory environment. The above recommendation can, however, provide researchers with the facility necessary to carry out design and research of this nature.

12.2.3. Improved clutch model

In Section 6.6 the reasons for opting for a simplistic clutch model were laid out. During the system development period, it was, however, found that certain shortcomings did exist in the chosen model. These were evident mainly in the area of vehicle pull-away where it was difficult to obtain repeatable results, meaning that comparative data could only be obtained if "running start" accelerations were performed. It is suggested that more research be done in this area, as it proved to be more important to the functioning of the system than was originally thought. Research conducted by Szadkowski et al., (1992) should be helpful in this regard.

As an alternative to the manual transmission model used, it is also recommended that the possibility of using an automatic transmission model be investigated. The inclusion of such a model would also be beneficial as far as future driving cycle control is concerned, since there would be only one input to control (i.e. throttle) as opposed to the two required with a manual transmission (i.e. throttle and clutch pedal). A study on the transient characteristics of automatic transmissions, including detailed dynamic modelling, has been conducted by Kim et al. (1994) and should prove useful in this regard.

12.3. SOFTWARE ASPECTS

A large element of the testing facility consisted of the development and integration of software routines. During this process, and after evaluation of the system, the following software aspects were identified as warranting further attention, as they would add significantly to the usefulness of the system.

12.3.1. Vehicle speed controller

As an initial approach to the problem of vehicle speed control, a basic vehicle model was developed and implemented, making sure that the virtual vehicle responded correctly to

external driver input. It was considered practical to make sure that the basic model was behaving correctly before attempting any computer control strategies. Time scales, however, prevented the implementation of such a control strategy, and the author was limited to the investigation and discussion of several control approaches. Based on these investigations, the following vehicle speed control strategy is recommended for future implementation.

It is firstly advisable that the modelling approach suggested by Jacobson (1995) be used when designing a vehicle speed controller, i.e. modelling with natural causality from the driver to the vehicle (see Figure 4.8). This means that input to the vehicle model should be provided by the driver box (see Figure 4.5), and the output being vehicle and engine speeds. Internal combustion engines inherently include time delays due to thermal, flow and mechanical reasons, which is also evident from the form of mathematical models that have been derived for them. It is therefore suggested that the inclusion of a Smith predictor be considered with the control strategy chosen for this application. Advantages of the Smith predictor were discussed in Section 9.3.

As the vehicle speed demand profile is available in advance, a general predictive controller can make use of this data and should therefore have an advantage over controllers using only currently available data. It is suggested that *a priori* speed profile data also be used to facilitate smoother transitions during gear shifting. By modifying the vehicle speed profile such that the target speed exceeds that of the original profile prior to gear shifts, it can be ensured that the difference between actual and demanded vehicle speeds is close to zero once a gear shift has been completed. This will prevent the simulated driver from abruptly moving the throttle or brake, thereby facilitating smoother driver input.

A final comment regarding the choice of controller algorithm is concerned with its self-learning, or adaptation, ability. As engine test-beds are designed for the testing of different engine types and sizes, it will greatly ease the work of researchers if a vehicle speed controller has the capability of optimising itself for any engine being tested. If this is not the case, engineers would continually have to adjust and optimise the controller depending on the type of engine being tested. It is therefore recommended that further research be conducted into this area with the aim of implementing a suitable, adaptive control algorithm in future.

12.3.2. Reliable time-base

In Section 8.2 the need for an accurate time base was explained. Since the programme ran in a Windows environment, it proved to be very difficult to establish a reliable time base from which to work. The method eventually chosen did work satisfactorily, but commanded 100% of the CPU resources due to its polling nature. It is recommended that a more efficient method of timing the application be sought. One that comes to mind is that of using system interrupts to trigger relevant events. As it is dangerous (and not to be recommended) to set interrupts within the Windows environment, it is advisable to use an external source to set interrupts at the required times. Many computer boards can be programmed to do this, and since they rely on their own internal clocks, one can be assured of a reliable time-base. This approach will result in making more efficient use of the CPU, and should lead to a more robust application.

12.3.3. Conventional testing abilities

Although the primary purpose of the dynamic test-bed was to simulate vehicle loads on engines, it would be prudent to enhance the system's functionality by including the conventional testing capabilities necessary to perform many common types of engine testing, e.g. durability testing, power curves, timing swings, etc. Among other things, this requires the ability to independently control engine torque and speed according to specified profiles. Although this is very close to what was achieved by the current system, it does differ in that engine torque instead of vehicle speed is the controlled variable. It is envisaged that standard tests should be automated and fully configurable, therefore requiring minimum user intervention.

13. REFERENCES

American Eagle Technology, 1995, *Eagle Technology – Data Acquisition Products*.

Astrom K. J., and Wittenmark, B., 1987, *Computer Controlled Systems: Theory and Design*, Prentice-Hall, Inc., Englewood Cliffs, New York.

Atul B. P. and Nitin S. R., 1993, *Computer Simulation of an I.C. Engine During Cranking by a Starter Motor*, SAE Paper no. 930626.

Beckwith T. G., Marangoni R. D., Lienhard J. H., 1993, *Mechanical Measurements*, Fifth Edition, Addison Wesley Publishing Company, 147-152.

Benedict T. R. and Bordner G. W., July 1962, *Synthesis of an Optimal Set of Radar Track-While-Scan Smoothing Equations*, IRE Transactions on Automatic Control.

Blanchard B. S. and Fabrycky W. J. ,1998, *Systems Engineering and Analysis*, Third Edition, Prectice Hall International Series in Industrial and Systems Engineering.

Bosch GmbH, 1993, *Automotive Handbook*, Third Edition, 323-324, 483-488.

Brown D. G. and Thompson S., 1983, *A Novel Approach to Engine Torque Speed Control,* SAE Paper no. 831302.

Bunker B. J., Franchek M. A., Thomason B. E., 1997, *Robust Multivariable Control of an Engine-Dynamometer System*, IEEE Transactions on Control Systems Technology, Vol. 5, No. 2, March 1997.

Burr Brown Corporation, 1993, *Universal Active Filter - UAF42.*

Cassidy J. F., 1972, *A Comparison of Dynamic Exhaust Emissions Tests: Chassis Dynamometer versus Engine Dynamometer*, SAE Paper no.720455.

Cassidy J. F. and Rillings J. H., 1972, *Transient Engine Testing by Computer Control,* SAE Paper no. 720454.

Cole D., 1972, *Elementary vehicle dynamics*, Course notes in Mechanical Engineering, The University of Michigan, Ann Arbor, Michigan.

Conradie P. A., 1995, *The Development of a Dynamic Engine-Testing Facility,* University of Stellenbosch, Final Year Project in the Degree B.Ing (Mech).

Del Giacomo N., Ferentino C., Marino P. and Rinaldi L., 1990, *Characterisation of a Dynamic Test Bed for Internal Combustion Engine,* SAE Paper no. 90064.

Fullmer R. R., Tuken T. and Van Gerpen J. H., 1992, *Adaptive Torque Control of a Diesel Engine for Transient Test Cycles*, SAE Paper no. 920238.

Gallacher A. M. and Krebl W. H., 1995, *Dynamic Engine Testing: Why?*, SAE Paper no. 952301.

Gerald C. F. and Wheatly P. O., 1989, *Applied Numerical Analysis*, Fourth Edition, Addison-Wesley Publishing Company, 264-278.

Germane G. J. and Heaton H. S., 1980, *A Dynamic Test Facility with Motoring Using a Digital Computer*, SAE Paper no. 800412.

Gillespie T. D., 1992, *Fundamentals in vehicle dynamics*, Second Edition, Society of Automotive Engineers Inc, 23-28, 110-118.

Hong, C-W., 1995, *An automotive dynamics performance simulator for vehicular powertrain system design*, Internation Journal of Vehicle Design, Vol 16, Nos 2/3, 264-281.

Hong, C-W., 1996, *Dynamic simulation of road vehicle performance under transient accelerating conditions*, Part D: Journal of Automobile Engineering, Proceedings of the Institution of Mechanical Engineers, Vol. 210.

Hughes E., 1987, *Hughes Electrical Technology*, Sixth Edition, Longman Scientific & Technical, 397-398, 552-557

Jacobson B., 1995, *On Vehicle Driving Cycle Simulation*, SAE Paper no. 950031

Kim Y. H., Yang J. and Lee J. M., 1994, *A Study on the Transient Characteristics of Automatic Transmission with Detailed Dynamic Modelling*, SAE Paper no. 941014.

Krebl W. H., 1995, *Engine Test Beds – Yesterday – Today – Tomorrow*, SAE Paper no. 952299.

Krempl P., Schindler W. and Schiefer E., 1985, *Dynamic measurements of particulate mass emission on light-duty diesel engines under steady state and transient conditions,* SAE Paper no. 850269.

Kuo B. C., 1979, *Mathematical Modelling of Permanent-Magnet Step Motors*, in Step Motors and Control Systems, Ed., Benjamin C. Kuo, SRL Publishing Company, Champaign, III., 87-113.

Lander C. W., 1987, *Power Electronics,* Second Edition, McGraw-Hill Book Company, (UK Limited), 1-5, 293-313.

Leonhardt S., Schmidt C., Voigt K. and Isermann R., 1992, *Real-Time Simulation of Drive Chains for Use in Dynamical Engine Test Stands*, American Control Conference.

Ljung L., 1987, *System Identification : Theory For The User,* Prentice-Hall International, Inc.

Ljung L., 1993, *System Identification Toolbox User's Guide*, The MathWorks, Inc.

Miao H. C. and Hewko L. O., 1992, *Dynamic Modelling and Simulation of an Automotive Engine Cranking System*, SAE Paper no. 920292.

Monk J. and Comfort J., 1970, *Mathematical model of an Internal Combustion Engine and Dynamometer Test Rig*, Measurement and Control, volume 3, June 1970.

Morris R. L., Hopkins H. G. and Borcherts R. H., 1981, *An Identification Approach to Throttle-Torque Modelling*, SAE Paper no. 810448.

Noble A. D., Beaumont A. J. and Mercer A. S., 1988, *Predictive Control Applied to Transient Engine Testing,* SAE Paper no. 880487.

Ogata K., 1990, *Modern Control Engineering*, Second Edition, Prentice-Hall International, Inc.

Pfeiffer K. and Isermann R., June 1993, *Driver Simulation used in Dynamical Engine Test Stand for Exhaust Emission Test Cycles,* Proceedings of the American Control Conference.

Phillips C. L., Nagle H. T., 1995, *Digital Control Systems Analysis and Design*, Third Edition, Prentice-Hall International, Inc.

Roberts P. D, and Dallard K. E., 1974, *Discrete PID Controller with a Single Tuning Parameter*, Measurement and Control, volume 7, December 1974, 469-473.

Shafai E. and Geering H. P., June 1989, *Emulation of Vehicle Dynamics on an Engine Test Bed*, Proceedings of the American Control Conference.

Shigley J. E., *Mechanical Engineering Design*, 1986, McGraw-Hill Book Company, 603-604.

Siemens AG, April 1993, *Simoreg K - Instruction Manual.*

Siemens AG, February 1999, *Loading Device for Engine Test beds with Dynamometer in Three-Phase Design*, Technical Description, 1SR9 Loading Device with SIMOVERT VC MASTER DRIVES converter and digital closed-loop control.

Sultan M. C., Tang D L, Chang M F, 1990, *An Engine and Starting System Computer Simulation,* SAE Paper no. 900779.

Szadkowski A. and Morford R. B., 1992, *Clutch Engagement Simulation: Engagement Without Throttle*, Dana Corporation, SAE Paper no. 920766.

Szadkowski A. and McNerney G. J., 1992, *Clutch Engagement Simulation: Engagement With Throttle*, Dana Corporation, SAE Paper no. 922483.

Tuken T., Fullmer R. R. and Van Gerpen J., 1990, *Modeling, Identification, and Torque Control of a Diesel Engine for Transient Test Cycles,* SAE Paper no. 900235.

Tuken T., and Van Gerpen J. H., 1992, *A Modified Pole-Zero Assignment Algorithm*, In preparation.

Uys J. B., 1991, *Dinamika van starre liggame*, Departement Toegepaste Wiskunde, Universiteit van Stellenbosch.

Voigt K. U., 1991, *A Control Scheme for a Dynamical Combustion Engine Test Stand*, IEE Control '91, Edinburgh, U.K. March 25-28.

Von Thun H. J., 1987, *A New Dynamic Combustion Engine Test Stand with Real-Time Simulation of the Vehicle Drive-Line,* SAE Paper no. 870085.

Voos W., 1992, *Dynamic Engine Testing,* SAE Paper no. 920254.

Ziegler J. C., and Nichols N. B., 1942, *Optimum Settings for Automatic Controllers*, Trans. of the ASME volume 64, 759-768.

14. APPENDIX A

Functional Block Diagrams describing the CAE system

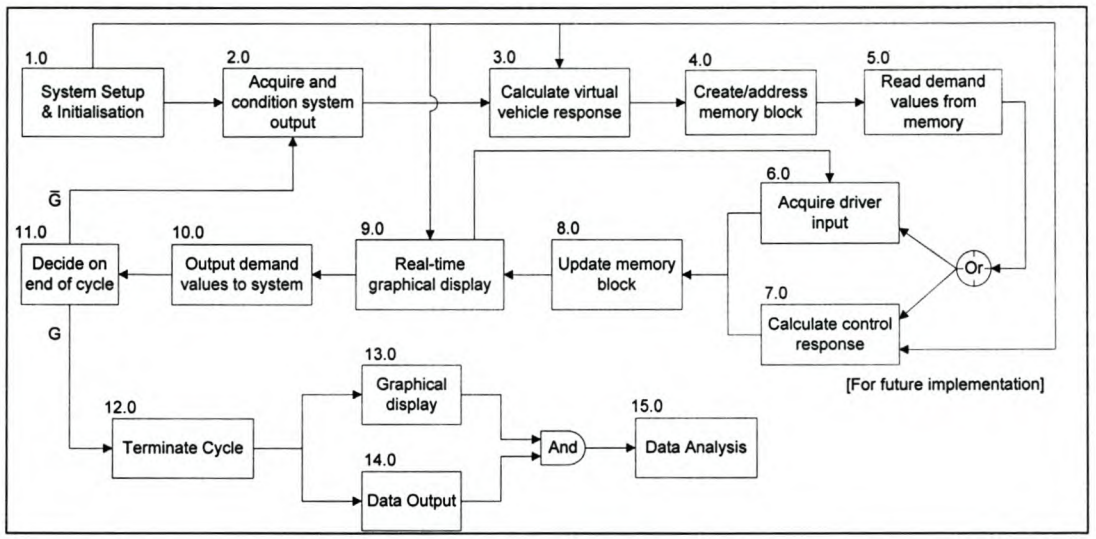

Figure A.0. Top level functional block diagram of the CAE system

Table A.0. Top level functional block diagram of the CAE system: descriptions

Block	Description
1.0	The system is setup and initialised including.: (a) opening/editing/creation of configuration files, (b) interpolation between cycle node points (cycle mode), (c) creation of memory space (cycle mode).
2.0	All relevant data is acquired from the system. Filtering of data occurs and load-cell torque is corrected as discussed in point 3.1.2.1) of the needs identification section.
3.0	The computer model is used to calculate the "virtual vehicle" response to acquired engine torque and speed readings.
4.0	Memory block created (*free-style* mode) or addressed (*cycle-mode*) as required.
5.0	Demanded vehicle speed values are read from memory block if in *cycle-mode.*
6.0	Acquire and filter driver input if cycle is controlled by human. Inputs include: (a) accelerator pedal position, (b) brake pedal position,

	(c) clutch pedal position, (d) gear selection. Control response from driver determined using graphical feedback (block [8.0]) and demanded vehicle speed (block [5.0]) if in cycle mode.
7.0	Calculate control response using control algorithm (see Section 9). Virtual vehicle response (block [3.0]) used for control feedback purposes.
8.0	Currently addressed memory block is updated with all the latest system data.
9.0	Display pertinent information in graphical format for user. User configurable setup.
10.0	Output engine speed demand, (obtained in block [3.0]) and throttle demand values (blocks [6.0] or [7.0]) to system.
11.0	If end of cycle is reached cycle is terminated (block [12.0]), else next system data is acquired (block [2.0]).
12.0	Cycle is terminated, setting all relevant outputs to zero.
13.0	Relevant data is graphed for user inspection and analysis.
14.0	Data is saved to file in spreadsheet compatible format, including necessary headings and date/time stamps.
15.0	Data analysis is performed by user (if req.)

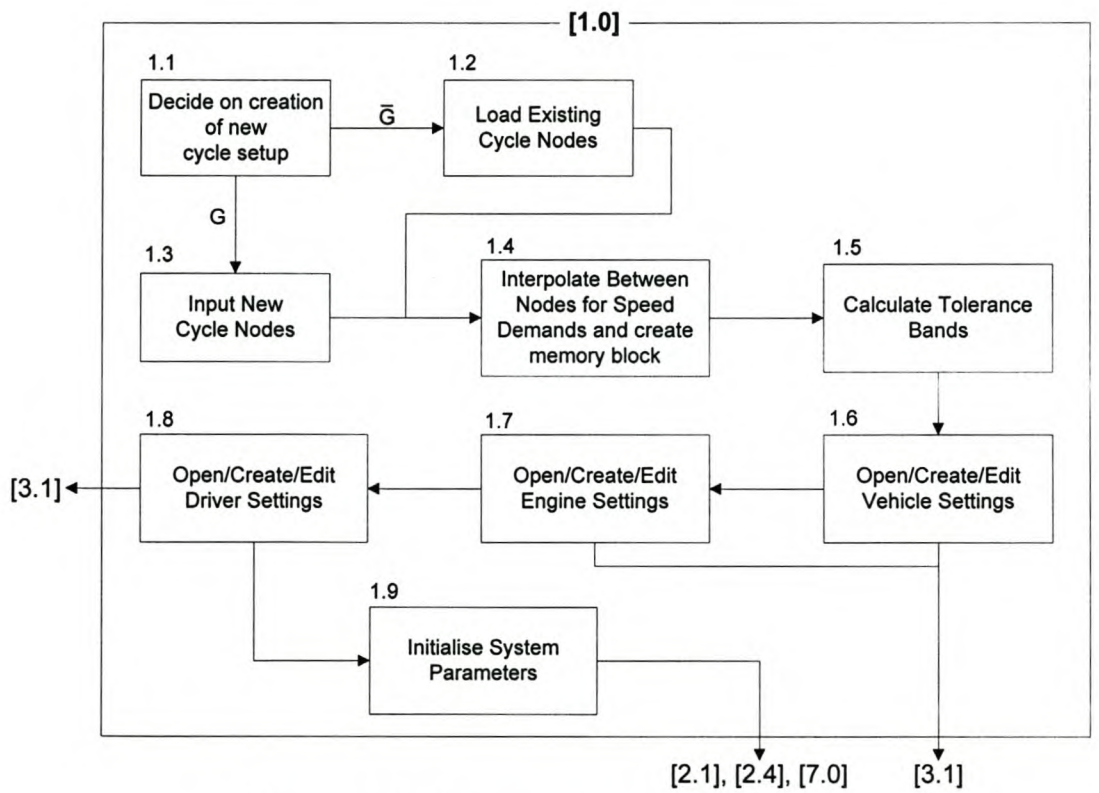

Figure A.1.0. System setup and initialisation

Table A.1.0. System setup and initialisation: descriptions

Block	Description
1.1	A new cycle setup can either be created (block [1.3]), or an existing cycle can be opened (block [1.2]).
1.2	Load existing cycle file from disk.
1.3	New cycle nodes are entered by the user (if in cycle mode).
1.4	Upon completion of node entering, the cycle file is saved at which time speed demand values at each time interval is obtained by means of interpolation. Memory blocks are allocated to each time step having enough space to hold all relevant data at that point in the cycle.
1.5	Permissible tolerance bands are calculated, adhering to standard formats as used by legislative bodies.
1.6	Vehicle settings are opened, created or edited by the user as required
1.7	Engine settings are opened, created or edited by the user as required
1.8	Driver settings are opened, created or edited by the user as required
1.9	All parameters used in the program are initialised, user interface set as required and timers & counters started.

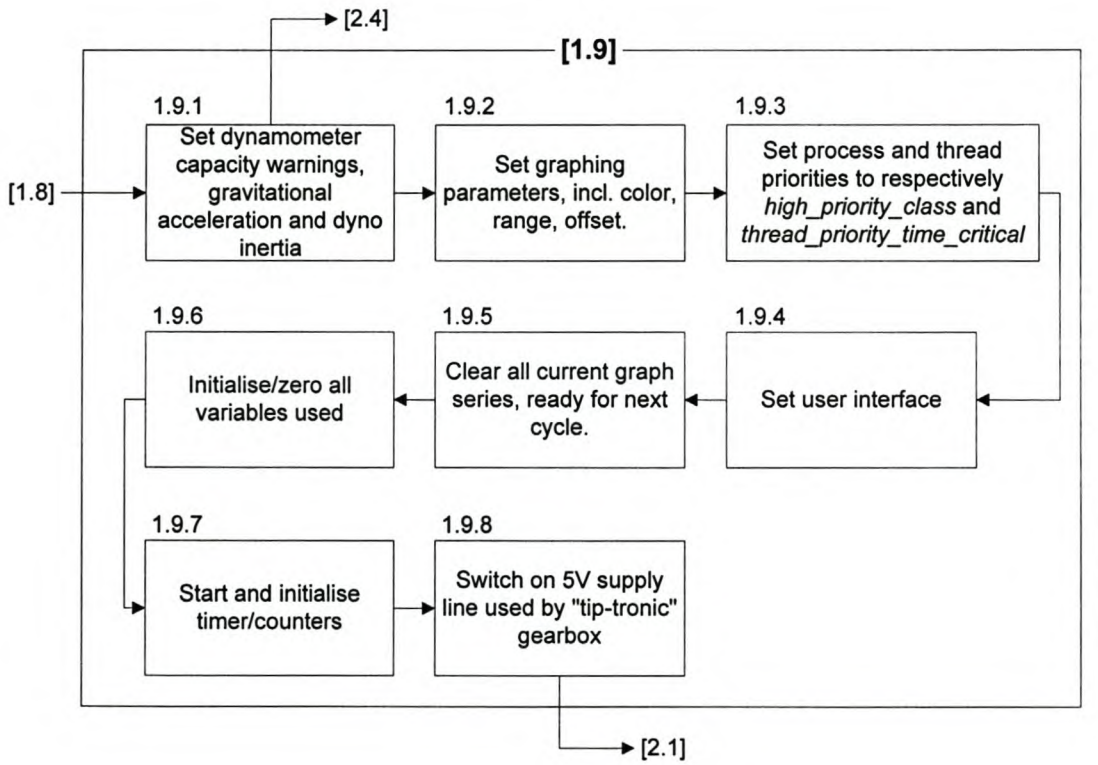

Figure A.1.9. Initialise system parameters

Table A.1.9. Initialise system parameters: descriptions

Block	Description
1.9.1	Dynamometer capacity settings are entered, together with the gravitational acceleration and dynamometer inertia. Dynamometer capacity settings are used by safety routines during the running of cycles.
1.9.2	Graphing parameters are set. These include graph color, range and offset.
1.9.3	New cycle nodes are entered by the user (if in cycle mode).
1.9.4	The user interface is set. Menu items are disabled to prevent interference with program execution in terms of CPU allocation time.
1.9.5	All current graphs are erased leaving the main viewing area ready for the next cycle.
1.9.6	All variables used during cycle execution are initialised/zeroed.
1.9.7	Timers/counters are initialised and started.
1.9.8	The "tip-tronic" gearbox receives its power from the computer board and this 5V supply is switched on here.

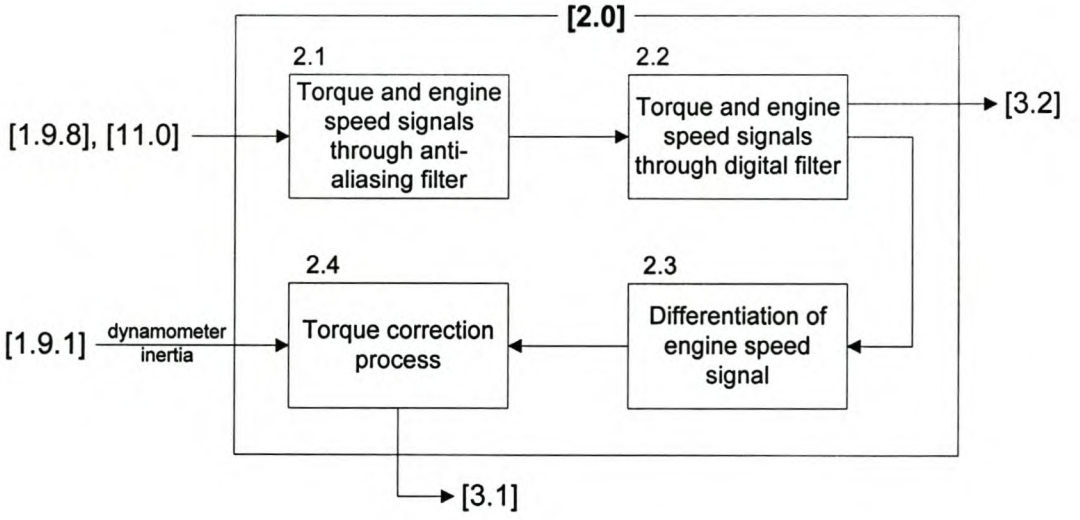

Figure A.2.0. Acquire and condition system output

Table A.2.0. Acquire and condition system output: descriptions

Block	Description
2.1	Speed and torque signal are filtered through an analogue anti-aliasing filter.
2.2	Speed and torque signal are filtered through a digital filter to further improve signal-to-noise ratio.
2.3	The speed signal is differentiated by means of a *tracking filter*, yielding dynamometer acceleration.
2.4	Torque correction is performed by multiplying dynamometer inertia with acceleration and adding to load-cell torque.

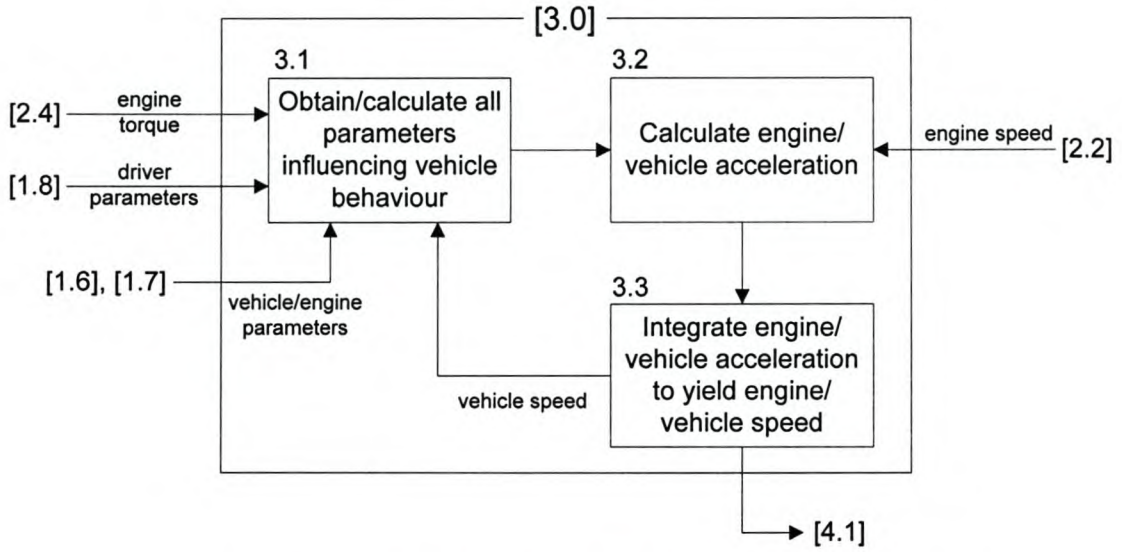

Figure A.3.0. Calculate virtual vehicle response

Table A.3.0. Calculate virtual vehicle response: descriptions

Block	Description
3.1	All parameters influencing vehicle behaviour (relevant torques and loads) are calculated/obtained. Tractive force is obtained by subtracting all load forces from the engine torque (block [2.4]) multiplied by the applicable gear and final ratios. Vehicle and engine parameters are obtained from blocks [1.6] and [1.7]. Vehicle speed, necessary in calculating drag and rolling forces is obtained from block [3.3].
3.2	Engine and vehicle accelerations are determined by dividing the respective torques by the engine and effective vehicle inertias.
3.3	Engine and vehicle accelerations obtained in block [3.2] are integrated, yielding engine/vehicle speeds.

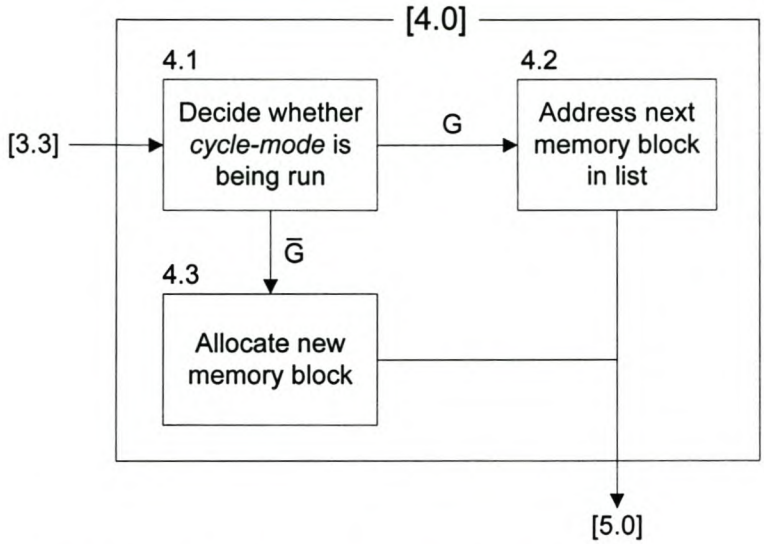

Figure A.4.0. Create/Address memory block

Table A.4.0. Create/Address memory block: descriptions

Block	Description
4.1	If in *cycle-mode*, the next memory block in the list (created in block [1.4]) is addressed (block [4.2]). If in *free-style* mode, a new block of memory is allocated (block [4.3])
4.2	The next memory block in the list (created in block [1.4]) is addressed by the system for storage and retrieval of data.
4.3	A new block of memory is allocated for the program in which to store data as it becomes available from the system.

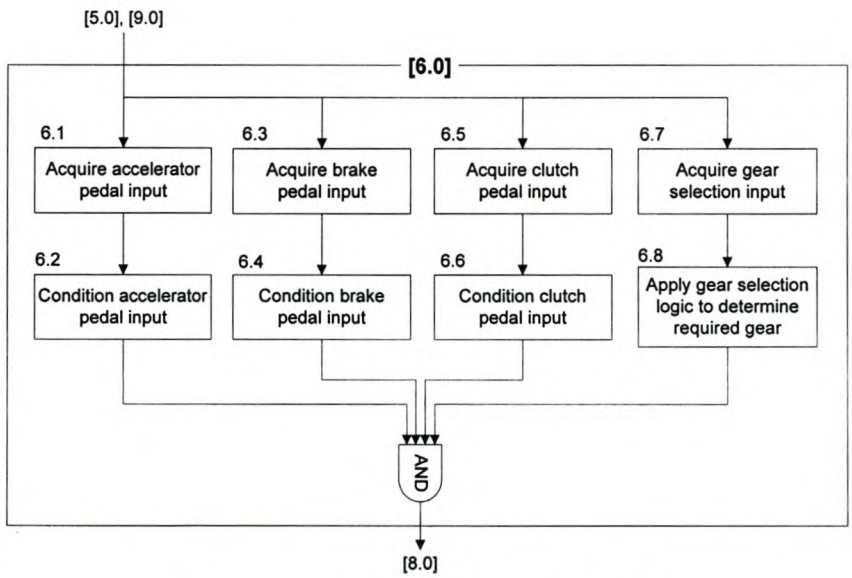

Figure A.6.0. Acquire driver input

Table A.6.0. Acquire driver input: descriptions

Block	Description
6.1	Accelerator pedal input is acquired from the driver. Graphical feedback generated in [9.0] is used for control purposes.
6.2	Accelerator pedal input is conditioned by filtering signal and clipping to within calibrated values.
6.3	Brake pedal input is acquired from the driver.
6.4	Brake pedal input is conditioned by filtering signal and clipping to within calibrated values.
6.5	Clutch pedal input is acquired from the driver.
6.6	Clutch pedal input is conditioned by filtering signal and clipping to within calibrated values.
6.7	"Tip-tronic" style gear selection is acquired from the driver.
6.8	Gear selection logic is applied in determining the gear selection currently required.

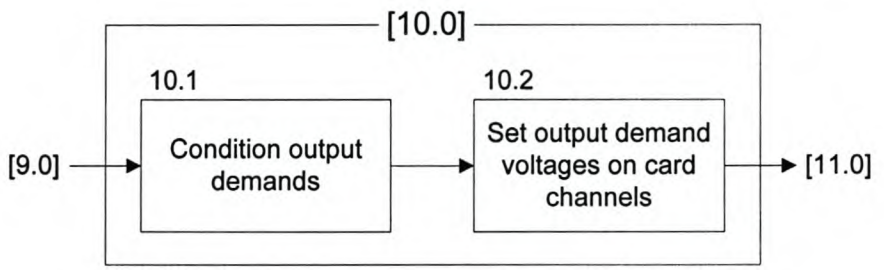

Figure A.10.0. Output demand values to system

Table A.10.0. Output demand values to system: descriptions

Block	Description
10.1	Speed demand values are generated at block [3.0], while throttle demand values are generated either at blocks [6.0] or[7.0], depending on whether the cycle is controlled by human or computer. The demand values are converted to appropriate voltages using calibration factors determined beforehand.
10.2	Demand values (voltages) are set on the appropriate channels of the D/A card.
11.0	If the end of the cycle has been reached, the cycle is terminated (block [12.0]), else the next system data is acquired and conditioned (block [2.0])

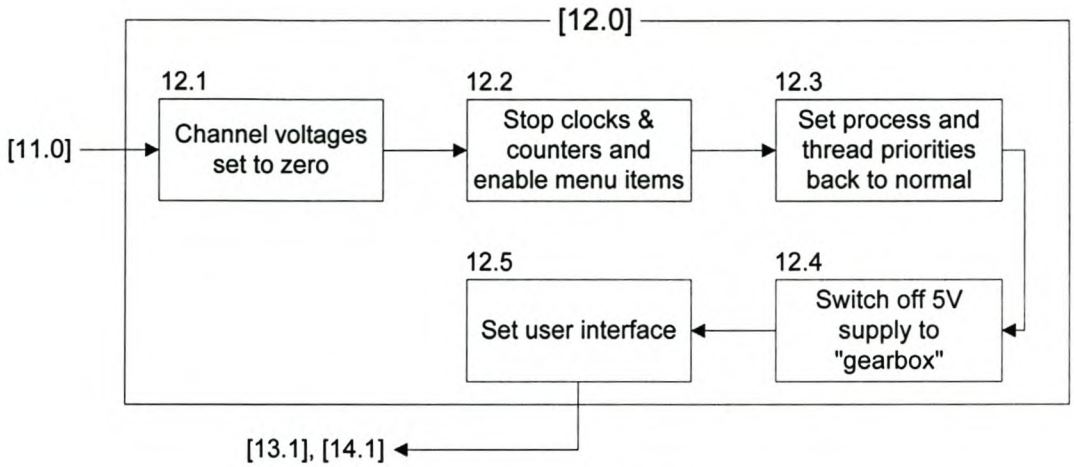

Figure A.12.0. Terminate cycle

Table A.12.0. Terminate cycle: descriptions

Block	Description
12.1	All channel voltages on the output card are set to zero.
12.2	Card clocks and counters are stopped. Menu items disabled during system initialisation (block [1.9]) are again enabled.
12.3	Process and thread priorities are set back to normal.
12.4	The 5V supply to the "tip-tronic" gearbox is switched off.
12.5	User interface is set such that a next cycle can be run.

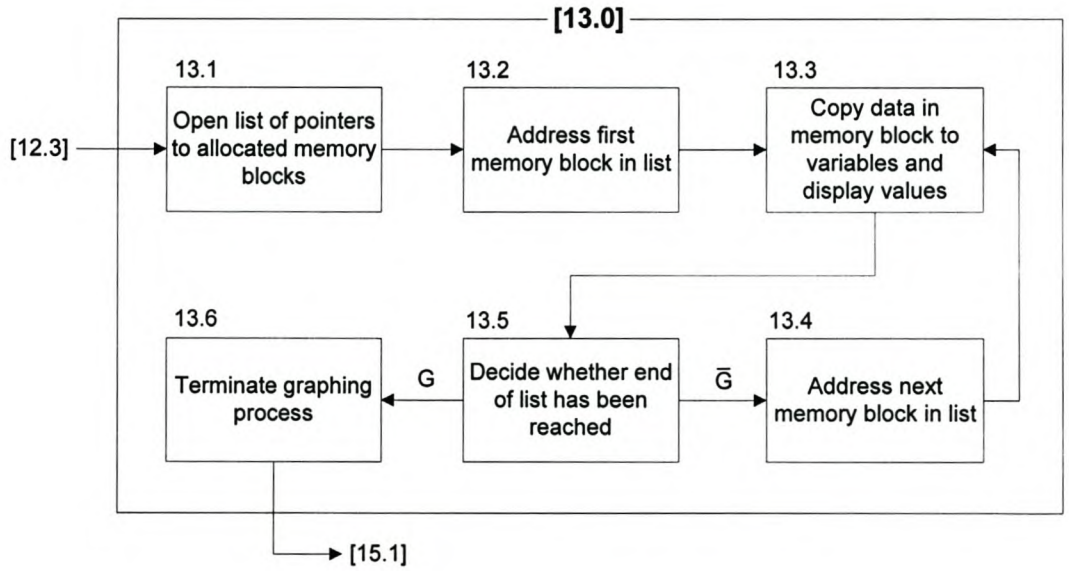

Figure A.13.0. Graphical display

Table A.13.0. Graphical display: descriptions

Block	Description
13.1	The list of pointers to memory locations created in block [4.0] is opened.
13.2	First memory block in the list is addressed
13.3	All data in the memory block is copied to variables and sent to a graphing object that displays them on the screen.
13.4	If the end of the list has not yet been reached, the next memory block in the list is addressed.
13.6	If the end of the list has been reached, the graphing procedure is terminated and the list closed.

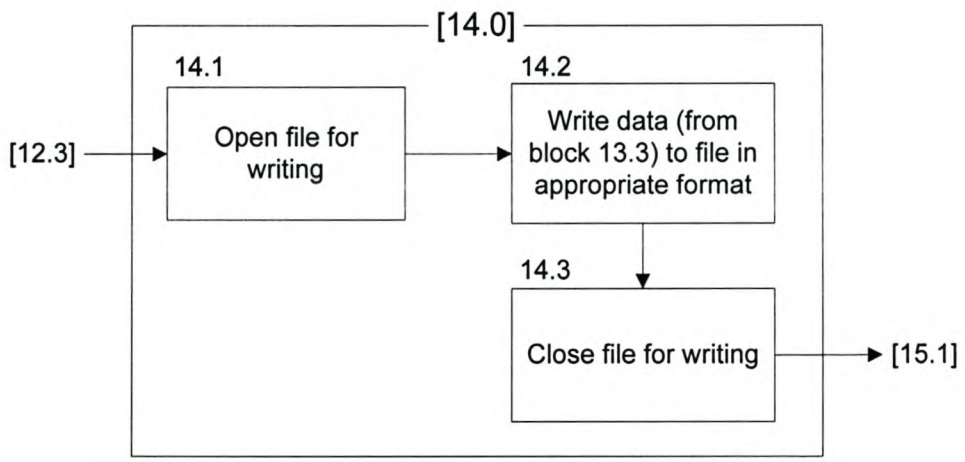

Figure A.14.0. Data Output

Table A.14.0. Data Output: descriptions

Block	Description
14.1	A file (as setup by the user) is open for writing.
14.2	Data (from block [13.3], used also for graphing) is written to hard disk in the appropriate format such that it can easily be imported into spreadsheet applications. Data files are also time-stamped to ensure trace-ability.
14.3	The file is closed for writing.

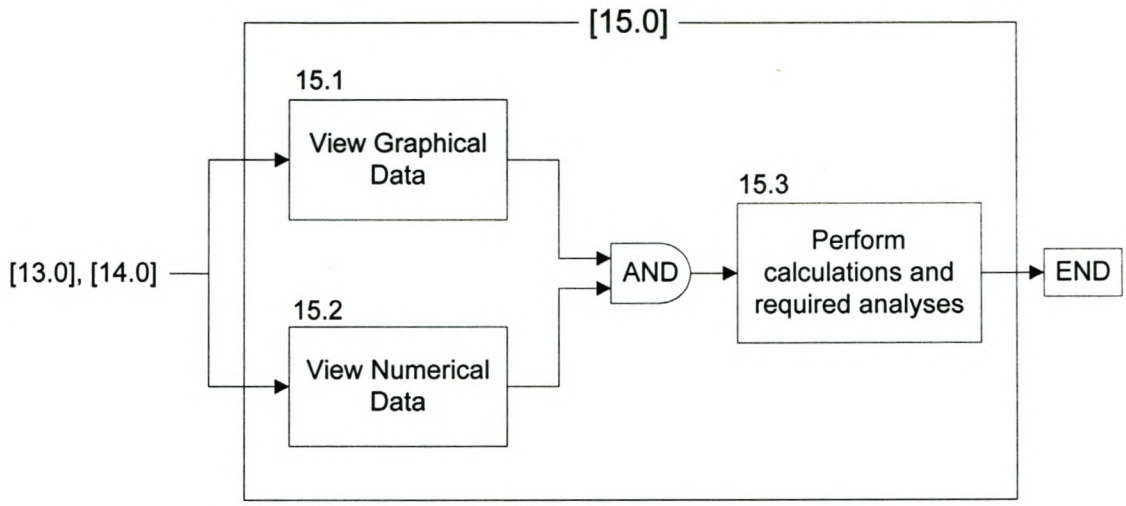

Figure A.15.0. Data analysis

Table A.15.0. Data analysis: descriptions

Block	Description
15.1	Graphical data produced in block [13.0] is manipulated and viewed.
15.2	Numerical data produced in block [14.0] is manipulated and viewed
15.3	Required data analysis is performed by manipulation of data and necessary calculations.

15. APPENDIX B

Technical specifications of PC-30GA computer board

Analogue Inputs	Number:	16 single-ended, 8 differential
	Resolution:	12 bits, 1 part in 4096
	Total System Accuracy:	±1 LSB max (affected by environment)
	Differential Non-Linearity:	±3/4 LSB max
	Integral:	±0.05% FS
	Full-Scale Range:	Bi-Polar: ±5V, ±10V
		Uni-Polar: 0 to 10V
	A/D Sample Rate:	100 kHz
	Input Impedance:	10GΩ/20pF (On Channel); 10GΩ/100pF (Off Channel)
	Programmable Gains:	Ranges: 1, 10, 100, 1000
		Error: Adjustable to 0
		Accuracy: 0.25% max, 0.05% typical
		CMRR: 1% max, 0.1% for gain = 100
		Monotonic: 0 to 70°C
	Temperature Drift:	6pppm/°C (full scale)
		1ppm/°C (bi-polar zero)
		±30ppm/°C (gain)
	A/D FIFO Buffer:	16 Samples
	Channel-Scan Gain List:	up to 31 channels
	Block Scan Mode:	up to 256 channels
	Aperture Uncertainty:	PC-30F/G-S4/16: 300ps (ch 0-3), 20ns (ch 0-15)
Analogue Outputs	Number:	2 @ 12 bits, 2 @ 8 bits
	Accuracy:	±1 LSB (12 bits), 0 LSB (8 bits)
	Differential Non-Linearity:	±0.5 LSB
	Output Ranges:	±5V, ±10V (bi-polar); 0-10V, 0-13V (uni-polar)
	Gain/Offset Error:	0.25 LSB typical, 1 LSB max (uni-polar)
		0.25 LSB typical, 2 LSB max (bi-polar)
	Gain Ranges:	x1, x2
	Settling Time:	10µs max into 500 pF, 2KΩ load
	Throughput:	100 kHz minimum
	Max current output:	5 mA

Digital I/O	Number of Lines:	24; 3 ports of 8 bits each
	Compatibility:	Intel-8255 compatible TTL
	Interface:	Simple I/O, strobed I/O, handshake I/O
	Counters/Timers:	3 (2 used for A/D)
	Frequency:	2 to 8 MHz
	Internal Clock:	2 MHz, crystal controlled
	Clock Divider:	16-bit pre-scaler, 16-bit divider
	External Trigger:	TTL compatible input
PC Interface	Base Address:	0000H to 1FE0H, DIP switch selectable
	Registers:	32 8-bit registers, register-compatible with PC30D series
	Interrupts:	IRQ 2 to IRQ 15
	DMA:	Dual-channel, levels 5, 6, or 7
	Power Requirements:	+5V @ 500 mA (typical); ±12V for user application only
	Relative Humidity:	0% to 90% non-condensing
	Operating Temperature:	0 °C to 70 °C

Technical specifications of PC-14B computer board

Digital I/O	Number:	48, in 6 x 8 bits
Lines	Compatibility:	TTL
	Input Logic Low:	0.8V
	Input Logic High:	2.0V
	Input Load Current:	±10μA max.
	Current Sink:	I_{sink} = 1.7mA @ 0.45V
	Current Sink:	I_{source} = 200μA @ 2.4V
	Output Drive Current:	4mA max @ V_{out} = 1.5V
Counter/Timers	Number:	3
	Compatibility:	TTL
	Resolution:	16 bits
	Input Frequency:	8 MHz
	On-board Clock:	2 MHz
Ext Interrupt	Compatibility:	TTL
	Sensitivity:	Rising edge
	Pulse Width:	20 ns minimum
PC Interface	Wait States:	0, 1, 2, 4 or 8
	PC-14B I/O Connectors:	1 50-pin DIL connectors, 1 25-pin auxiliary connector
	Operating Temperature:	0°C to 70°C

16. APPENDIX C

Transformation of linear inertia to rotational inertia

From Newton, resultant tractive force available at the wheel equals vehicle mass times acceleration:

$$F_t = Ma \tag{C.1}$$

Vehicle velocity equals tyre radius times angular velocity:

$$V = R\omega_v \tag{C.2}$$

This can now be differentiated to yield angular vehicle acceleration:

$$a = R\alpha_v \tag{C.3}$$

Resultant traction torque ($T_c G_{tf} - T_v$) available at the wheel, equals the resultant traction force times the wheel radius:

$$T_t = F_t R \tag{C.4}$$

From equation (C.1) and (C.4):

$$T_t = MaR \tag{C.5}$$

Substituting equation (C.3) into (C.5) yields:

$$T_t = MR^2\alpha_v \tag{C.6}$$

Resultant traction torque is also equal to effective vehicle inertia times angular acceleration:

$$T_t = J_v\alpha_v \tag{C.7}$$

From equations (C.6) and (C.7), the following relationship is found:

$$J_v = MR^2 \tag{C.8}$$

This result is in accordance with the inertia of a point-mass as deducted by J.B. Uys (1991).

17. APPENDIX D

Schematic of Anti-Aliasing filter design

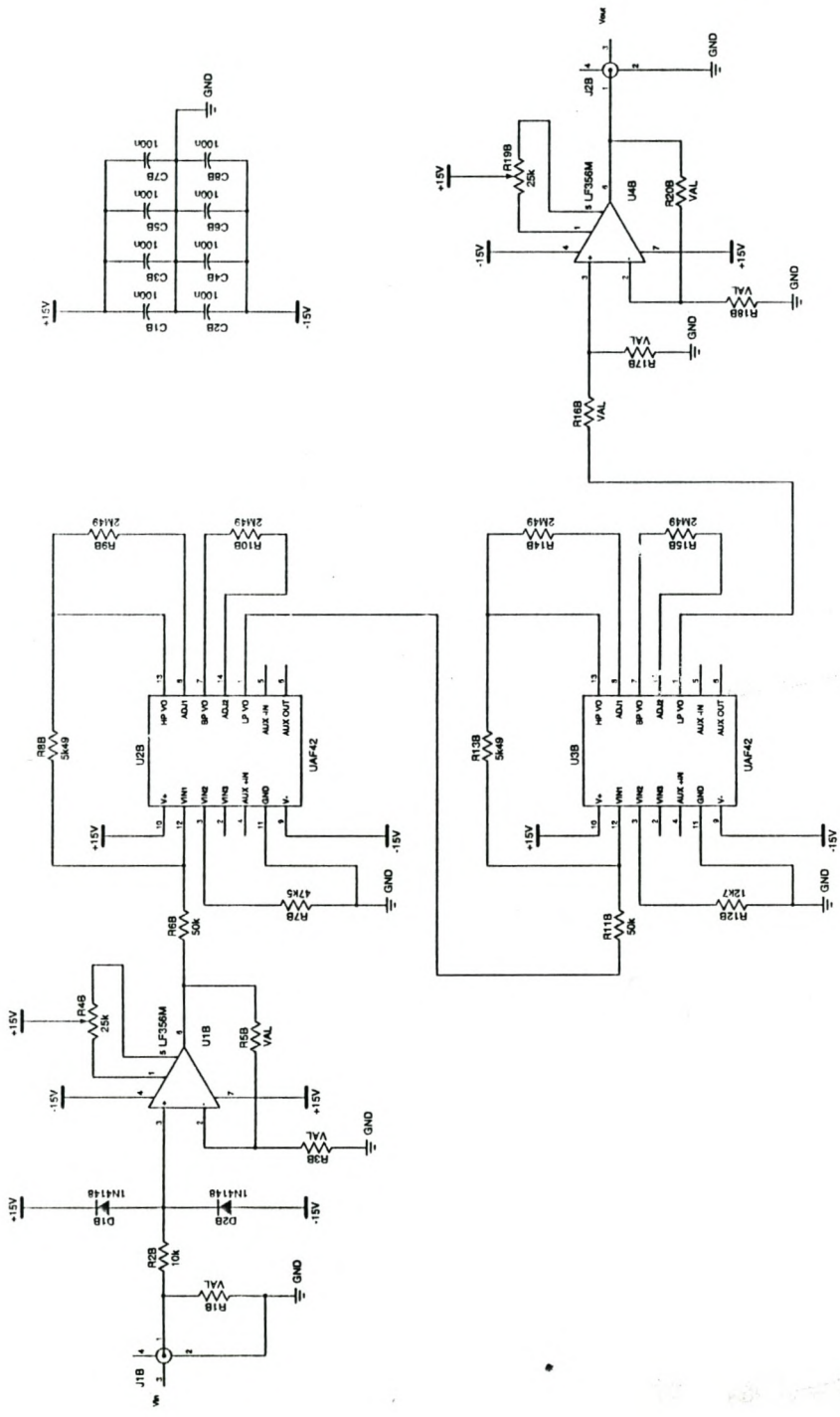

Figure D.1. Anti-aliasing filter circuit layout

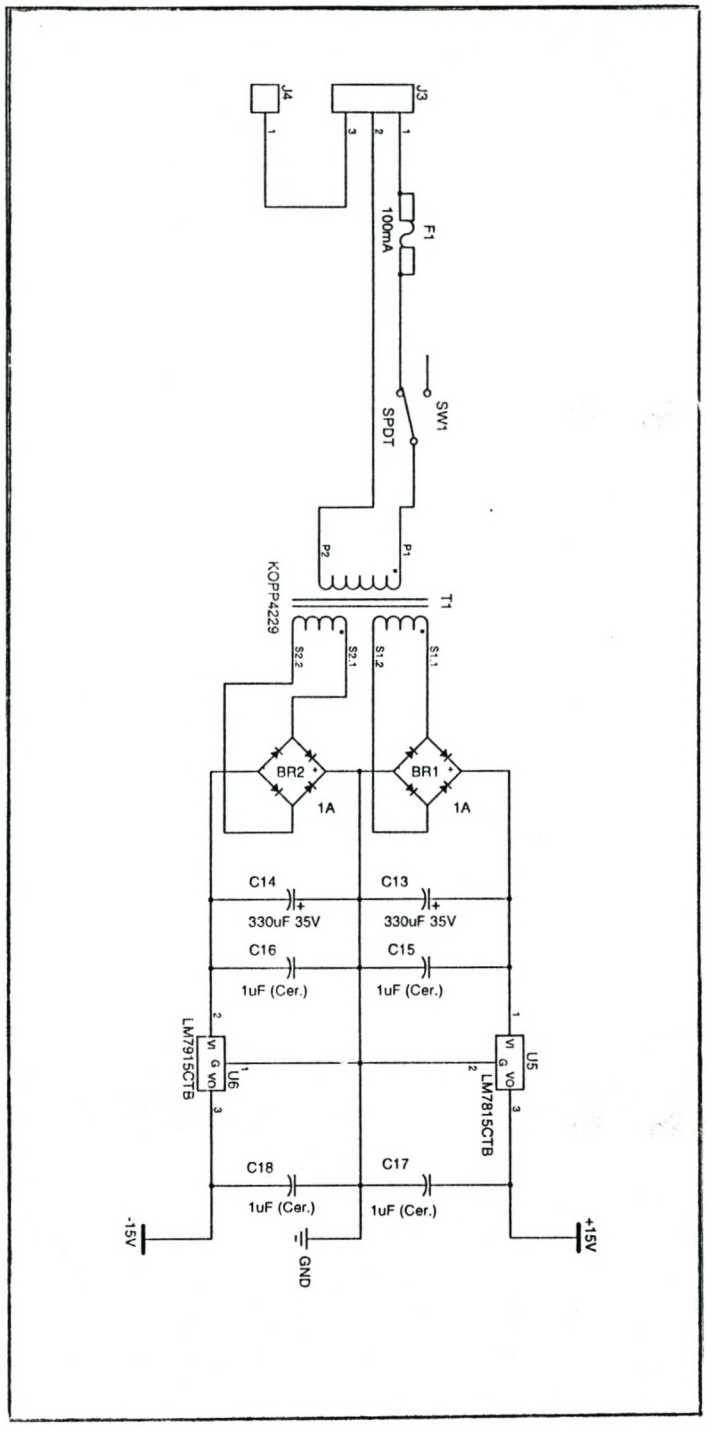

Figure D.2. Anti-aliasing filter power supply circuit